DISSERTATION

In Partial Fulfillment of the Requirements for the Degree of Doctor of Philosophy

from TELECOM ParisTech

Specialization : Electronic and Communications

Bassem Zayen

Spectrum Sensing and Resource Allocation Strategies for Cognitive Radio

Defense scheduled on the 19th of November 2010 before a committee composed of :

President	Dirk Slock, EURECOM, France
Reporters	Guevara Noubir, CCIS, Northeastern University, Boston, USA
	Constantinos Papadias, AIT, Greece
Examiners	Slim Alouini, KAUST, Kingdom of Saudi Arabia
	Mischa Dohler, CTTC, Spain
Thesis supervisor	Aawatif Hayar, EURECOM, France

THÈSE

Présentée pour obtenir le grade de docteur

de TELECOM ParisTech

Spécialité : Eléctronique et Communications

Bassem Zayen

Stratégies d'accès et d'allocation des ressources pour la radio cognitive

Soutenance prévue pour le 19 novembre 2010 devant le jury composé de :

Président	**Dirk Slock, EURECOM, France**
Rapporteurs	**Guevara Noubir, CCIS, Northeastern University, Boston, USA**
	Constantinos Papadias, AIT, Greece
Examinateurs	**Slim Alouini, KAUST, Kingdom of Saudi Arabia**
	Mischa Dohler, CTTC, Spain
Directeur de thèse	**Aawatif Hayar, EURECOM, France**

Abstract

Cognitive radio is a promising technique for efficient spectrum utilization. It dynamically monitors activity in the primary spectrum and adapts its transmission to available spectral resources. The blind spectrum sensing and resource allocation in cognitive radio are being addressed in this thesis.

In the first part of this thesis, we will show how methods relying on traditional sample based estimation methods, such as the energy detector and autocorrelation based detector, suffer at low signal to noise range. This problem is attempted to be solved by investigating how model selection and information theoretic distance measures can be applied to do spectrum sensing. Results from a thorough literature survey indicate that the Kullback-Leibler distance between signal and noise distributions and the information theoretic distance are promising when trying to devise novel spectrum sensing techniques. Two novel detection algorithms based on the distribution analysis and the dimension estimation of the primary user received signal are proposed. Furthermore, we derive also closed-form expressions of false alarm probabilities for a given threshold for both detectors. Detection performance of the two proposed detectors in comparison with some reference detectors will be assessed. Detection performance will be also assessed by applying the detectors to real signal captured by EURECOM RF Agile Platform. Simulations show good results for the two proposed techniques in terms of local spectrum holes detection and primary user presence detection. An extensive analysis on cooperative communications for cognitive radio networks will be discussed. In particular, we will study collaborative sensing as a means to improve the performance of the proposed detectors and show their effect on cooperative cognitive radio networks.

In the second part of this thesis, we will address the problem of resource allocation in the context of cognitive radio networks and we will propose two user selection strategies. The two new strategies are based on outage probability to mange the quality of service of the cognitive radio system. We will derive in a first step a distributed user selection algorithm under a cognitive capacity maximization and outage probability constraints. Specifically, we allow secondary users to transmit simultaneously with the primary user as long as the interference from the secondary users to the primary user that transmits on the same band remains within an acceptable range. We impose that secondary users may transmit simultaneously with the primary user as long as the primary user in question does not have his quality of service affected in terms of outage probability. The second algorithm investigates multiuser multi-antenna channels using a beamforming strategy. The proposed strategy tries to maximize the system throughput and to satisfy the signal-to-interference plus-noise ratio constraint, as well as to limit interference to the primary user. In the proposed algorithm, secondary users are first pre-selected to maximize the per-user sum capacity subject to minimize the mutual interference. Then, the cognitive radio system verifies the outage probability constraint to guarantee quality of service for the primary user. Both theoretical and simulation results based on a realistic network setting, for the two proposed strategies, provide substantial throughput gains, thereby illustrating interesting features in terms of cognitive radio network deployment while maintaining quality of service for the primary system.

Résumé

La radio cognitive est une technique prometteuse pour l'utilisation efficace du spectre. Elle doit surveiller l'activité dynamique dans le spectre du primaire et adapter la transmission des utilisateurs secondaires pour une meilleure allocation des ressources spectrales. La détection spectrale aveugle et l'allocation des ressources pour la radio cognitive sont traitées dans cette thèse.

L'objectif de la première partie de cette thèse est de voir si la sélection des modèles ou l'estimation de la dimension spatiale du signal primaire ainsi que la théorie de l'information et les mesures de distance pourraient être utilisés pour améliorer les performances de détection du spectre d'une manière aveugle et dans des zones à faible rapport signal à bruit. Grâce à un effort de recherche approfondie, deux nouvelles méthodes de détection basées sur l'analyse de la distribution et l'estimation de la dimension du signal primaire reçu ont été proposées et analysées. En outre, nous avons dérivé des expressions théoriques de la probabilité de fausse alarme pour un seuil donné pour les deux détecteurs. Les performances de détection des deux techniques proposées en comparaison avec quelques détecteurs de référence sont évaluées. Ces performances sont également évaluées en appliquant les détecteurs à des signaux réels captés par la plate-forme d'EURECOM. Les simulations montrent des résultats encourageants en termes de détection des trous dans le spectre du primaire ainsi la détection binaire de la présence de l'utilisateur primaire. Une analyse sur l'application des deux techniques proposées en communication coopérative pour les réseaux radio cognitive est présentée également.

Dans la deuxième partie de cette thèse nous adressons le problème d'allocation de ressources dans le contexte des réseaux radio cognitive et nous présentons et analysons deux stratégies de sélection d'utilisateurs secondaires basées sur la probabilité outage pour gérer la qualité de service du système. La première stratégie explore l'idée de combiner la diversité des gains multiutilisateurs avec des techniques de partage spectrale pour essayer de maximiser la somme des capacités des utilisateurs secondaires tout en maintenant la probabilité outage de l'utilisateur primaire non dégradée d'une manière distribuée. La deuxième stratégie traite le problème de beamforming pour minimiser l'interférence dans le contexte de la radio cognitive pour un système d'utilisateurs secondaires MIMO et propose une méthode de sélection d'utilisateurs basée sur la probabilité outage. Dans l'algorithme proposé, les utilisateurs secondaires sont d'abord présélectionnés pour maximiser la somme des capacités des utilisateurs secondaires sous réserve de minimiser les interférences mutuelles. Ensuite, le système radio cognitive vérifie la contrainte de probabilité outage pour garantir la qualité de service du système primaire. Les résultats théoriques et expérimentaux en utilisant des conditions réel, pour les deux stratégies proposées, montrent des gains de débit important, illustrant ainsi des caractéristiques intéressantes en termes de déploiement du réseau radio cognitive, tout en garantissant une qualité du service pour le système primaire et secondaire.

Acknowledgements

I am indebted to many people for their guidance and support of any form, leading to the completion of this thesis.

I would like first to thank Dr. Aawatif Hayar, my supervisor, for offering me the opportunity to pursue my doctoral studies at EURECOM, for her insightful guidance, and for being available whenever I needed her support.

I would also like to thank my thesis jury members, Prof. Dirk Slock, Prof. Guevara Noubir, Prof. Constantinos Papadias, Prof. Slim Alouini, and Prof. Mischa Dohler for their time, interest, and helpful comments.

I would like also to extend my thanks to our Department Head Prof. Christian Bonnet, to the secretaries, and to all my colleagues and friends at EURECOM for the excellent and truly enjoyable ambiance. My warmest thanks extend to my dear friends, in France, back in Tunisia and in many other corners of the globe, for all the unforgettable moments I shared with them over the past years.

Finally, I want to express my gratitude to my family for their unconditional love, support, and encouragement. I would never thank enough my father Moncef and my mother Jalila for their love, trust, and support. Thank you for bringing so much sincere love and happiness to my life.

Table of Contents

List of Figures

List of Tables

Acronyms

Here are the main acronyms used in this document. The meaning of an acronym is usually indicated once, when it first occurs in the text. The English acronyms are also used for the French summary.

AD	Autocorrelation Detector
AIC	Akaike Information Criterion
AWGN	Additive White Gaussian Noise
BER	Bit Error Rate
BS	Base Station
CD	Cyclostationary Detector
CDF	Cumulative Density Function
CFAR	Constant False Alarm Rate
CH	Cluster Head
CR	Cognitive Radio
CRN	Cognitive Radio Network
CSI	Channel State Information
DAD	Distribution Analysis Detector
DC	Digital Convertor
DED	Dimension Estimation Detector
DED-AIC	Dimension Estimation Detector using Akaike Information Criterion
DED-MDL	Dimension Estimation Detector using Minimum Description Length
ED	Energy Detector
DFT	Discrete Fourier Transform
DoF	Degrees of Freedom
DVB-T	Digital Video Broadcast-Terrestrial
ETSI	European Telecommunications Standards Institute
FC	Fusion Centre
FCC	Federal Communications Commission
FFT	Fast Fourier Transform
FPGA	Field Programmable Gate Array
GLRT	Generalized Likelihood Ratio Test
GSM	Global System for Mobile communications
GUI	Graphical User Interface
i.i.d.	independent and identically distributed
IDFT	Inverse Discrete Fourier Transform
KL	Kullback-Leibler
KLD	Kullback-Leibler Detector
LHS	Left-Hand-Side

LOS	Line-Of-Sight
LTE	Long Term Evolution
MDL	Minimum Description Length
MIMO	Multiple-Input Multiple-Output
MLE	Maximum Likelihood Estimator
MMED	Maximum-Minimum Eigenvalue Detection
NLOS	Non-Line-Of-Sight
NTIA	National Telecommunications and Information Administration
OFDM	Orthogonal Frequency Division Multiplexing
OFDMA	Orthogonal Frequency Division Mutiple Access
PHY	PHYsical
PSD	Power Spectral Density
PU	Primary User
QoS	Quality of Service
RF	Radio Frequency
RHS	Right-Hand-Side
ROC	Receiver Operating Characteristics
RTOS	Real-Time Operating System
SE	Significant Eigenvalue
SINR	Signal-to-Interference-plus-Noise Ratio
SIR	Signal-to-Interference Ratio
SN	Sensor Network
SNR	Signal-to-Noise Ratio
SU	Secondary User
TTI	Transmission Time Interval
UMTS	Universal Mobile Telecommunications System
UWB	Ultra-Wide Band
WiMAX	Worldwide Interoperability for Microwave Access
WRAN	Wireless Regional Area Network

Introduction

Motivation

The discrepancy between current-day spectrum allocation and spectrum use suggests that radio spectrum shortage could be overcome by allowing a more flexible usage of the spectrum. Flexibility would mean that radios could find and adapt to any immediate local spectrum availability. A new class of radios that is able to reliably sense the spectral environment over a wide bandwidth detects the presence/absence of legacy users (*primary users*) and uses the spectrum only if the communication does not interfere with primary users (PUs). It is defined by the term *cognitive radio* [1] [2] [3]. Cognitive Radio (CR) technology has attracted worldwide interest and is believed to be a promising candidate for future wireless communications in heterogeneous wideband environments.

The original definition of CR is wide, as it envisions the wireless node as a device with cognitive capabilities utilizing all available environmental parameters. According to [1], examples of parameters the CR can exploit are knowledge of time, user location, user preferences, knowledge of its own hardware and limitations, knowledge of the network and knowledge of other users in the network. This initial definition of CR is conceptual, and deviates somewhat from the common contemporary working definition of CR. A sub set of CR that has received a substantial amount of focus is the Spectrum Sensing and Resource Allocation for Cognitive Radio. This is a radio that dynamically monitors activity in its available electromagnetic spectrum and adapts its transmission to available spectral resources. The most common scenario is an unlicensed secondary user (SU) wishing to utilize idle parts of the spectrum when transmission from the licensed PU is absent. It has become a standard practice to simply use the wide term CR also when referring to limited sub definitions such as Spectrum Sensing or Resource Allocation for Cognitive Radio. This is for instance reflected in modern redefinitions. A typical example is this definition of CR from the U.S. National Telecommunications and Information Administration (NTIA) [4] :

> **Cognitive Radio** A radio or system that senses its operational electromagnetic environment and can dynamically and autonomously adjust its radio operating parameters to modify system operation, such as maximize throughput, mitigate interference, facilitate interoperability, access secondary markets.

This definition is a slight misnomer, since it only refers to a more limited adaptive radio, and not to the complete cognitive device, utilizing all available parameters from its environment, as presented by the pioneer Mitola in [1]. However, this redefinition of CR appears to have been widely adopted. To stick with this practice, the NTIA definition of CR will be the working definition in this thesis. But the reader should still be aware of the fact that the original concept of CR was coined around a concept where a complete set of environmental parameters, and not only spectral parameters, was considered. Therefore, the thesis is divided into two parts : Part I discusses the spectrum sensing topic and proposes two blind sensing schemes ; Part II investigates the resource

allocation subject and proposes two distributed and centralized resource allocation strategies.

The research was split in the following sections :

1. Analysis of the problem at hand to limit the scope.
2. Literature survey on background information and current techniques in spectrum sensing and resource allocation.
3. Analysis of a selection of the conventional approaches to identify problems for spectrum sensing and resource allocation.
4. Literature survey in the areas suggested in the problem outline. It was related to distribution and dimension analysis of a communication signal to decide on potential new blind spectrum sensing approaches.
5. Study when SUs are allowed to transmit simultaneously with the PU and maintaining a quality of service (QoS) for the PU using outage probability. Then investigation in new resource allocation strategies to provide a solution to the problem.
6. Proposing a novel spectrum sensing schemes and resource allocation strategies and providing insight through a theoretical analysis and simulations.

From the list above it becomes obvious that the research for both topics is divided in two main parts. The first part revolving around literature surveys and theoretical analysis, the second part being founded on computer aided simulation. All simulations have been performed utilizing the software package Matlab® R2009a.

Thesis [1] Objectives and Structure

As it has been presented in the motivation section, the CR research area is very open. A particularly problem in the context of CR, when we seek to optimize the secondary system capacity, is to guarantee a QoS to PUs. There is a large number of proposals for all communication layers treating the increase of restrictions to spectrum utilization [6], but the QoS issue still has not been clearly defined. In addition, it is unclear how secondary system opportunism is compatible with the support of QoS for both, CR systems and primary systems. The U.S. Federal Communications Commission (FCC) proposed the concept of "*interference temperature*" as a way to have unlicensed transmitters sharing licensed bands without causing harmful interference [7, 8]. Rather than merely regulate transmitter power at fixed levels, as it has been done in the past, the scheme would have governed transmitter power on a variable basis calculated to limit the energy at victim receivers, where interference actually occurs. As a practical matter, however, the FCC abandoned the interference temperature concept recently [9] due to the fact that it is not a workable concept. While offering attractive promises, CRs face various challenges, starting from defining the fundamental performance limits of this radio technology, in order to achieve the capability of using the spectrum in an opportunistic manner. Specifically, CR is required to detect spectrum holes in the spectrum band and to determine if the spectrum allocation meets the QoS requirements of different users. This decision can be made by assessing the channel capacity, known as the most important factor for spectrum characterization.

The purpose of the thesis is to present an analysis of the QoS problem along with a proposed solution, while maintaining a limited scope to provide coherency and depth. The QoS problem will be tackled in this thesis into two ways : Spectrum Sensing and Resource Allocation.

1. The work reported herein was partially supported by the European project SENDORA (SEnsor Network for Dynamic and cOgnitive Radio Access [5]) and the National project GRACE (Gestion de Spectre et Radio Cognitive).

Part I : Blind Spectrum Sensing Techniques

CR has been proposed as the means to promote efficient utilization of the spectrum by exploiting the existence of spectrum holes. The spectrum use is concentrated on certain portions of the spectrum while a significant amount of the spectrum remains unused. It is thus key for the development of CR to invent fast and highly robust ways of determining whether a frequency band is available or occupied. This is the area of spectrum sensing for CR which is the first study part in this thesis.

It is stated that current spectrum sensing techniques suffer from challenges in the low signal to noise range (SNR). The reasons for this have to be analyzed. It is suggested that higher order statistics or information theoretic criteria are possible areas to look for a solution to overcome the problem. It is apparent that the problem at hand is wide and challenging. To meet the outlined demands, it is important that the scope is limited to provide a tangible base for the thesis. In addition, blind detection of spectrum holes in the frequency band is a very challenging requirement. As the names imply, blind spectrum sensing algorithms make sensing decisions without any prior knowledge, whereas non-blind approaches utilize some form of a priori knowledge about the underlying signals. Typical known signal features can be modulation type, carrier frequency or pulse shape. Although the importance of blind sensing in the conception of CR devices, only few algorithms exist in the literature. The blind detection is the second challenge to be raised in this part of thesis.

Hence the first step in the research has been to analyze the problem and to decide on the correct approach. The first chapter gives a literature survey on background information and current techniques in spectrum sensing. This chapter analysis also a selection of the conventional approaches to identify problems in the low signal to noise region and to decide on a potential new approach. Alongside the presentation of the survey results, a simultaneous discussion of their relevance is given. A conclusion is made on results that were important enough to pursue further. Based on the findings from the literature survey, two novel detectors are proposed and analyzed.

Chapter 2 presents the first blind spectrum sensing technique based on distribution analysis of the PU received signal. The proposed detector tries to analyze the Kullback-Leibler distance between signal and noise distributions. It compares the distribution of the received signal with the Gaussian distribution. The idea is to decide if the distribution of the observed signal fits the Gaussian model. The proposed algorithm, called the distribution analysis detector (DAD), exploits Akaike weights information derived using Akaike information criterion (AIC) as a reliability index in order to decide if the distribution of the received signal fits the noise distribution or not [10, 11].

In Chapter 3 we propose the second blind sensing method based on the investigation of the dimension (entropy) of the received signal. Particularly we focus on analyzing the number of significant eigenvalues which are computed using the AIC criteria and the Minimum Description Length (MDL) criteria to conclude on the nature of the sensed band [11, 12]. Specifically, the slope change of the signal space dimension curve (from positive to negative trend) is representative of the transition from a vacant band to an occupied band (and vice versa). Based on these results we propose the dimension estimation detector (DED).

In the last two chapters the proposed novel detectors are compared with the reference detectors presented in Chapter 1 in terms of detection performance. Performance is mainly assessed through simulations utilizing synthetic signals, but also on an authentic real signal captured by the EURECOM RF Agile Platform in order to provide perspective and to strengthen the findings from the simulations. We performed the detection capacity of the DAD and DED detectors in terms of PU signal detection as well as of spectrum holes detection using sliding window technique even if the analyzed band is not synchronized with the PU signal band. We derives also closed-form expressions of false alarm probabilities for both detectors.

Part II : Resource Allocation Techniques

If the CR can successfully determine with a high degree of certainty that a specific part of the spectrum is idle, it can then transmit on these frequencies without interfering with the licensed owner of the spectrum and thus achieving a better spectral resource efficiency. Therefore, the CR protocol must adapt its signal to fill this void in the spectrum domain. Therefore, a SU device transmits over a certain time or frequency band only when no other user does. The requirement of no interference is extremely rigid to avoid disturbing licensed users. This is exactly the setup in the second part of this thesis where the CR behavior is generalized to allow SUs to transmit simultaneously with PU in the same frequency band. It can be done as long as the level of interference to PUs remains within an acceptable range. It is proposed in this thesis to combine CR with multi-user diversity technology to achieve strategic spectrum sharing and self-organizing communications.

Chapter 4 provides a summary of the approach chosen to attack the topic, and explains how the research was structured. This chapter starts by briefly introducing a number of theoretical concepts of importance to the following analysis. It is assumed that the reader is familiar with basic concepts from signal processing and communications. So the theory chapter will be structured more as a review of essential fundamental topics and a as brief introduction to peripheral topics where the reader might not be familiar with. A number of references providing further depth are provided. A big part of Chapter 4 provides the main findings from a thorough literature survey aimed at investigating the potential of centralized and distributed resource allocation techniques. Following this chapter an overview of the problem context is presented and a current centralized user selection solution that will act as a reference is described.

A starting point when trying to devise new user selection algorithms is to search for multi-user technologies where each user tries to manage its local resources (e.g. rate and power control, user scheduling). This search is based only on locally observable channel conditions such as the channel gain between the access point and a chosen user, and possibly locally measured noise and interference. This has been the main focus in Chapter 5 where we present a distributed user selection strategy based on outage probability. Specifically, we allow SUs to transmit simultaneously with the PU as long as the interference from the SUs to the PU that transmits on the same band remains within an acceptable range. We impose that SUs may transmit simultaneously with the PU as long as the PU in question does not have his QoS affected in terms of outage probability. We consider that PUs operate at a desired rate (depending on their respective QoS demands). Based on PU channel statistics, we determine the outage failure or in other words the probability that the PU of interest is actually under that rate. From a practical point of view the outage probability as well as the requested rate can be broadcasted before the start of the communication by the primary system, and it is used as a preamble for the PU to get informed which data rate is requested. This preamble can also be overheard by SUs who can then learn about these outage values. The proposed method guarantees also a certain QoS to SUs and ensures the continuity of service even when the detected spectrum holes become occupied by the PU, this is done by the outage probability control.

In Chapter 6 we adopt the same framework as in Chapter 5 by using the outage probability as protection constraint for the PU. We propose in this chapter a centralized user selection strategy combined with an efficient transmit beamforming technique using a multiuser SU system. The proposed strategy tries to maximize the system throughput and to satisfy the signal-to-interference-plus-noise ratio (SINR) constraint, as well as to limit interference to the PU. In the proposed user selection algorithm, SUs are first pre-selected to maximize the per-user sum capacity subject to minimize the mutual interference. Then, the CR system verifies the outage probability constraint

to guarantee QoS for the PU. Finally a number of SUs are selected from those pre-selected SUs. We also compare the results obtained by the proposed method to those obtained in Chapter 5.

Part I

Blind Spectrum Sensing Techniques

Chapter 1

Spectrum Sensing for Cognitive Radio Applications

1.1 Introduction

This chapter provides background material to understand the spectrum sensing problem and the results presented in this part of thesis. The concept of CR will be explained along with the principles of spectrum sensing. We will present also some topics in spectrum sensing that have been of great interest in recent research. We will especially focus on blind spectrum sensing, which is the area of concentration chosen for the presented research. Therefore, selected existing spectrum sensing algorithms will be introduced. Furthermore, we will describe some examples of feature spectrum sensing algorithms including the cyclostationarity based detector and the autocorrelation based detector, and examples of blind sensing algorithms including the energy detector, the maximum-minimum eigenvalue detector and the Kullback-Leibler based detector. These algorithms will serve as references when evaluating the novel approaches resulting from the research.

Apart from that, this chapter will provide a number of simulations aimed at assessing the performance of the presented reference detectors. They will be compared with the two proposed detectors in Chapter 2 and Chapter 3. Besides we will introduce the common simulation scenarios used to test the detection algorithms. Three different scenarios with different properties have been chosen to evaluate spectral detection performance. The reader is assumed to be familiar with common digital modulation and communication principles. All simulation scenarios follow the Monte Carlo principle, where detection results are obtained as the average of a number of simulations. For each iteration of the Monte Carlo simulation, a test statistic is computed on the basis of the signal samples in one block, and a binary decision is made by comparing the test statistic to a predetermined detection threshold.

The remaining chapter is organized as follows. We start by explaining some challenges associated with spectrum sensing in Section 1.2. Section 1.3 presents the spectrum sensing goal. We will show in Section 1.4 some examples of feature detectors, that exploit knowledge about the signal to be detected as well as blind sensing detectors. We will also give some fundamental limits for detection by presenting some simulation results using the three different scenarios and by studying the complexity required for sensing of each detector. In Section 1.5 we will show the concept of cooperative detection. Finally we provide a summary of the contributions of the thesis in Section 1.6.

1.2 Challenges

Before getting into the details of spectrum sensing techniques, some challenges associated with the spectrum sensing for CR are given in this section.

Sensing Time PUs can claim their frequency bands anytime while CR is operating in that band. In order to prevent interference to and from primary licence owners, CR should be able to identify the presence of PUs as quick as possible and should vacate the band immediately. Hence, sensing methods should be able to identify the presence of PUs within a certain duration. This requirement possesses a limit on the performance of sensing algorithms and creates a challenge for CR [13].

Complexity Sensing methods can also be compared from the implementation point of view by estimating the hardware cost and energy efficiency through computational complexity of the sensing algorithm. The complexity issue in the sensing algorithm design is, however, only partially resolved [13]. One aim of this thesis is to develop low-complexity sensing algorithms.

Cooperation Cooperation between the users affected by such effects improve sensing performance significantly [14]. When the CR is suffering from shadowing by a high building over the sensing channel, it definitely can not sense the presence of the PU appropriately due to the low received SNR. Therefore, CR accesses the channel in the presence of the PU. To address this issue, multiple CRs can be coordinated to perform spectrum sensing cooperatively. Several recent works have shown that cooperative spectrum sensing can greatly increase the probability of detection in fading channels [14].

Other Challenges Some other challenges that need to be considered while designing effective spectrum sensing algorithms include hardware requirements, presence of multiple SUs, coherence times, multi-path and shadowing, competition, robustness, heterogeneous propagation losses and power consumption [13].

Some challenges for spectrum sensing have been presented. The lack of a priori knowledge of the signal is limited to blind spectrum sensing. Robust performance in low signal to noise ratios and maintaining a low computational complexity are essential to both. The requirement for reliability and accuracy in the low SNR region is the most important in general. This is also the problem that will receive the main focus in this research.

1.3 Spectrum Sensing Goal

The CR concept proposes to furnish the radio systems with the abilities to measure and to be aware of parameters related to the availability of spectrum and the radio channel characteristics. The spectrum sensing radio system adopted in this work is given in details in this section. An example test scenario for the presented sensing algorithms is given in Figure 1.1. This scenario allows us to combine different PU signals with a variety of channel models and to generate a signal received by the sensor. Then suitable sensing algorithms can be applied and evaluated. A sensor network (SN) is deployed in the area to detect the spectrum usage in the corresponding frequency band. A sensing unit composed of sensor nodes has detection capabilities and communicates detection results to a fusion centre (FC) entity that aggregates the information coming from the sensing unit and that proposes an interface with global spectrum monitoring. A secondary network (base station (BS) and SUs), deployed in the area, takes advantage from this interface provided by the FC entity to perform communications in an opportunistic manner. If PU transmissions are detected

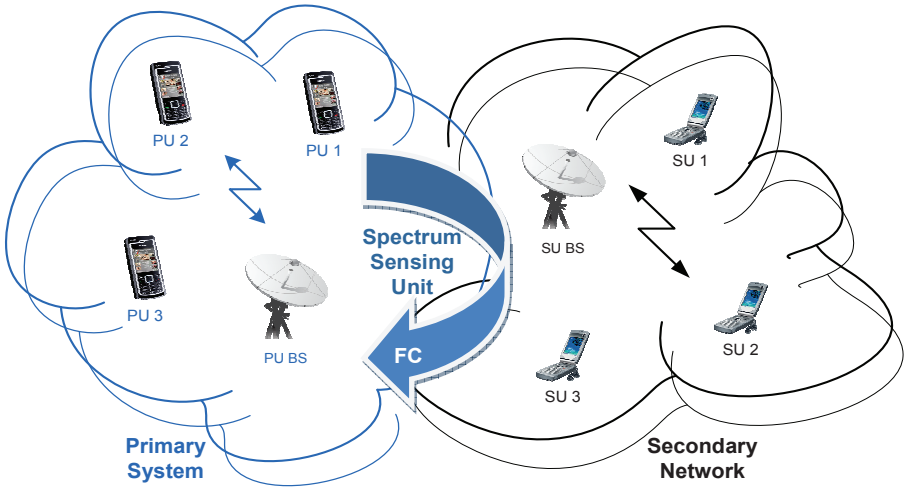

FIGURE 1.1 – An example of a wireless sensor network aided cognitive radio scenario : primary system, spectrum sensing unit and secondary network.

by the SN in the corresponding band, the FC shall receive the information and forward it to the SN. The SUs shall adapt their transmissions to avoid harmful interferences generated by the PUs.

The transmitted signal by one PU is convolved with a multi-path channel where Gaussian noise is added. The received signal at a sensor node, denoted by the $(q \times 1)$ complex vector $\mathbf{x}$ (also called *observation* in some chapters of this thesis), can be modeled as

$$\mathbf{x} = \mathbf{A}\mathbf{s} + \mathbf{n} \tag{1.1}$$

where $\mathbf{A}$ $(q \times p)$ complex matrix is the channel matrix whose columns are determined by the unknown parameters associated with each signal. $\mathbf{s}$ $(p \times 1)$ complex vector is a PU transmitted signal and $\mathbf{n}$ $(q \times 1)$ vector is a complex, stationary, and Gaussian noise with zero mean and covariance matrix $E\{\mathbf{n}\mathbf{n}^H\} = \sigma^2\mathbf{I}$.

The goal of spectrum sensing is to decide between the following two hypothesizes [2] [3] :

$$\mathbf{x} = \begin{cases} \mathbf{n} & \mathrm{H}_0 \\ \mathbf{A}\mathbf{s} + \mathbf{n} & \mathrm{H}_1 \end{cases} \tag{1.2}$$

We decide that a spectrum band is unoccupied if there is only noise, as defined in H_0. On the other hand, once there exists a PU signal besides noise in a specific band, as defined in H_1, we say that the band is occupied. Thus the probability of false alarm can be expressed as

$$P_{FA} = Pr(\mathrm{H}_1 \mid \mathrm{H}_0) = Pr(\mathbf{x} \text{ is present} \mid \mathrm{H}_0) \tag{1.3}$$

and the probability of detection is

$$\begin{aligned} P_D =& 1 - P_{MD} \\ =& 1 - Pr(\mathrm{H}_0 \mid \mathrm{H}_1) \\ =& 1 - Pr(\mathbf{x} \text{ is absent} \mid \mathrm{H}_1) \end{aligned} \tag{1.4}$$

where P_{MD} indicates the probability of a missed detection. The decision threshold is determined by using the required probability of false alarm P_{FA} given by (1.3). The threshold γ for a given false alarm probability is determined by solving the equation

$$P_{FA} = Pr(\Upsilon(\mathbf{x}) > \gamma | \mathrm{H}_0) \tag{1.5}$$

where $\Upsilon(\mathbf{x})$ denotes the test statistic for the given detector.

Based on the previously mentioned challenges and requirements, the spectrum sensing strategies can be broadly classified as *non-cooperative detection strategies* and *cooperative detection strategies*. Each of these strategies has its own advantages and disadvantages and is further elaborated in the following section. In this section, we will describe these spectrum sensing methods and we will discuss also the open research topics in this area.

1.4 Non-Cooperative Sensing

The non-cooperative detection strategies for spectrum sensing only rely on the local information from a secondary node that is actually sensing the spectrum. This information is only used by the node that does the sensing and is not shared among SUs. There are several non-cooperative spectrum sensing techniques that were proposed for CR. The non-cooperative sensing strategies are categorized in two families : feature detection strategies and blind detection strategies. In the following section we will describe the state of the art spectrum sensing algorithms and widely used representative methods in each of these categories.

1.4.1 Feature Detection Strategies

The feature detection approaches assume that a PU is transmitting information to a primary receiver when a SU is sensing the primary channel band. The elaboration of sensing techniques that use some prior information about the transmitted signal is interesting in terms of performance. In fact, feature detection algorithms employ knowledge of structural and statistical properties of PU signals when making the decision. Such properties include for example the cyclostationarity property, the autocorrelation property or the finite alphabet property.

1.4.1.1 Cyclostationarity Based Detection

The most known feature sensing technique is the CD [15]. Cyclostationary processes are random processes for which statistical properties such as mean and autocorrelation change periodically as a function of time. The theory of cyclostationarity is relevant to various fields like telecommunications, mechanics, biology, econometrics etc. [16]. For example, in mechanics, periodicity is due to gear rotation and in econometrics, it is due to seasonality. In telecommunications and radar applications periodicity is due to modulation, sampling, multiplexing and coding operations [16].

Wireless communication signals typically exhibit cyclostationarity at multiple cyclic frequencies that may be related to the carrier frequency, symbol, chip, code or hop rates, as well as their harmonics, sums and differences. These periodicities can be exploited to design powerful sensing algorithms for CRs. Cyclostationarity based detectors have the potential to distinguish among the PUs, SUs, and interference exhibiting cyclostationarity at different cyclic frequencies. Moreover, random noise commonly does not possess the cyclostationarity property. Cyclostationarity based detection has received a considerable amount of attention in the literature. Recent bibliography on cyclostationarity, including a large number of references on cyclostationarity based detection, is provided in [16].

The cyclic autocorrelation function at some lag l and some cyclic frequency α can be estimated from samples **x** by

$$\hat{r}_l(\mathbf{x},\alpha)=\frac{1}{p-l}\sum_{n=0}^{p-l-1} x_{n+l}x_n^* e^{-j\alpha n} \qquad l \geq 0 \tag{1.6}$$

where p is the length of the PU signal in samples. The cyclic autocorrelations are non-zero for cyclostationarity based PU. This property is exploited to detect a PU by testing whether the expected value of the estimated cyclic autocorrelation is zero or not. In [17], an optimum spectral correlation detector in stationary additive white Gaussian noise (AWGN) is presented. However, the scheme requires lot of information related to the PU like signal phase, modulation type and its parameters, such as carrier frequency, pulse shape and symbol rate, which makes the scheme impractical. In [18], authors have proposed a generalized likelihood ratio test (GLRT) for detecting the presence of a cyclic frequency with an asymptotic constant false alarm rate (CFAR). However, it may be desirable to test the presence of multiple cyclic frequencies to improve the detector performance. In [19], authors introduce a GLRT detector based on multiple cyclic frequencies, where the CFAR property is retained over the set of cyclic frequencies. It is particularly suitable for signals with multiple significant cyclic frequencies.

A GLRT may be obtained from the likelihood ratio test by replacing the unknown parameters with their maximum likelihood estimates. Assuming that **s** is cyclic with cycle frequency α,

$$\hat{\mathbf{r}}=[\text{Re}\left\{\hat{r}_{l_1}(\alpha)\right\},...,\text{Re}\left\{\hat{r}_{l_K}(\alpha)\right\},\text{Im}\left\{\hat{r}_{l_1}(\alpha)\right\},...,\text{Im}\left\{\hat{r}_{l_K}(\alpha)\right\}] \tag{1.7}$$

denotes a $1 \times 2K$ vector containing the real and imaginary parts of the estimated cyclic autocorrelations for K time delays at the cyclic frequency stacked in a single vector [18]. The GLRT statistic is given by [18]

$$\Upsilon_{CD}(\mathbf{x})=\hat{\mathbf{r}}\hat{\Sigma}^{-1}\hat{\mathbf{r}}^T \tag{1.8}$$

where $\hat{\Sigma}$ is an estimate of the covariance matrix $\Sigma \cong cov\left\{\hat{\mathbf{r}}\right\}$ [18].

To detect the cyclostationary over the received signal we make the choice of the statistical test proposed by Dandawate and Giannakis [15]. This test uses the asymptotic properties of the cyclic autocorrelation function estimates. It has been shown in [15] that under hypothesis H_0, regardless of the distribution of the input data, the distribution of $T(\mathbf{x})$ converges asymptotically to a central χ^2 distribution with $2p$ degrees of freedom where p is an integer with $p \geq 1$. This makes it possible to analytically calculate the probability of false alarm for a large enough observation length T for a given threshold. This leads to an asymptotically constant false alarm rate test. Under H_0, one can write :

$$\lim_{T\to\infty} \Upsilon_{CD}(\mathbf{x})=\chi^2_{2p} \tag{1.9}$$

Hence, the (asymptotic) probability of false alarm for this detector with threshold γ_{CD} is given by

$$P_{FA,CD}=1-G\left(\frac{\gamma_{CD}}{2},K\right) \tag{1.10}$$

where $G(.)$ is the (lower) incomplete gamma function [20].

The main advantage of the cyclic autocorrelation function is that it differentiates the noise energy from the modulated signal energy. Therefore, a CD can perform better than other detectors in discriminating against noise due to its robustness to the uncertainty in noise power. However, it is computationally complex and requires a significantly long observation time.

1.4.1.2 Autocorrelation Based Detection

Many communication signals contain redundancy, introduced for example to facilitate synchronization, by channel coding or to circumvent inter-symbol interference. This redundancy occurs as non-zero average autocorrelation at some time lag l. Based on the system model given in Section 1.3, the autocorrelation function at some lag l can be estimated from :

$$\hat{r}_l(\mathbf{x}) = \frac{1}{p-l} \sum_{n=0}^{p-l-1} x_{n+l} x_n^* \qquad l \geq 0 \tag{1.11}$$

Any signal except for the white noise case will have values of the autocorrelation function different from zero at some lags larger than zero. Although some might be exactly zero depending on the zero crossings. In practice, this simplistic view will be obscured by the fact that we have to estimate the autocorrelation function locally on stochastic signals and noise. This will inevitably generate spurious values that are not accounted above. The autocorrelation function is proportional to the received signal variance and its use in spectral sensing is therefore also dependent on either knowing the variance of the noise without signal or deriving reliable estimates of the variance based on long signal observations. If we assume that the noise level is constant, then the observed variance of the received signal is lower bounded by the noise itself. Several options for deriving the noise variance or some average received signal variance are open.

In [21], authors have proposed an autocorrelation-based detector for orthogonal frequency division multiplexing (OFDM) signals. OFDM has developed into a popular scheme for wideband digital wireless. This detector is limited to the case when the PU is using OFDM. Another autocorrelation-based detector was proposed in [22]. This detector relies on the fact that the autocorrelation function of the oversampled communication signal exhibits non-zero values at non-zero lags, whereas for the white noise (i.e., no signal) these values will be zero. We present in this section a summary of the autocorrelation-based detector given in [22].

To detect the existence/non existence of a signal we use functions of the autocorrelation lags where the autocorrelation is based on (1.11). Therefore, the autocorrelation-based decision statistic is given by [22]

$$\Upsilon_{AD}(\mathbf{x}) = \sum_{l=1}^{L} w_l \frac{\mathrm{Re}\left\{\hat{r}_l\right\}}{\hat{r}_0} \tag{1.12}$$

where the number of lags, L, is selected to be an odd number. The weighting coefficients w_l could be computed to achieve the optimal performance. They are given by

$$w_l = \frac{L+1+|l|}{L+1} \tag{1.13}$$

With decision threshold γ_{AD}, the probability of false alarm of this detector is

$$P_{FA,AD} = Q\left(\gamma_{AD}\left[\frac{\gamma_{AD}^2}{p} + \frac{1}{2p}\sum_{l=1}^{L} w_l^2\right]^{-\frac{1}{2}}\right) \tag{1.14}$$

where Q is the generalized Marcum Q-function [20].

1.4.1.3 Other Feature Sensing Methods

Other feature spectrum sensing methods include matched filtering and multitaper spectral estimation. Matched filtering is known as the optimum method for detection of PUs when the transmitted signal is known [23]. The main advantage of matched filtering is the short time to achieve a certain probability of false alarm or probability of a miss detection [24] as compared to other methods that are discussed in this section. However, matched filtering requires the CR to demodulate received signals. Hence, it requires knowledge of the PUs signaling features such as bandwidth, operating frequency, modulation type and order, pulse shaping, frame format, etc. Multitaper spectral estimation is proposed in [25]. The proposed algorithm is shown to be an approximation to maximum likelihood power spectral density (PSD) estimation. For wideband signals it is nearly optimal. Although the complexity of this method is less than the maximum likelihood estimator, it is still computationally demanding.

1.4.2 Blind Detection Strategies

Completely blind spectrum sensing techniques that do not consider any prior knowledge about the PU transmitted signal are more convenient to CR. A few methods that belong to this category have been proposed, but all of them suffer from the noise uncertainty and fading channels variations.

1.4.2.1 Energy Detection

One of the most popular blind detectors is the energy detector (ED) [26]. This detector is the most common method for spectrum sensing because of its non-coherency and low complexity.

Conventional energy detectors can be simply implemented like spectrum analyzers. The energy detector measures the received energy during a finite time interval and compares it to a predetermined threshold. The test statistic of the energy detector is

$$\Upsilon_{ED}(\mathbf{x}) = \sum_{i=1}^{p} |x_i|^2 \tag{1.15}$$

The performance of the energy detector in AWGN is well known and can be written in closed form. The probability of false alarm is given by

$$P_{FA,ED}=1 - G\left(\frac{2\gamma_{ED}}{\sigma^2}, p\right) \tag{1.16}$$

where G denotes the cumulative distribution function [20] of a χ^2 distributed random variable with $2p$ degrees of freedom. γ_{ED} is the detection threshold of the ED and σ^2 is the noise variance [26].

The energy detector is universal in the sense that it does not require any knowledge about the signal to be detected. On the other hand, for the same reason it does not exploit any potentially available knowledge about the signal. Moreover, the noise power needs to be known to set the decision threshold and to control the false alarm probability. It is very common that the noise power levels vary depending on time and locations. Consequently, there may be a need to estimate the noise power from a signal-free data set in order to obtain a constant false alarm probability detector performance.

1.4.2.2 Model Selection Based Detection

Sub Space Analysis Based Detection One of the main contributions in this work is the investigation of the sub space analysis in spectrum sensing. We propose in this context the dimension estimation detector (DED) which will be presented and analyzed in Chapter 3. This detector exploits the sub space analysis of the PU received signal using AIC and MDL criteria as model selection tools [27] [11]. The same idea was applied in [28] and [29], published after our work, to develop two spectrum sensing algorithms exploiting the maximum or/and the minimum eigenvalue as detection rule. However, in [28] and [29], the model selection has not been considered. This work will be presented in Subsection 1.4.2.3.

Distribution Analysis Based Detection The second contribution in this part is the distribution analysis detector (DAD). To develop the DAD detector, we will compute the Kullback-Leibler distance between signal and noise distributions using AIC criteria and Akaike weight as model selection tools. Chapter 2 will describe this detector.

Kullback-Leibler Based Detection [1] The Kullback-Leibler detector (KLD) was developed for comparison with the DAD detector. Note that, this work in under progress and the simulation results which will be presented later are a preliminary step for this idea. We will give in this subsection the basic idea of this detector and the work done until now.

The Kullback-Leibler (KL) divergence, or relative entropy, is a measure of the distance between two probability distributions. The KL divergence between the two continuous probability density functions $f(x)$ and $g(x)$ is defined as

$$D(f||g)=E\left[\log\frac{f(x)}{g(x)}\right] \tag{1.17}$$

where the expectation is taken with respect to f. $D(f||g)$ is only finite if the support set of f is contained in the support set of g. Another important property of the KL divergence is that it is non negative and in general non-symmetric.

The literature surveys in the two papers [30] and [31] were good references for more elaborate KL divergence estimators. [30] suggests estimating the characteristic function of a normalized version of the input signal, composing a toeplitz matrix of the characteristic function, computing its eigenvalues and using these eigenvalues to estimate the KL divergence. The estimation procedure is founded in the relationship between the sum of the eigenvalues of an autocorrelation matrix and the integral of the spectrum given by Szego's theorem. [31] presents a completely different approach. The algorithm given suggests estimating the KL divergence between two distributions through estimating their cumulative density functions. The analysis and ideas presented in the paper are thorough and consistent, and the author implies that the estimation variance of the algorithm only scales with the number of input samples.

The proposed algorithm depending on estimating the KL divergence is given on closed form as [31]

$$\Upsilon_{KLD}(\mathbf{x}) = D(f||g)=-\kappa-\frac{1}{p}\sum_{i=1}^{p}\ln\left(p\Delta G(x_i)\right) \tag{1.18}$$

1. This work is a collaboration between our team in EURECOM and the Norwegian university of science and technology (NTNU) team. Acknowledgements to Professor Tor Audun Ramstad at NTNU and Jorgen Berle Christiansen mastere student at NTNU for the collaboration we had.

where $\kappa = 0.577215$ is the Euler-Mascheroni constant, p is the number of input samples, $\Delta G(xi) = G(x_i) - G(x_i - 1)$ and G denotes the CDF such that $g(x) = G'(x)$. The probability of false alarm for a given detection threshold is given as

$$P_{FA,KLD}{=}Q\left(\sqrt{\frac{p}{\pi^2/6-1}}\gamma_{KLD}\right) \tag{1.19}$$

where $Q(.)$ denotes the cumulative distribution function [20] of a χ^2 distributed random variable with $2p$ degrees of freedom.

1.4.2.3 Maximum-Minimum Eigenvalue Based Detection

In [28] and [29], two sensing algorithms are suggested. One is based on the ratio of the maximum eigenvalue to the minimum eigenvalue, the other is based on the ratio of the average eigenvalue to the minimum eigenvalue. It is assumed that the signal to be detected is highly correlated. Let **R** be the covariance matrix of the received signal. Then, under H_0, all eigenvalues of **R** are equal. However, under H_1 some eigenvalues of **R** will be larger than others. A detector exploiting this property is called maximum-minimum eigenvalue detector (MMED) and was proposed in [28]. It will be described briefly in the context of this section. Considering N observations $\mathbf{x}_n$ received in a sequence, the sample covariance matrix can be defined as

$$\hat{\mathbf{R}}{=}\frac{1}{N}\sum_{n=1}^{N}\mathbf{x}_n\mathbf{x}_n^T \tag{1.20}$$

Let $\lambda_n|_{n=1,\ldots,N}$ be the eigenvalues of **R**. There are two eigenvalue-based detectors proposed in [28]. The first detector uses the ratio of the largest eigenvalue to the smallest eigenvalue and compares it to a threshold. So the test statistic of the first proposal of [28] is based on a condition number

$$\Upsilon_{MMED}(\mathbf{x}){=}\frac{\max\lambda_n}{\min\lambda_n} \tag{1.21}$$

The probability of false alarm of the MMED is given by

$$P_{FA,MMED}{=}1-F_1\left(\frac{\gamma_{MMED}\left(\sqrt{N}-\sqrt{p}\right)^2-\left(\sqrt{N-1}-\sqrt{p}\right)^2}{\left(\sqrt{N-1}-\sqrt{p}\right)\left(\frac{1}{\sqrt{N-1}}+\frac{1}{\sqrt{p}}\right)^{\frac{1}{3}}}\right) \tag{1.22}$$

where F_1 is the cumulative distribution function (CDF) of the Tracy-Widom distribution of order 1, N is the number of PU observations and p is the length of each observation. The distribution function is defined as

$$F_1{=}\exp\left(-\frac{1}{2}\int_t^\infty\left(q(u)+(u-t)q^2(u)\right)du\right) \tag{1.23}$$

where $q(u)$ is the solution of the nonlinear Painleve II differential equation

$$q"(u){=}uq(u)+2q^3(u) \tag{1.24}$$

With the above expressions for the probability of false alarm, the expected detection performance can be evaluated. In [32] the authors propose a research perspective of the MMED considering a finite number of cooperative receivers and a finite number of samples. They calculate in this paper the exact decision threshold as a function of the desired probability of false alarm for the MMED detector.

Bandwidth	8MHz
Mode	2K
Guard interval	1/4
Channel models	Rayleigh/Rician (K=1)
Maximum Doppler shift	100Hz
Frequency-flat	Single path
Sensing time	1.25ms
Location variability	10dB

TABLE 1.1 – The transmitted DVB-T primary user signal parameters

1.4.2.4 Other Blind Sensing Methods

Another blind technique called multi resolution sensing was proposed in [33]. This technique produces a multi resolution PSD estimate using a tunable wavelet filter that can change its center frequency and its bandwidth [34]. In [35], wavelets are used for detecting PU signals in blind manner. The wavelet based approach is efficiently used for wideband spectrum sensing where a wideband signal spectrum is decomposed into elementary building blocks of sub-bands that are well characterized by local irregularities in frequency [35]. The wavelet transform is then employed in order to detect and to estimate the local spectral irregular structure that carries important information about the frequency location and power spectral densities of the sub-bands. Others methods that exploit a recorded form of the covariance matrix are also derived in the literature [36].

1.4.3 Summary of Presented Methods and Simulations

Actual sensing results and performance studies will be provided in this subsection. The primary system used is a DVB-T system. Its communications are considered as PU communications. DVB-T abbreviates Digital Television Broadcast - Terrestrial, and as the name implies it is a standard for wireless digital transmission of TV signals. The standard is administered by the European Telecommunications Standards Institute (ETSI). The official ETSI web page can be found at [37]. The choice of the DVB-T primary user system is justified by the fact that most of the primary user systems utilize the OFDM modulation format. The channel models implemented are AWGN, Rician and Rayleigh channels. The latter two correspond to the two different types of propagation that have to be handled in practice, namely line-of-sight (LOS) and Non-line-of-sight (NLOS). Slow fading is simulated by adding log-normal shadowing. The simulation scenarios are generated by using different combinations of parameters given in Table 1.1. The evaluation framework for all simulations has been implemented in Matlab®.

Three different scenarios with different properties have been chosen to evaluate the spectral detection performance. It is assumed that the reader is familiar with common theoretical concepts. Results presented in this part are obtained as the average of a number of Monte Carlo simulations. For the Monte Carlo simulation, each signal block consists of one symbol which contains 2048 samples. 500 iterations are performed in the simulation. The threshold is computed for the detectors to have a probability of false alarm $P_{FA} = 0.05$.

OFDM is the modulation of choice for the three simulation scenarios to be used as evaluation tools in this report. In OFDM, a wideband channel is divided into a set of narrowband orthogonal subchannels. OFDM modulation is implemented through digital signal processing via to the FFT algorithm [38].

Scenario 1 : OFDM signal in AWGN channel We consider here a DVB-T OFDM signal in an AWGN channel. It is assumed that the detection performance in AWGN will provide a good impression of the performance, but it is necessary to extend the simulations to include signal distortion due to multipath and shadow fading.

Scenario 2 : OFDM signal in Rayleigh multipath fading with shadowing This scenario utilizes the same DVB-T OFDM signal as scenario 1, but to make the simulations more realistic, the signal is subjected to Rayleigh multipath fading and shadowing following a log normal distribution in addition to the AWGN. The maximum Doppler shift of the channel is 100Hz and the standard deviation for the log normal shadowing is 10dB. Since the fading causes the channel to be time variant, it is necessary to apply longer averaging than in scenario 1 to obtain good simulation results. Thus the number of iterations in the Monte Carlo simulation is increased from 500 to 1000.

Scenario 3 : OFDM signal in Rician multipath fading with shadowing The third simulation scenario utilizes also a DVB-T OFDM signal in Rician multipath fading with shadowing. The K-factor for the Rician fading is 10, which represents a very strong line of sight component. The maximum Doppler shift of the channel and the standard deviation for the log normal shadowing are the same as in the second scenario.

Simulations are important in assessing the performance of the presented spectrum sensing algorithms. The three scenarios provide different attributes so that the performance can be assessed under different conditions, providing fair conditions before making conclusions. Figure 1.2 presents the detection performances of the presented detectors in the three proposed simulation scenarios. The simulations are split in two main parts. Part one presents the probability of detection versus SNR with a fixed $P_{FA} = 0.05$. Part two evaluates the algorithms in terms of receiver operating characteristics (ROC). In these simulations, the sensing time is set to $1.12ms$.

Figures 1.2 (a), (b) and (c) show the P_D versus SNR at a constant false alarm rate for the five sensing detectors (CD, AD, ED, MMED and KLD) in the three proposed scenarios. From these figures, we show that the ED has lost its detecting ability when decreasing the SNR. For sufficiently low SNR, robust detection becomes impossible. The same can be observed for the KLD. These results come from the fact that the theoretical analysis for the ED and KLD algorithms assume the noise variance to be known, and the underlying noise to have a perfect stationary Gaussian distribution. This assumption does not hold. In reality, the noise variance will usually not be completely stationary. The assumption about the distribution of the noise is also known to be weak. On the other hand, we find that if knowledge of signal parameters is provided, the CD and AD can still perform a high probability of detection. Since this group of detection algorithms requires a priori knowledge about the received signal, they are not blind and are therefore not directly relevant to the work presented in this thesis. The two proposed detectors in this thesis will be compared with the KLD and MMED as reference algorithms. In the following chapters we will show as well the difference between these detectors and the proposed ones. Results in Figures 1.2 (d), (e) and (f) present the ROC curves. All detectors work at a SNR $= -7$dB condition. From these curves we show that the CD and AD outperform the others detectors. These results confirm the ones presented in Figures 1.2 (a), (b) and (c).

Complexity of signal detection process is also a great concern for CR other than detection performance. Complexity terminology will be the asymptotic $O - notation$, which is standard when analyzing algorithms. For readers who are not familiar with this notation, it will be briefly introduced. The notation is used to describe an asymptotic upper bound and is defined as

$$O(g(n))=\{f(n) : \exists \text{ positive constants } c \text{ and } n_0 \text{ such that } 0 \leq f(n) \leq cg(n) \ \forall \ n \geq n_0\} \tag{1.25}$$

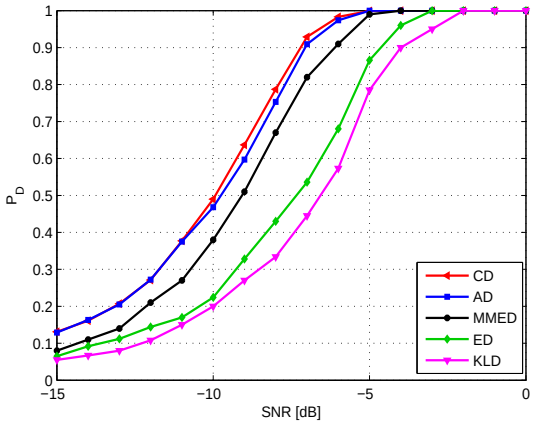

(a) P_D vs. SNR : Scenario 1

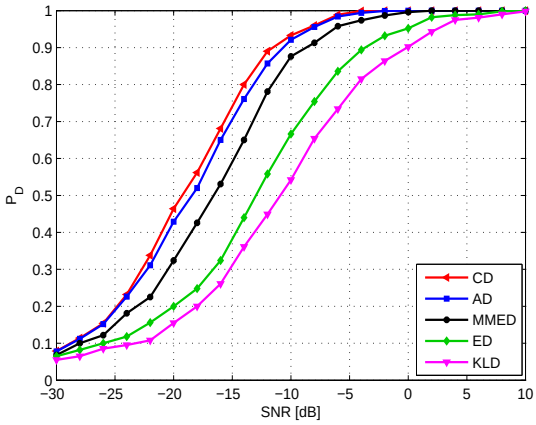

(b) P_D vs. SNR : Scenario 2

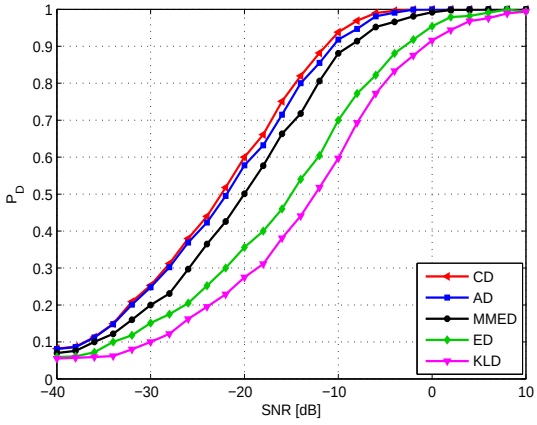

(c) P_D vs. SNR : Scenario 3

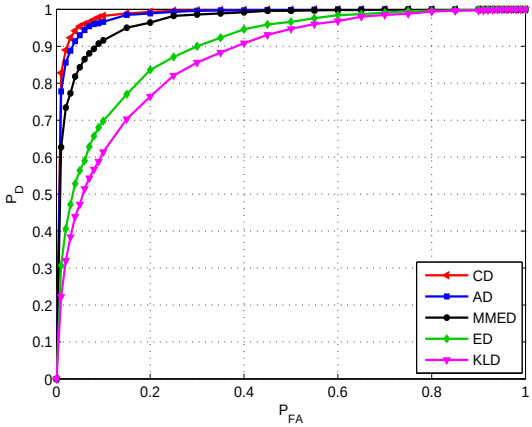

(d) ROC curves : Scenario 1

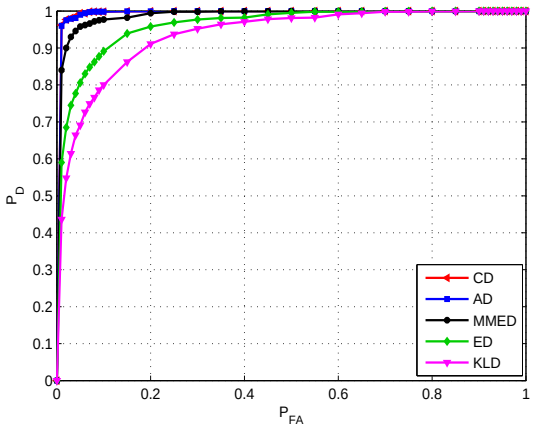

(e) ROC curves : Scenario 2

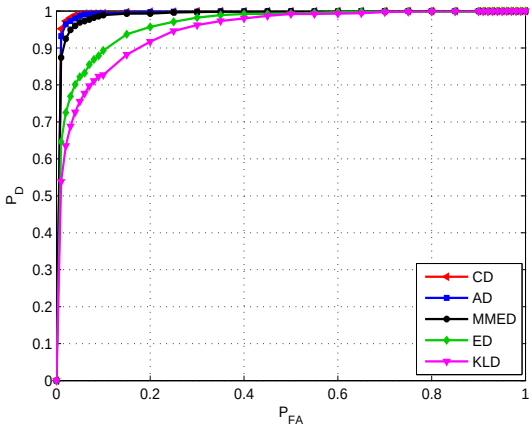

(f) ROC curves : Scenario 3

FIGURE 1.2 – Monte Carlo simulation results assessing detection performance of a number of spectrum sensing algorithms using an DVB-T OFDM primary user system : Probability of detection versus SNR curves with $P_{FA} = 0.05$ and ROC curves with SNR $= -7$dB and sensing time $= 1.12ms$.

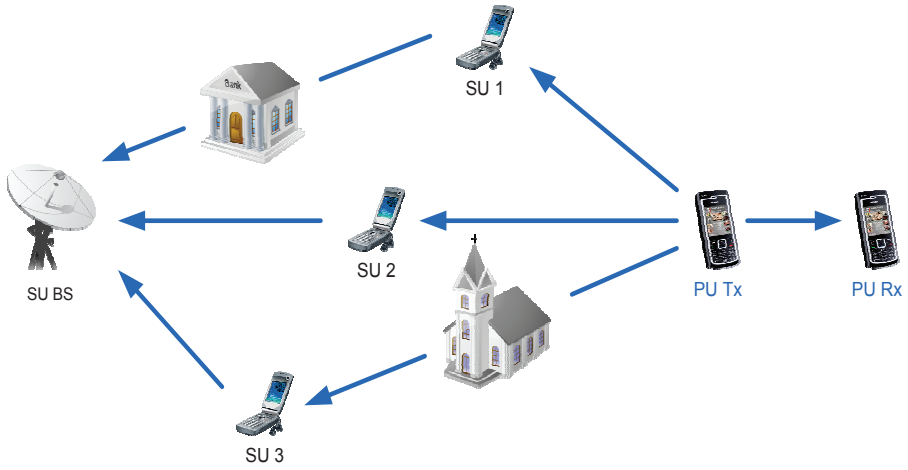

FIGURE 1.3 – Cooperative spectrum sensing in cognitive radio networks : SU 1 is shadowed over the reporting channel and SU 3 is shadowed over the sensing channel.

This definition is taken from [39]. This book is an excellent reference on algorithms and analysis of algorithms.

We summarize the number of multiplications required for each technique in Table 1.2. Note that p refers to the number of samples and N to the size of the covariance matrix (i.e. number of observations). From this table, we conclude that the CD, AD and MMED detectors are the most complex among all, while ED is the least complex among them. For more information about the complexity study of spectrum sensing methods see [40].

1.5 Cooperative Sensing

The estimation of traffic in a specific geographic area can be done locally (by one SU only). Alternatively information from different SUs can be combined. In the literature, cooperation is discussed as a solution to problems that arise in spectrum sensing due to noise uncertainty, fading and shadowing.

In Figure 1.3, SU 1 is shown to be shadowed by a high building over the sensing channel. In this case, the CR cannot reliably sense the presence of the PU due to the very low SNR of the received signal. Then, this CR assumes that the observed channel is vacant and begins to access this

Sensing Method	Complexity
CD	$p^2 + O(p\log(p))$
AD	$p + O(p\log(p))$
ED	p
MMED	$Np + O(N^3)$
KLD	$O(p)$

TABLE 1.2 – Complexity comparison of the different sensing techniques.

channel while the PU is still in operation. To address this issue, multiple SUs can be coordinated to perform spectrum sensing cooperatively.

The challenges of cooperative sensing include the development of efficient information sharing algorithms and increased complexity. Cooperative sensing decreases also the probability of misdetections and the probability of false alarms considerably. In addition, cooperation can solve the hidden PU problem and can decrease sensing time. It can also mitigate the multi-path fading and shadowing effects, which improve the detection probability. However, the cooperation causes adverse effects on resource-constrained networks due to the additional operations and overhead traffic. The advantages and disadvantages of local and cooperative sensing methods are tabulated in Table 1.3.

Cooperative sensing can be implemented in two fashions : *centralized* or *distributed*. These two methods will be explained in the following sections.

Centralized Sensing In centralized sensing, a central unit collects sensing information from SUs, identifies the available spectrum and broadcasts this information to other SUs or directly controls the CR traffic.

The binary sensing results are gathered at a central place which is known as access point [41]. The goal is to mitigate the fading effects of the channel and to increase detection performance. For the sensing algorithms presented in [41], the resulting detection and false alarm rates are given in [42]. In [43], the sensing results are combined in a central node, termed as master node, for detecting TV channels. Hard and soft information combining methods are investigated for reducing the probability of missed opportunity. The results presented in [43] show that soft information-combining outperforms hard information-combining method in terms of the probability of missed opportunity.

Distributed Sensing In the case of distributed sensing, cognitive nodes share information among each other but they make their own decisions when they have to determine which part of the spectrum they can use. Distributed sensing is more advantageous in the sense that there is no need for a backbone infrastructure.

A distributed collaboration algorithm is proposed in [41]. The collaboration is performed between two SUs. The user that is closer to primary transmitter has a better chance of detecting the PU transmission and cooperates with a user far away. An algorithm for pairing SUs without a centralized mechanism is also proposed. In [44], a distributed sensing method is proposed where SUs share their sensing information among themselves. Only final decisions are shared in order to minimize the network overhead due to collaboration.

In this work the cooperative spectrum sensing is performed as follows :

Step 1 Every SU performs local spectrum measurements independently and then makes a binary decision.

Sensing Method	**Advantages**	**Disadvantages**
Non-cooperative Sensing (Local sensing)	Computational and implementation simplicity	Hidden node problem Multipath and shadowing
Cooperative Sensing	Reduced sensing time Higher accuracy Mitigate the multi-path fading and shadowing effects	Traffic overhead The need for a control channel Additional operations

TABLE 1.3 – Local versus cooperative sensing.

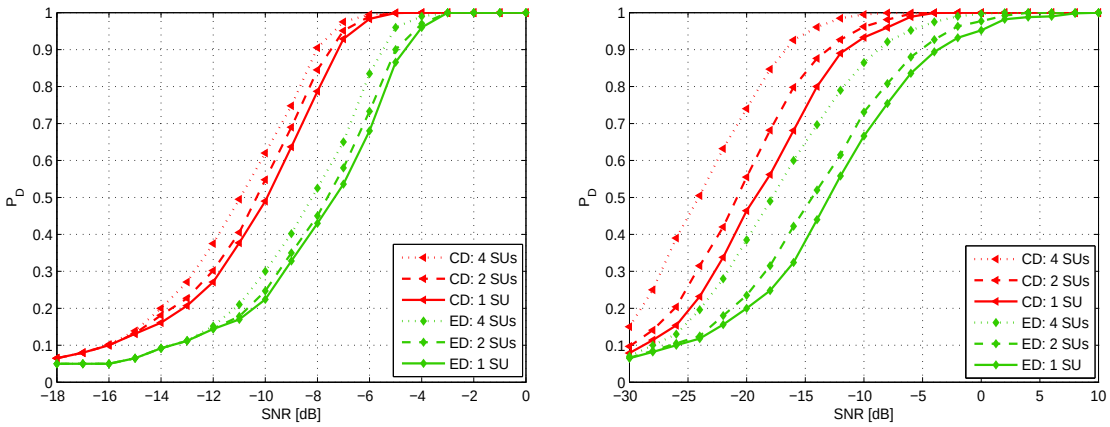

(a) Scenario 1 (b) Scenario 2

FIGURE 1.4 – Monte Carlo simulation results assessing detection performance of ED and CD algorithms in terms of PU signal detection in cooperative way using an DVB-T OFDM primary user signal in AWGN channel and Rayleigh multipath fading with shadowing channel : Probability of detection versus SNR curves with sensing time = $1.12ms$.

Step 2 All the SUs forward their binary decisions to a FC.

Step 3 The FC combines those binary decisions and makes a final decision to infer the absence or presence of the PU in the observed band.

In the above mentioned cooperative spectrum sensing algorithms, each cooperative partner makes a binary decision based on its local observation and then forwards one bit of the decision to the FC. At the FC, all one-bit decisions are fused together according to an ”OR” logic. This cooperative sensing algorithm is referred to as decision fusion.

Figure 1.4 shows the performance evaluation of ED and CD detectors in a cooperative way using scenario 1 and scenario 2. Remember that only on scenarios 2 we use a multipath fading with shadowing channel. From the presented results we show that the detection performance of the two detectors is improved as the number of cooperative users is increased especially in a heavily shadowed environment (scenario 2). These results prove that the two cooperative detection schemes allow to mitigate the multi-path fading and shadowing effects, which improves the detection probability.

1.6 Conclusion

This chapter presented the topic of spectrum sensing for CR and explained how spectrum sensing algorithms can be divided in the two groups of blind and feature algorithms. In addition, the chapter ended by providing a motivation for why only blind spectrum sensing is being investigated in this research. Some reference detectors have been presented. An intuitive explanation of the algorithms along with the important mathematical descriptions should provide the reader with a sound perspective of common blind and feature spectrum sensing algorithms. This is important as the two following chapters will start analyzing the problems with these algorithms in the low signal to noise ratio region, and will present two novel approaches that attempt to mitigate these problems.

Chapter 2

Distribution Analysis Based Detection

2.1 Introduction

Literature review in the last chapter shows that there are many proposed strategies and corresponding techniques to achieve efficient spectrum sensing under various conditions. In this chapter, we propose a blind sensing detector based on the distribution analysis of the PU received signal. This detector analysis the Kullback-Leibler distance between signal and noise distributions. We assume that the envelope of Gaussian noise can be modeled using Rayleigh distribution and the one of signal data can be modeled by Rician distribution. To develop the distribution analysis detector (DAD), we will exploit model selection tools like Akaike information criterion (AIC) and Akaike weights [10]. AIC criteria was first introduced by Akaike in [11] for model selection. It was shown in [11] that the classical maximum likelihood principle can be considered to be a method of asymptotic realization of an optimum estimate with respect to a very general information theoretic criterion [11]. This criterion was recently used in the literature to estimate the number of significant eigenvalues of the covariance matrix of a given observation vector [45]. The main goal within our contribution is to exploit Akaike weights information in order to decide if the distribution of the received signal fits the noise distribution. Therefore, the Akaike weights derived using AIC criterion are used as detection rule to decide on the best fit of the distribution of the received signal. The proposed detector will be compared with the ones presented in the previous chapter.

The flow of the chapter is as follows. In Section 2.2, we give a short review of the basic ideas of the model selection strategy and we formulate the AIC criterion, which will be used as a base to develop the DAD algorithm presented in this chapter, and the DED algorithm given in Chapter 3. Section 2.3 analyzes the Akaike weight information and Section 2.4 provides the motivation as to why the norm of the Gaussian noise can be modeled using Rayleigh distribution and the signal data can be modeled as a Rician distribution. In Section 2.5, we present the derivation of AIC and Akaike weight in our context. The detection algorithm will be developed in Section 2.6 and a theoretical probability of false alarm will be evaluated in Section 2.7. Performance evaluation and advantages of the proposed detector are described in Section 2.8 and a comparison with detectors presented in Chapter 1 is given. We present also in this section the complexity study of this sensing algorithm. To complete this study, we will perform in Section 2.9 a sensing demonstration based on the OpenAirInterface platform at EURECOM. The demonstration is composed of two nodes : a PU with a varying transmission gain and four possible carrier frequencies, and a SU implementing the DAD algorithm and the ED and CD algorithms, for comparison. The sensing results as well as their corresponding measured SNR over the four carrier frequencies are displayed in real time. Finally, Section 2.10 presents the conclusions of this study.

2.2 Model Selection Strategy

It is assumed that the samples of the received signal are distributed according to an original probability density function f, called the operating model. The operating model is usually unknown, since only a finite number of observations is available. Therefore, approximating probability model must be specified using the observed data, in order to estimate the operating model. The approximating model is denoted as g_θ, where the subscript θ indicates the U-dimensional parameter vector, which in turn specifies the probability density function. In information theory, the Kullback-Leibler distance describes the discrepancy between the two probability functions f and g_θ and is given by [11] :

$$\begin{aligned} D(f\|g_\theta) &= E\{\log f_X(X)\} - E\{\log g_\theta(X)\} \\ &= \int f_X(x)\log f_X(x)dx - \int f_X(x)\log g_\theta(x)dx \\ &= -h(X) - \int f_X(x)\log g_\theta(x)dx \end{aligned} \tag{2.1}$$

where the random variable X is distributed according to the original but unknown probability density function f, and $h(.)$ denotes differential entropy. This distance measure is not directly applicable, since the original probability density function f is not known. It is known, however, that the Kullback-Leibler distance is nonnegative, i.e., $D(f\|g_\theta) \geq 0$. This implies that the Kullback-Leibler discrepancy,

$$-\int f_X(x)\log g_\theta(x)dx = h(X) + D(f\|g_\theta) \tag{2.2}$$

approaches the differential entropy of X from above for increasing quality of the model g_θ. The differential entropy of X is reached if and only if $f = g_\theta$. Applying the weak law of large numbers, the second term in (2.2) can be approximated by averaging the log-likelihood values given the model over N independent observations $\mathbf{x}_1, \mathbf{x}_2, ..., \mathbf{x}_N$ according to :

$$-\int f_X(x)\log g_\theta(x)dx \approx -\frac{1}{N}\sum_{n=1}^{N} g_\theta(\mathbf{x}_n) \tag{2.3}$$

The log-likelihood depends on the estimated vector θ, which itself is a function of the actual observations $\mathbf{x}_1, \mathbf{x}_2, ..., \mathbf{x}_N$. If another set of observations $\tilde{\mathbf{x}}_1, \tilde{\mathbf{x}}_2, ..., \tilde{\mathbf{x}}_N$ is used, a different Kullback-Leibler discrepancy would be obtained. The expected Kullback-Leibler discrepancy is given by :

$$-E_\theta\left\{\int f_X(x)\log g_\theta(x)dx\right\} \tag{2.4}$$

where the expectation is taken with respect to the distribution of the estimated parameter vector θ. This expression (2.4) cannot be computed, but estimated.

The information theoretic criteria was first introduced by Akaike in [11] for model selection. Assuming a candidate model, the idea is to decide if the distribution of the observed signal fits the candidate model. The AIC criterion is an approximately unbiased estimator for (2.4) and is given by :

$$\text{AIC} = -2\sum_{n=1}^{N}\log g_{\hat{\theta}}(\mathbf{x}_n) + 2U \tag{2.5}$$

The parameter vector θ for each family should be estimated using the minimum discrepancy estimator $\hat{\theta}$, which minimizes the empirical discrepancy. This is the discrepancy between the approximating model and the model obtained by regarding the observations as the whole population. The maximum likelihood estimator is the minimum discrepancy estimator for the Kullback-Leibler discrepancy.

2.3 Model Selection Using Akaike Weight

In this section, we analyze the Akaike weight information introduced by Akaike in [10] and [11] in order to decide if the distribution of the received signal fits the suitable distribution or not. Consider a probability distribution parameterized by an unknown parameter θ, associated with either a known probability density function or a known probability mass function, denoted as f_θ. As a function of θ with $\mathbf{x}_1, \mathbf{x}_2, ..., \mathbf{x}_N$ fixed, the likelihood function is :

$$\begin{aligned} L(\theta) &= f_\theta(\mathbf{x}_1, \mathbf{x}_2, ..., \mathbf{x}_N) \\ &= \prod_{n=1}^{N} f_\theta(\mathbf{x}_n) \end{aligned} \tag{2.6}$$

Commonly, one assumes that the data drawn from a particular distribution are i.i.d. with unknown parameters. This considerably simplifies the problem because the log-likelihood can then be written as follows :

$$L(\theta) = \sum_{n=1}^{N} \log f_\theta(\mathbf{x}_n) \tag{2.7}$$

The maximum of this expression can then be found numerically using various optimization algorithms. The method of maximum likelihood estimates θ by finding the value of θ that maximizes $L(\theta)$. Maximum likelihood estimator (MLE) is one of the most used methods to estimate functions parameters. This contrasts with seeking an unbiased estimator of θ, which may not necessarily yield the MLE but which will yield a value that (on average) will neither tend to overestimate nor under-estimate the true value of θ. The maximum likelihood estimator may not be unique, or indeed may not even exist. The MLE of the parameters of θ is computed over a set of samples of length N. We assume that the samples are independent identically distributed (i.i.d.). The log-likelihood function $L^*(\theta)$ is given by :

$$L^*(\theta) = \sum_{n=1}^{N} \log g_\theta(\mathbf{x}_n) \tag{2.8}$$

Consequently, the MLE expression of θ in our case is :

$$\hat{\theta} = \arg_\theta \max \frac{1}{N} \sum_{n=1}^{N} \log g_\theta(\mathbf{x}_n) \tag{2.9}$$

The AIC is hence described by the following form :

$$\text{AIC} = -2L^*(\hat{\theta}) + 2U \tag{2.10}$$

where U indicates the dimension of the parameter vector θ.

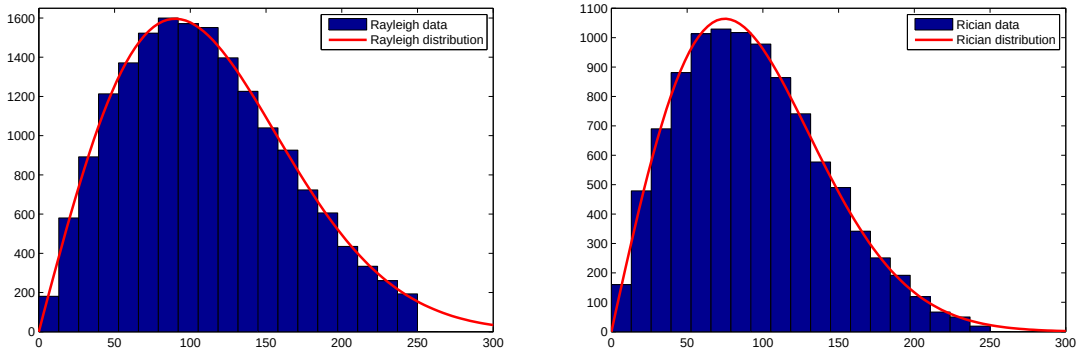

(a) Noise block (b) Data block

FIGURE 2.1 – Histogram of the envelope of a captured noise block and data block using an UMTS signal versus desired Rayleigh and Rician distribution computed analytically, respectively.

Akaike weights can be interpreted as estimate of the probabilities that the corresponding candidate distribution show the best modeling fit. It provides another measure of the strength of evidence for this model, and is given by :

$$\mathrm{W}_j = \frac{e^{-\frac{1}{2}\Phi_j}}{\sum_{i=1}^{N} e^{-\frac{1}{2}\Phi_i}} \tag{2.11}$$

for a given distribution j, where Φ_j denotes the AIC difference defined by :

$$\Phi_j = \mathrm{AIC}_j - \min_i \mathrm{AIC}_i \tag{2.12}$$

where $\min_i \mathrm{AIC}_i$ denotes the minimum AIC value over all PU signals observations.

2.4 Probability Distribution of a Communication Signal

The probability distribution of communication signals is of vital importance to the analysis for the DAD detector, as the research is aimed at finding distribution based methods to perform spectrum sensing in CR. It is hard to completely characterize such distributions due to the stochastic nature of many communication signals, however there are some common properties. In fact, recall that the distribution of a sum of independent random variables is the convolution of their distributions [46]. Hence, when the SNR is low, the noise distribution will dominate in the convolution and the resulting distribution will tend to become close to Gaussian even if the signal has an arbitrary non Gaussian distribution, and the envelope (norm) distribution of the signal is close to Rayleigh distribution [46]. This property is verified by Figure 2.1 (a) when we use a UMTS signal with low SNR. Another important property is the contribution of the dominant propagation paths on the distribution of the communication signal. The envelope distribution of the received communication signal tend to become close to Rician even if the input has a non Rician distribution [47] [23]. Figure 2.1 (b) plots the histogram of the envelope of data block samples using a UMTS signal compared with the desired Rician distribution computed analytically. We tested also other communication signal types (GSM, WiFi, DVB-T OFDM with different channel models, etc.), and we found similar results. Hence, for the proposed DAD detector, we assume that the norm of the Gaussian noise can be modeled using Rayleigh distribution and the signal data can be modeled as a Rician distribution.

Therefore, the operating model f (i.e. the original probability density function given in (2.2)) will be compared with Rice and Rayleigh probability density functions. In addition, the AIC equation is a function of Rice and Rayleigh distributions. As a first step, we proceed in this section to the derivation of parameter vector θ for both Rayleigh and Rice distribution.

Rayleigh distribution The probability density function for the Rayleigh distribution is given by :

$$g_{Rayleigh}(x \mid \sigma) = \frac{x}{\sigma^2} \exp\left(\frac{-x^2}{2\sigma^2}\right) \tag{2.13}$$

which leads to a log-likelihood function :

$$L^*_{Rayleigh}(\sigma) = \sum_{i=1}^{p} \log x_i - p \log \sigma^2 - \frac{1}{2\sigma^2} \sum_{i=1}^{p} x_i^2 \tag{2.14}$$

where the parameter $\theta = (\sigma)$. The MLE of the parameter σ is given by :

$$\hat{\sigma}^2 = \frac{1}{2p} \sum_{i=1}^{p} x_i^2 \tag{2.15}$$

Rice distribution The probability density function for the Rice distribution is given by :

$$g_{Rice}(x \mid v, \sigma) = \frac{x}{\sigma^2} \exp\left(\frac{-(x^2+v^2)}{2\sigma^2}\right) I_0\left(\frac{xv}{\sigma^2}\right) \tag{2.16}$$

where $I_0\left(\frac{xv}{\sigma^2}\right)$ is the modified Bessel function of the first kind with order zero. The approximated probability density function leads to the following log-likelihood function :

$$L^*_{Rice}(v, \sigma) = \log\left(\frac{\prod_{i=1}^{p} x_i}{\sigma^{2p}} \exp\left(-\frac{\sum_{i=1}^{p}\left(x_i^2+v^2\right)}{2\sigma^2}\right) \prod_{i=1}^{p} I_0\left(\frac{x_i v}{\sigma^2}\right)\right) \tag{2.17}$$

Parameters v and σ are given by the solution of the following set of equations [48] :

$$\begin{cases} v - \frac{1}{p}\sum_{i=1}^{p} x_i \frac{I_1\left(\frac{x_i v}{\sigma^2}\right)}{I_0\left(\frac{x_i v}{\sigma^2}\right)} = 0 \\ 2\sigma^2 + v^2 - \frac{1}{p}\sum_{i=1}^{p} x_i^2 = 0 \end{cases} \tag{2.18}$$

where $I_1\left(\frac{x_i v}{\sigma^2}\right) = -I_0\left(\frac{x_i v}{\sigma^2}\right) + \frac{\sigma^2}{2xv} I_0\left(\frac{x_i v}{\sigma^2}\right)$ is the modified Bessel function with order one. When $\frac{x_i v}{\sigma^2} \gg 0.25$ and $I_0\left(\frac{x_i v}{\sigma^2}\right) = \frac{exp\left(\frac{x_i v}{\sigma^2}\right)}{\sqrt{2\pi \frac{x_i v}{\sigma^2}}}$, (2.18) can be expressed as :

$$\begin{cases} v^2 + \frac{1}{p}\sum_{i=1}^{p} x_i v - \frac{\sigma^2}{2} = 0 \\ v^2 - \frac{1}{p}\sum_{i=1}^{p} x_i^2 + 2\sigma^2 = 0 \end{cases} \tag{2.19}$$

Resolving (2.19), the MLE for the parameters v and σ can be expressed as :

$$\hat{v} = \frac{-2\sum_{i=1}^{p} x_i + \sqrt{4\left(\sum_{i=1}^{p} x_i\right)^2 + 5p\sum_{i=1}^{p} x_i^2}}{5p} \tag{2.20}$$

$$\hat{\sigma}^2 = -\frac{1}{2}v^2 + \frac{1}{2p}\sum_{i=1}^{p} x_i^2 = -\frac{1}{2}\left(\frac{-2\sum_{i=1}^{p} x_i + \sqrt{4\left(\sum_{i=1}^{p} x_i\right)^2 + 5p\sum_{i=1}^{p} x_i^2}}{5p}\right)^2 + \frac{1}{2p}\sum_{i=1}^{p} x_i^2 \tag{2.21}$$

and the parameter vector $\theta = (\sigma, v)$.

2.5 Akaike Information Criteria and Akaike Weight Formulation

In this section, we present the derivation of AIC and Akaike weight in our context. In order to show the results of comparison between distributions in a clear manner, we introduce the Akaike weights W_{Rice} and $W_{Rayleigh}$ derived from AIC values [49]. Akaike weights for Rice and Rayleigh can be expressed as :

$$W_{Rice}=\frac{exp\left(-\frac{1}{2}\Phi_{Rice}\right)}{exp\left(-\frac{1}{2}\Phi_{Rice}\right)+exp\left(-\frac{1}{2}\Phi_{Rayleigh}\right)} \tag{2.22}$$

$$W_{Rayleigh}=\frac{exp\left(-\frac{1}{2}\Phi_{Rayleigh}\right)}{exp\left(-\frac{1}{2}\Phi_{Rayleigh}\right)+exp\left(-\frac{1}{2}\Phi_{Rice}\right)} \tag{2.23}$$

where

$$\Phi_{Rice}=\text{AIC}_{Rice}-\min\left(\text{AIC}_{Rice},\text{AIC}_{Rayleigh}\right) \tag{2.24}$$

$$\Phi_{Rayleigh}=\text{AIC}_{Rayleigh}-\min\left(\text{AIC}_{Rayleigh},\text{AIC}_{Rice}\right) \tag{2.25}$$

and

$$\text{AIC}_{Rice}=-2L_{Rice}+2U_{Rice} \tag{2.26}$$

$$\text{AIC}_{Rayleigh}=-2L_{Rayleigh}+2U_{Rayleigh} \tag{2.27}$$

where $U_{Rayleigh}=1$ and $U_{Rice}=2$.

2.6 Distribution Analysis Detector (DAD)

Sub-bands Detection The proposed method is based on the sliding window technique shown in Figure 2.2. As an example, we use in this figure a frame divided into nw sub-bands. In the first step, we select a sliding window size with T samples and slide the window over the spectral band to obtain AIC values for each analysis windows. A time-lag sliding window of L samples was used to scan all the signals. The size of the analyzed spectrum band and the number of the sliding windows are denoted by p and $nw=\frac{p}{T}$, respectively. Therefore, we choose the size of the observed window in order to estimate parameters θ for Rayleigh and Rice distributions. In the second step of the DAD detector, we compute the value of AIC and then Akaike weights for the two distributions. Once we get the corresponding Akaike weights, we shift the window by L samples till the end of the band. The Akaike weights allow us not only to decide if the distribution of the received signal fits the suitable distribution, but also provide information about the relative approximation quality of this distribution.

PU Signal Detection According to the proposed sliding window technique, the DAD detector can be formulated as a binary hypothesis test. If PU is present, the Akaike weight of Rician distribution is higher than Akaike weight of Rayleigh distribution, and if PU is absent, we have the opposite. Therefore, the generalized blind DAD algorithm is given by :

$$\Upsilon_{DAD}(\mathbf{x})=\begin{cases} W_{Rice}-W_{Rayleigh}<\gamma_{DAD} & \text{noise} \\ W_{Rice}-W_{Rayleigh}>\gamma_{DAD} & \text{signal} \end{cases} \tag{2.28}$$

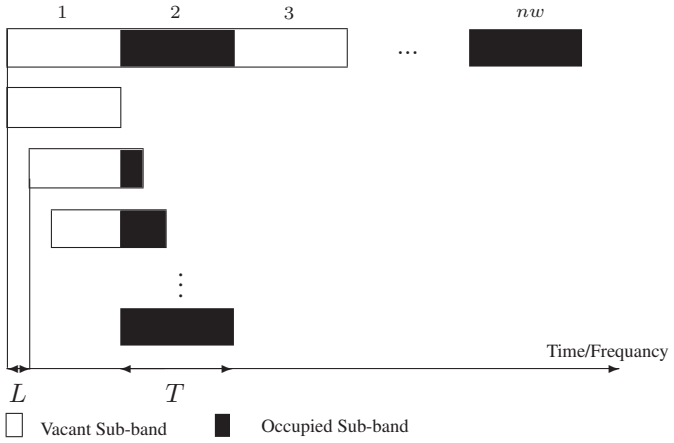

FIGURE 2.2 – Sliding window technique : We select a sliding window of size T samples and slide the window over the spectrum band to obtain AIC values and Akaike weight values for each analysis windows. A time-lag sliding window of L samples was used to scan all the frame.

According to the system requirement on $P_{FA,DAD}$, we calculate a proper threshold γ_{DAD}. If $\text{AIC}_{Rice} - \text{AIC}_{Rayleigh} > \gamma_{DAD}$, we declare that the PU is present, otherwise, we declare the PU is absent. The threshold expression depends only on $P_{FA,DAD}$ and is given in the following section.

2.7 DAD False Alarm Probability

Since spectrum sensing is actually a binary hypothesis test, the performance we focus on is the probability for identifying the signal when the PU is absent (the probability of false alarm $P_{FA,DAD}$). We will derive in this section a closed-form expression of $P_{FA,DAD}$. According to the sensing steps in Section 2.6, the false alarm occurs when the estimated decision $\Upsilon_{DAD}(\mathbf{x})$ is smaller than γ_{DAD} given that the PU is absent.

According to the presented sensing scheme, the false alarm probability for DAD detector can be expressed as

$$\begin{aligned} P_{FA,DAD} &= Pr\left(W_{Rice} - W_{Rayleigh} > \gamma_{DAD} | \mathrm{H}_0\right) \\ &= Pr\left(\frac{\exp\left(-\frac{1}{2}\Phi_{Rice}\right) - \exp\left(-\frac{1}{2}\Phi_{Rayleigh}\right)}{\exp\left(-\frac{1}{2}\Phi_{Rice}\right) + \exp\left(-\frac{1}{2}\Phi_{Rayleigh}\right)} > \gamma_{DAD} \middle| \mathrm{H}_0\right) \\ &= Pr\left(\frac{\exp\left(-\frac{1}{2}\text{AIC}_{Rice}\right) - \exp\left(-\frac{1}{2}\text{AIC}_{Rayleigh}\right)}{\exp\left(-\frac{1}{2}\text{AIC}_{Rice}\right) + \exp\left(-\frac{1}{2}\text{AIC}_{Rayleigh}\right)} > \gamma_{DAD} \middle| \mathrm{H}_0\right) \end{aligned} \tag{2.29}$$

According to AIC values for Rice and Rayleigh given in (2.26) and (2.27), we have

$$\begin{aligned} P_{FA,DAD} &= Pr\left(\frac{\exp\left(L_{Rice} - 1\right) - \exp\left(L_{Rayleigh}\right)}{\exp\left(L_{Rice} - 1\right) + \exp\left(L_{Rayleigh}\right)} > \gamma_{DAD} \middle| \mathrm{H}_0\right) \\ &= Pr\left(\frac{\exp\left(L_{Rice}\right) - e\exp\left(L_{Rayleigh}\right)}{\exp\left(L_{Rice}\right) + e\exp\left(L_{Rayleigh}\right)} > \gamma_{DAD} \middle| \mathrm{H}_0\right) \end{aligned} \tag{2.30}$$

where $e = \exp(1)$.

Using now (2.14) and (2.17), we obtain

$$P_{FA,DAD}=Pr\left(\frac{\frac{\prod_{i=1}^{p}x_i}{\sigma^{2p}}\exp\left(-\frac{\sum_{i=1}^{p}\left(x_i^2+v^2\right)}{2\sigma^2}\right)\prod_{i=1}^{p}I_0\left(\frac{x_iv}{\sigma^2}\right)-\frac{e\prod_{i=1}^{p}x_i}{\sigma^{2p}}\exp\left(-\frac{\sum_{i=1}^{p}x_i^2}{2\sigma^2}\right)}{\frac{\prod_{i=1}^{p}x_i}{\sigma^{2p}}\exp\left(-\frac{\sum_{i=1}^{p}\left(x_i^2+v^2\right)}{2\sigma^2}\right)\prod_{i=1}^{p}I_0\left(\frac{x_iv}{\sigma^2}\right)+\frac{e\prod_{i=1}^{p}x_i}{\sigma^{2p}}\exp\left(-\frac{\sum_{i=1}^{p}x_i^2}{\sigma^{2p}}\right)}>\gamma_{DAD}\middle|\mathrm{H}_0\right)$$

$$=Pr\left(\frac{e-\exp\left(-\frac{pv^2}{2\sigma^2}\right)\prod_{i=1}^{p}I_0\left(\frac{x_iv}{\sigma^2}\right)}{e+\exp\left(-\frac{pv^2}{2\sigma^2}\right)\prod_{i=1}^{p}I_0\left(\frac{x_iv}{\sigma^2}\right)}>\gamma_{DAD}\middle|\mathrm{H}_0\right) \tag{2.31}$$

Using now I_0 expression $\left(I_0\left(\frac{x_iv}{\sigma^2}\right)=\frac{exp\left(\frac{x_iv}{\sigma^2}\right)}{\sqrt{2\pi\frac{x_iv}{\sigma^2}}}\right)$, we have

$$P_{FA,DAD}=Pr\left(\frac{e-\exp\left(-\frac{pv^2}{2\sigma^2}\right)\prod_{i=1}^{p}\left(\frac{exp\left(\frac{x_iv}{\sigma^2}\right)}{\sqrt{2\pi\frac{x_iv}{\sigma^2}}}\right)}{e+\exp\left(-\frac{pv^2}{2\sigma^2}\right)\prod_{i=1}^{p}\left(\frac{exp\left(\frac{x_iv}{\sigma^2}\right)}{\sqrt{2\pi\frac{x_iv}{\sigma^2}}}\right)}>\gamma_{DAD}\middle|\mathrm{H}_0\right)$$

$$=Pr\left(e(1-\gamma_{DAD})>(1+\gamma_{DAD})\exp\left(-\frac{pv^2}{2\sigma^2}\right)\prod_{i=1}^{p}\left(\frac{exp\left(\frac{x_iv}{\sigma^2}\right)}{\sqrt{2\pi\frac{x_iv}{\sigma^2}}}\right)\middle|\mathrm{H}_0\right)$$

$$=Pr\left(\frac{e(1-\gamma_{DAD})}{1+\gamma_{DAD}}\left(\frac{2\pi v}{\sigma^2}\right)^{\frac{p}{2}}\exp\left(\frac{pv^2}{2\sigma^2}\right)>\frac{\exp\left(\sum_{i=1}^{p}x_i\right)}{\left(\prod_{i=1}^{p}x_i\right)^{\frac{1}{2}}}\middle|\mathrm{H}_0\right) \tag{2.32}$$

and finally we obtain

$$P_{FA,DAD}=Pr\left(\left(\prod_{i=1}^{p}x_i\right)^{\frac{1}{2}}<\frac{1+\gamma_{DAD}}{e(1-\gamma_{DAD})}\frac{\exp\left(\frac{p}{2}-\frac{pv^2}{\sigma^2}-\frac{pv^2}{2\sigma^2}\right)}{\left(\frac{2\pi v}{\sigma^2}\right)^{\frac{p}{2}}}\middle|\mathrm{H}_0\right)$$

$$=Pr\left(\prod_{i=1}^{p}x_i<\left(\frac{1+\gamma_{DAD}}{1-\gamma_{DAD}}\right)^2\left(\frac{2\pi v}{\sigma^2}\right)^{-p}\exp\left(p-\frac{3pv^2}{\sigma^2}-2\right)\middle|\mathrm{H}_0\right) \tag{2.33}$$

At hypothesis H_0, the distribution of the received signal is assumed as a Gaussian distribution. Therefore, the distribution of the envelope of this signal is Rayleigh. Substituting (2.15) into (2.19), we can find that $\frac{pv^2}{\sigma^2}\rightarrow 0$. If we introduce the Rician K-factor defined as the ratio of signal power in dominant component σ^2 over the (local-mean) scattered power v, the false alarm probability of the DAD detector can be approximated as

$$P_{FA,DAD}=Pr\left(\prod_{i=1}^{p}x_i<\left(\frac{1+\gamma_{DAD}}{1-\gamma_{DAD}}\right)^2(4\pi K)^{-p}\exp\left(p-2\right)\middle|\mathrm{H}_0\right) \tag{2.34}$$

Applying now the distribution of the product of p independent Rayleigh random variables [50], the product $\prod_{i=1}^{p}x_i$ satisfies the distribution of p independent Rayleigh random variables represented by its CDF [50] given by :

$$F(t)=\left(2^p\sigma^{2p}\right)^{-\frac{1}{2}}tG_{1,p+1}^{p,1}\left(\left(2^p\sigma^{2p}\right)^{-1}t^2\middle|\begin{matrix}\frac{1}{2}\\ \frac{1}{2},\ldots,\frac{1}{2},-\frac{1}{2}\end{matrix}\right) \tag{2.35}$$

where G denotes the Meijer G-function [50] defined by :

$$G_{1,p+1}^{p,1}\left(u\Big|_{\frac{1}{2},\ldots,\frac{1}{2},-\frac{1}{2}}^{\frac{1}{2}}\right)=\frac{1}{j2\pi}\int_{L}\frac{\left(\Gamma\left(\frac{1}{2}-s\right)\right)^{p-1}\Gamma\left(\frac{1}{2}+s\right)}{\Gamma\left(\frac{3}{2}+s\right)}u^{-s}ds \tag{2.36}$$

The contour L is chosen so that it separates the poles of the gamma products in the numerator. The Meijer G-function has been implemented in some commercial mathematical software packages. Finally, the probability of false alarm of the DAD algorithm can be approximated as

$$P_{FA,DAD}=F\left(\left(\frac{1+\gamma_{DAD}}{1-\gamma_{DAD}}\right)^{2}(4\pi K)^{-p}\exp\left(p-2\right)\right) \tag{2.37}$$

or, alternatively, the threshold can be expressed as

$$\gamma_{DAD}=\frac{\sqrt{(4\pi K)^{p}F^{-1}\left(P_{FA,DAD}\right)\exp\left(2-p\right)}-1}{\sqrt{(4\pi K)^{p}F^{-1}\left(P_{FA,DAD}\right)\exp\left(2-p\right)}+1} \tag{2.38}$$

Note that Meijer's G-function is a standard built-in function in most of the well known mathematical software packages, such as Matlab® which used in this work.

From (2.37), it is clear that the probability of false alarm is independent of noise variances σ^2. Therefore, the proposed sensing algorithm based on distribution analysis is robust in practical applications. This remark will be verified in the following section.

2.8 Performance Evaluation

In this section, we present some numerical examples to demonstrate the effectiveness of the proposed sensing scheme and to confirm the theoretical analysis.

2.8.1 Simulation and Analytical Results Comparison

In this subsection, we present a comparison between simulation and analytical results to confirm the theoretical results given in Section 2.7. For the proposed detector the threshold is computed based on p (the length of PU received signal in samples) and $P_{FA,DAD}$ value. Table 2.1 shows the comparison results for the thresholds γ_{DAD} for the DAD detector with $P_{FA}=0.05$ and for $P_{FA,DAD}$ using different p values. In the presented results SNR $=-7$dB. One can find that, the simulation results are slightly lower than the analytical results. This is due to the approximation we have used during the derivation of $P_{FA,DAD}$ and γ_{DAD} for the presented detector. The presented table confirms the very good match between simulation and theoretic results.

		$p=100$	$p=150$	$p=200$
Simulation results for DAD detector	$P_{FA,DAD}$	0.0571	0.0544	0.0502
	γ_{DAD}	0.9948	0.9814	0.9561
Analytical results for DAD detector	$P_{FA,DAD}$	0.0582	0.0563	0.0529
	γ_{DAD}	0.9965	0.9907	0.9614

TABLE 2.1 – Simulation and analytical results of thresholds values γ_{DAD} with $P_{FA}=0.05$ and probability of false alarm values for DAD detector with different p and SNR $=-7$dB.

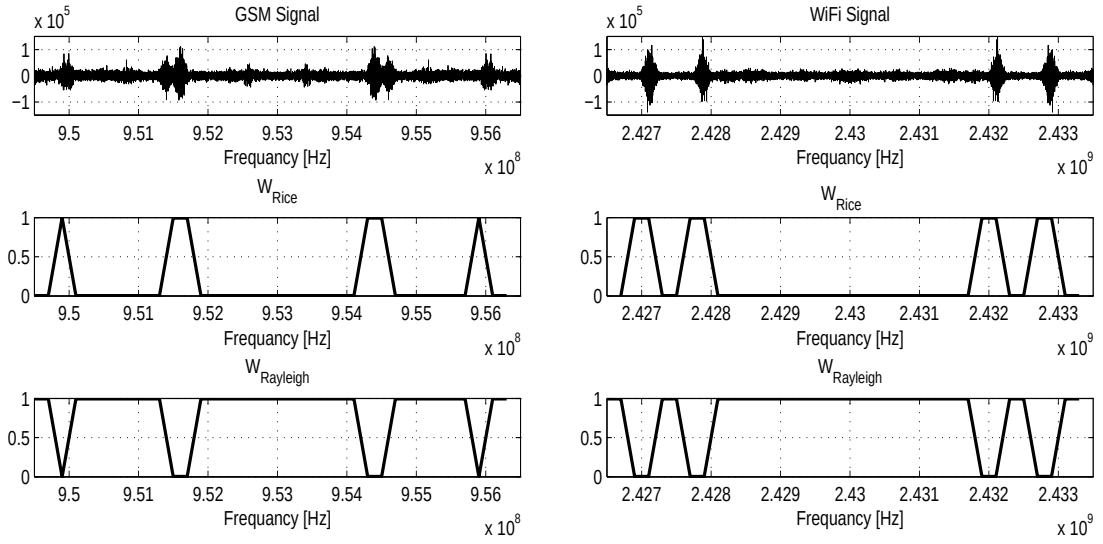

(a) GSM signal (b) WiFi signal

FIGURE 2.3 – Performance evaluation of the DAD detector in terms of PU vacant sub-bands detection for : (a) Baseband GSM signal at the carrier of 953MHz using sliding window technique with $T = 533$ samples which correspond to the GSM bandwidth (equal to 200kHz) and $L = 533$ samples, (b) Baseband WiFi signal at the carrier of 2430MHz using sliding window technique with $T = 1332$ samples which correspond to the WiFi bandwidth (equal to 500kHz) and $L = 1332$ samples.

2.8.2 Non-Cooperative Sensing Evaluation

In this subsection, the spectrum sensing is done locally. In a first step, we focus on the performance of the proposed detector in detecting vacant spectrum sub-bands in the PU band using the sliding window technique given by Figure 2.2. The validation of this detection mode is based on experimental measurements captured by EURECOM's RF Agile Platform [51]. We select a sliding window size T samples and slide the window over the spectrum band to obtain AIC values and Akaike weight values for each analysis windows. A time-lag sliding window of L samples was used to scan all the signal. The test statistic used in this case was given by (2.22) and (2.23). In a second step, we evaluate the performance of the proposed detector in terms of PU presence detection using the binary hypothesis test given in (2.28). We use in this part the scenarios test described in Section 1.4.3 using the DVB-T OFDM system.

Sub-bands Detection In order to evaluate the performances of the spectrum sensing method in terms of spectrum holes detection, measurements by the RF Agile Platform at EURECOM are considered [51]. RF Agile Platform covers an RF band from 200MHz to 7.5GHz, with a maximum bandwidth of 20MHz. It is able to receive and transmit almost all the existing commercial radio access technologies. Concerning the transmitted power, the target is comparable to existing GSM terminals (+21dBm). On the receiver side, the noise figure is from 8 to 12dB, depending on the frequency band. The RF equipment include up to 4 antennas and 4 RF chains. In addition, it allows for experimenting with system on-chip architectures for wireless communications.

At first stage, we focus on GSM signals at carrier of 953MHz with a bandwidth of 7680MHz. The received signal in the frequency domain is shown in Figure 2.3 (a). Time channel samples are stored in a vector of size p (with p equal to 20480 samples). Parameters v_{Rice}, σ_{Rice} and $\sigma_{Rayleigh}$ are estimated over $T = 533$ samples which correspond to the GSM bandwidth (equal to 200kHz). From Figure 2.3 (a), it is clear that only sub-bands around 950MHz, 951.5MHz, 954.5MHz and 956MHz contain data. The remaining sub-bands are idle. Figure 2.3 (a) depicts Akaike weight values for Rice and Rayleigh distributions obtained from the GSM signal. These results demonstrate that the DAD detector estimates efficiently the distribution of the received signal. In fact, when $W_{Rice} \rightarrow 1$ (or $W_{Rayleigh} \rightarrow 0$) we show that the PU is present, otherwise (i.e. $W_{Rice} \rightarrow 0$), we show that the PU is absent.

At second stage, we considered a WiFi signal at the carrier of 2430MHz. The size of the sliding window is around 500kHz. From Figure 2.3 (b) we can see that similar to the case of GSM signal, we obtain interesting results in terms of sub-bands detection for the proposed blind spectrum sensing technique.

PU Signal Detection We analyze now the performance of the DAD detector, in comparison with detectors presented in Chapter 1, in detecting primary signals. We use here the binary hypothesis test given by (2.28). We choose proper performance criteria given by the probability of false alarm P_{FA} and the probability of detection P_D, in the three proposed simulation scenarios presented in Subsection 1.4.3.

Figures 2.4 (a), (b) and (c) depict the detection comparison of the DAD detector with CD, ED and KLD detectors in the three proposed scenarios. From the simulation results, we see that the CD detector performs the best. Subsequent to the CD detector is the proposed DAD detector, with approximately 2dB reduced performance compared to the CD, and ED detector, approximately 3dB behind CD. The worst performance is obtained by the KLD detector, which shows a performance reduction of approximately 5dB compared to CD detector. The ROC curves in Figures 2.4 (d), (e) and (f) for all detectors can be observed to have very similar slopes. Hence, the proposed detector exhibit very interesting results in term of spectrum detection in a perfectly blind way.

Two things can be inferred from this. It is expected that if knowledge of signal parameters is provided, feature detectors are the optimal schemes for detecting the PU signal. These expectations are confirmed when considering the simulation results seen in Figure 2.4. As expected, the CD detector gives the best performance in the three scenarios cases. The other thing is to expect that the proposed DAD detector have best distribution estimation compared with the KLD. Recall that the KLD algorithm is based on the measurement of the distance between two probability distributions, the estimated received PU signal distribution and a generated Gaussian distribution. On the other hand, the DAD algorithm estimates distributions parameters directly from the received signal. This confirms that the proposed technique is the optimal for estimating the PU signal distribution.

When considering the simulation results for scenario 2 and scenario 3, another obvious fact is observed. It is clearly seen how introducing channel distortion in terms of multipath and shadow fading clearly deteriorates the detection performance. While the detection performance under AWGN dropped rapidly from 1 to P_{FA} over a range of about 10dB, the slope of the detection curve falls off considerably slower, extending the SNR range of the drop to at least 30dB, especially for scenario 3. Recall that the Rice factor for the multipath fading in scenario is K $= 10$, and that this corresponds to a very strong LOS component compared to the multipath components. Hence the Rician multipath fading is expected not to cause significant performance degradation. The shadow fading on the other hand, has a standard deviation of 12dB, and can be expected to decrease performance over a wide range of SNRs. This is clearly seen as the case in Figure 2.4 (c).

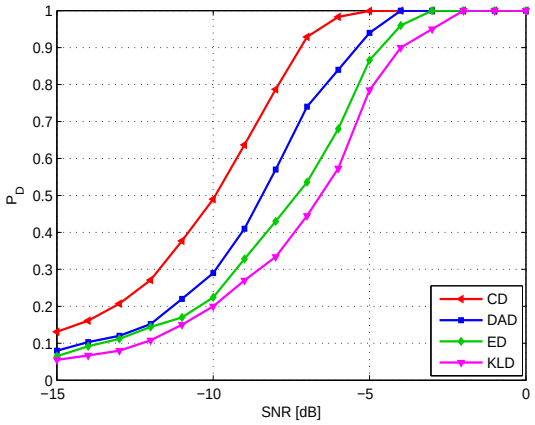

(a) P_D vs. SNR : Scenario 1

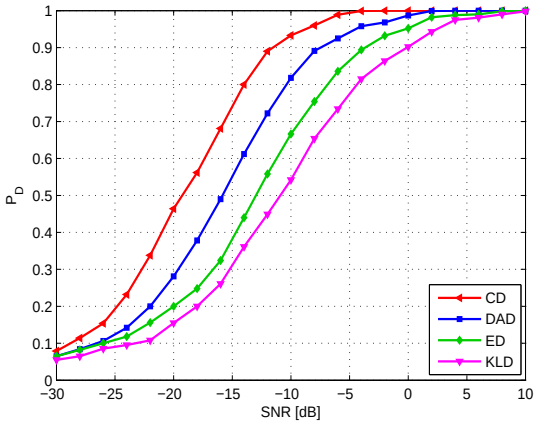

(b) P_D vs. SNR : Scenario 2

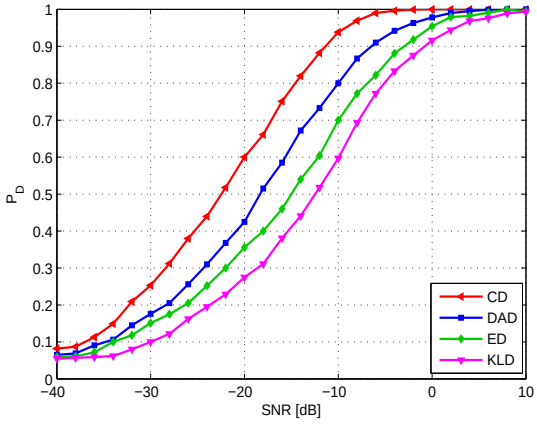

(c) P_D vs. SNR : Scenario 3

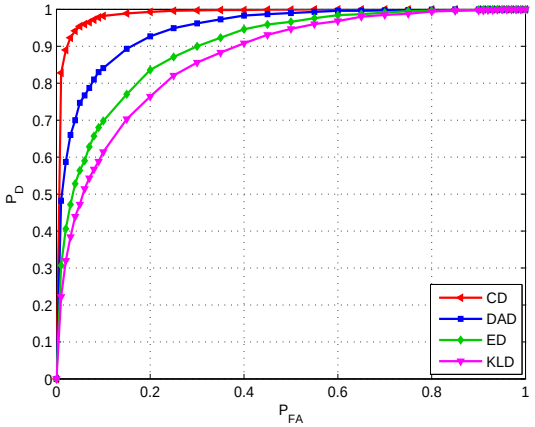

(d) ROC curves : Scenario 1

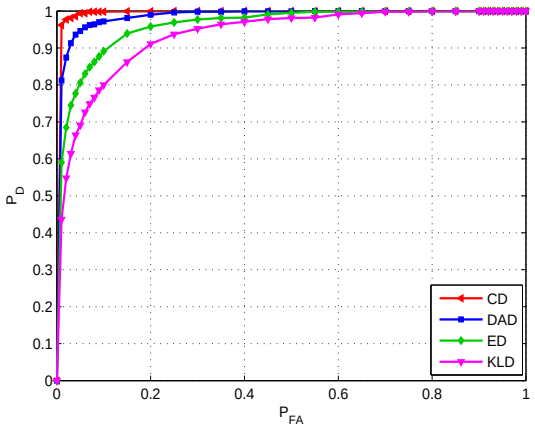

(e) ROC curves : Scenario 2

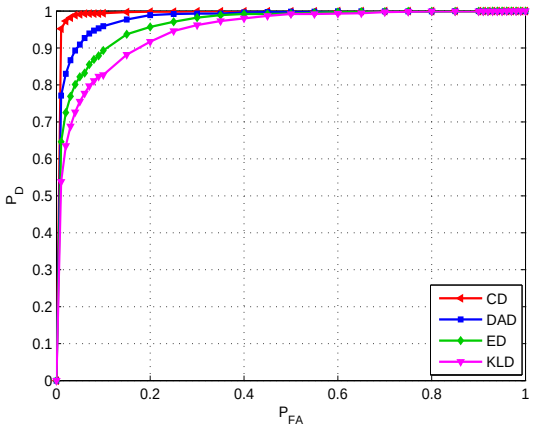

(f) ROC curves : Scenario 3

FIGURE 2.4 – Performance evaluation of the DAD detector in terms of PU signal detection in non-cooperative way using an DVB-T OFDM primary user system : Probability of detection versus SNR curves with $P_{FA} = 0.05$ and ROC curves with SNR $= -7$dB, and, sensing time = $1.12ms$ and $p = 2048$.

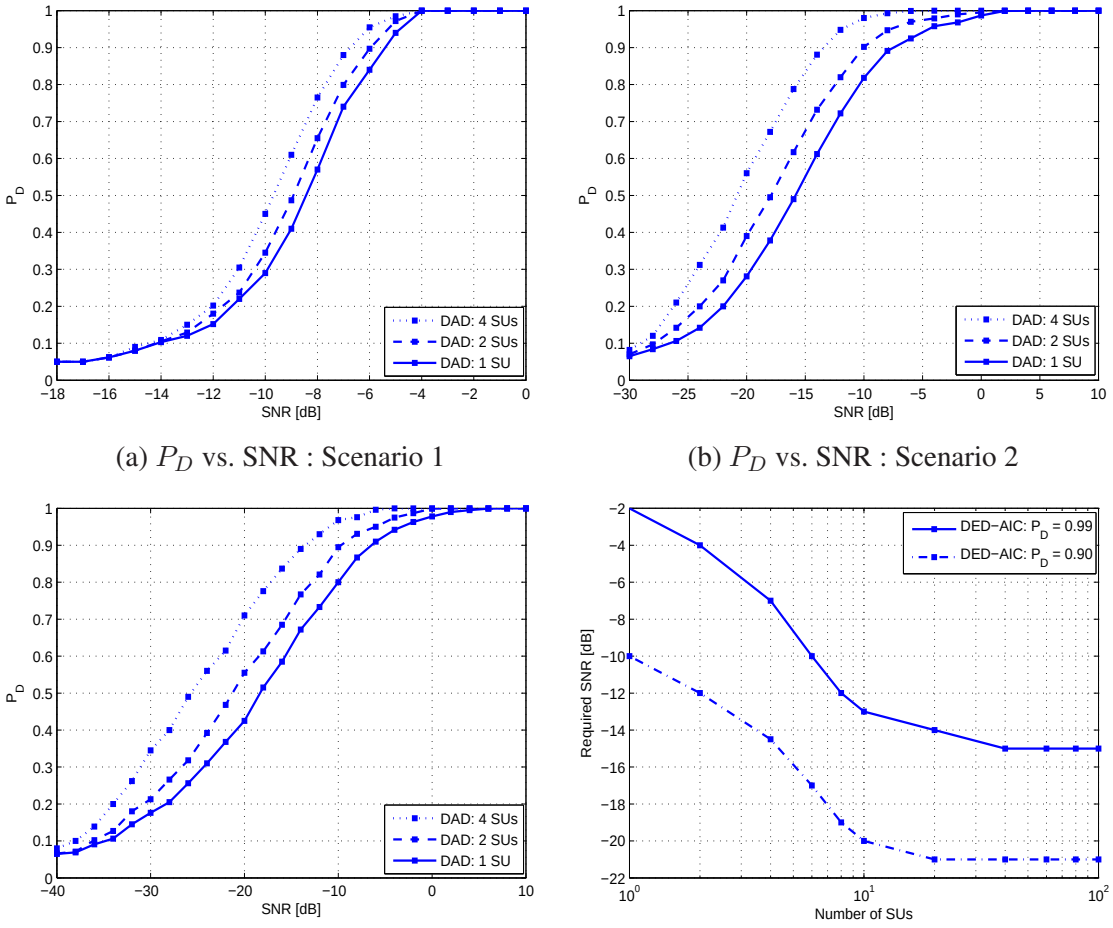

(a) P_D vs. SNR : Scenario 1

(b) P_D vs. SNR : Scenario 2

(c) P_D vs. SNR : Scenario 3

(d) SNR vs. M : Scenario 3

FIGURE 2.5 – Performance evaluation of the DAD detector in terms of PU signal detection in cooperative way using an DVB-T OFDM primary user system : Probability of detection versus SNR curves with $P_{FA} = 0.05$ and the required SNR versus the number of collaborating users M.

2.8.3 Cooperative Sensing Evaluation

In this part, we consider a wireless CRN with a collection of users randomly distributed over the geographical area. The cooperative sensing scenario system was described in Section 1.5. In this scenario, only binary decisions are sent to the FC to make the final global decision.

In Figures 2.5 (a), (b) and (c), we present the detection performances of the cooperative spectrum sensing method for multiple users in the three proposed simulation scenarios. These figures show the P_D versus SNR. From the presented results, it is seen that the detection performance of the DAD is improved as the number of cooperative users is increased. Performance gain of roughly 1dB for scenario 1 and 3dB using scenarios 2 and 3 is obtained from the cooperative sensing. This confirms that using cooperation between SUs allows for mitigation of the multi-path fading and shadowing effects.

Figure 2.5 (d) provides plots of SNR versus the number of collaborating users M for different P_D values using scenario 3. For each curve, the decision threshold is chosen such that $P_{FA} = 0.05$. The results show that there is significant improvement in the performance for spectrum sensing in

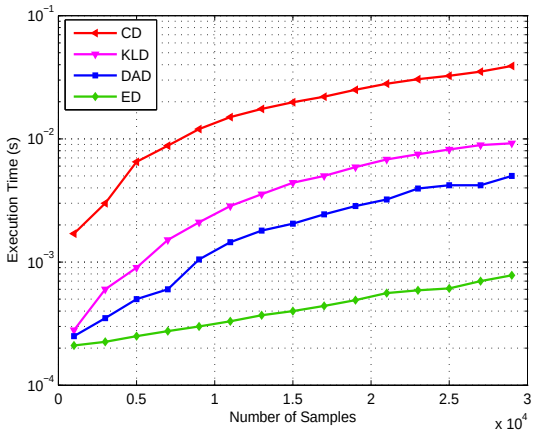

FIGURE 2.6 – Simulation results assessing the performance in terms of execution time for the DAD detector in comparison with three detectors : Execution time versus the number of samples of the received DVB-T OFDM primary user signal.

terms of SNR in detecting the PU by performing cooperative spectrum sensing, especially when the number of the cooperating cognitive users is large in the network. This is the main advantage gained by performing cooperative spectrum sensing by using the spectral sensing information obtained at the individual users. In fact, results indicate a significant improvement in terms of the SNR required for detection. In particular, to achieve $P_D = 0.99$, local spectrum sensing requires SNR $= -2$dB while collaborative sensing with $M = 10$ only needs SNR of -13dB for the individual users. In addition, we remark that the number of collaborating users increases with the value of probability of detection especially at low SNR region. As an example, having SNR $= -14$dB, more than 99% of the occupied bands can be correctly detected with 20 users. On the other hand, for the same SNR, 90% of occupied bands is detected with $M = 4$ collaborating users.

2.8.4 Complexity Study

Using the implementation steps of the DAD detector, we will study in this subsection the complexity required to derive its sensing algorithm. It will also provide simulation results assessing the performance in terms of execution time for the proposed algorithm in comparison with the reference algorithms described in Chapter 1.

The complexity of the algorithm is measured through the number of complex multiplications that the algorithm has to perform for the calculation of the test statistic. It is difficult to say anything exact about the computational complexity of the proposed algorithm since this depends on the implementation of the sub functions. However, when considering the pseudo code, some main points can be noted. Complexity of the DAD algorithm is dominated by the computation of $\hat{\sigma}^2$ and $\hat{v}$. The running time of $\hat{\sigma}^2$ and $\hat{v}$ depends on the implementation, but can in general be done in $2p$ time since it only requires $2p$ multiplications.

To get an impression of the relative performance, the execution times have been recorded for various input sizes. The input signal is circularly symmetric complex Gaussian noise. Execution time has been measured by using the Matlab® stopwatch function *tic/toc*. Simulations were performed on a laptop computer with a 1.6GHz CPU. Results from the simulations can be seen in Figure 2.6. From this figure, it becomes clear that the former discussion on DAD algorithm perfor-

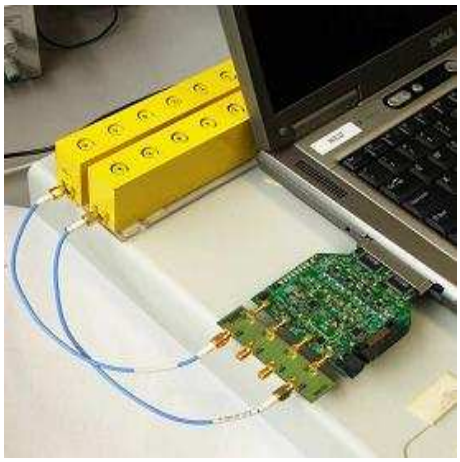

(a) CardBus MIMO I

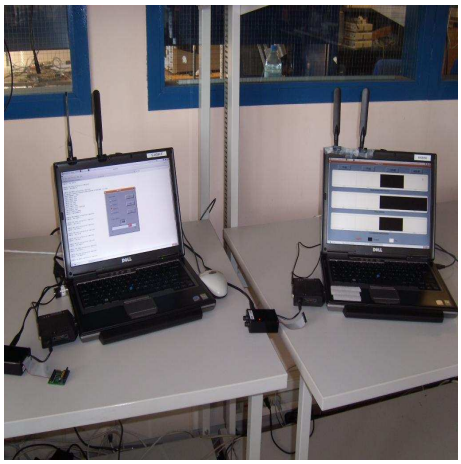

(b) The sensing demonstration.

FIGURE 2.7 – The sensing demonstration using two laptops, one for transmission and one for reception, equipped with the CardBus MIMO I data acquisition card and two antennas.

mance was accurate. The running time of the DAD algorithm clearly dominates when the number of input samples increases. It is also seen that the proposed algorithm have execution times that are of one to two orders of magnitude greater than the ED algorithm and smaller than CD algorithm. This was expected as the amount of computation to be performed for the ED and the DAD proposed detector is very limited.

2.9 Implementation of DAD using OpenAirInterface

In this section, we will present the sensing module implementation. This implementation is based on the OpenAirInterface platform available at EURECOM [51] [52]. The aim of the demonstration is first to illustrate the spectrum sensing concept and second to assess the detection performances of the proposed DAD detector which will be compared with ED and CD detectors. Only the sensing and transmission of sensing information will be performed for the three detectors. In the rest of this section, we will present the OpenAirInterfce platform and then the main steps of the demonstration.

2.9.1 OpenAirInterfce Platform

The spectrum sensing demonstration that we performed is based on the OpenAirInterface development platform at EURECOM [51]. The platform consists of dual-RF CardBus/PCMCIA data acquisition cards called CardBus MIMO I (see Figure 2.7 (a)). The RF section is time-division duplex and operates at 1.900-1.920GHz with 5MHz channels and 21dBm transmit power per antenna for an OFDM waveform. EURECOM has a frequency allocation for experimentation around its premises in Sophia Antipolis. The cards house a medium-scale FPGA (Xilinx X2CV3000) allowing for an embedded HW/SW system implementing the physical layer. Besides implementation in the FPGA, for advanced PHY algorithms and real-time testing prior to HW implementation, the physical (PHY) layer is usually run in real-time on the host PC under the real-time operating system (RTOS) RTAI. The PHY layer of the platform targets WiMax and UMTS LTE like networks and thus uses multiple-input multiple-output orthogonal frequency division multiples

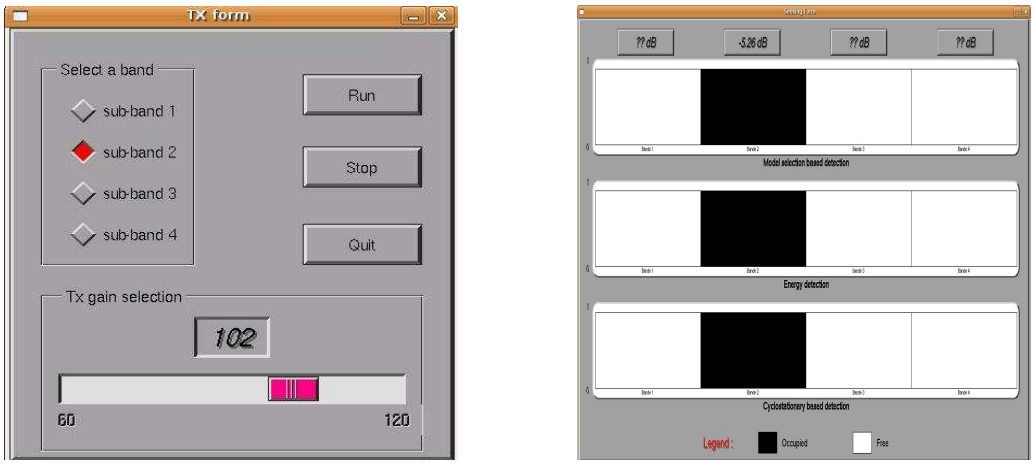

(a) GUI Transmitter (b) GUI Receiver

FIGURE 2.8 – Graphical user interface for the transmitter and the receiver side of the sensing demonstration.

access (MIMO-OFDMA) as modulation and multiple access technique. The MIMO-OFDMA system provides the means for transmitting several multiple-bitrate streams (multiplexed over subcarriers and antennas) in parallel. The physical resources are organized in frames of OFDM symbols. A nominal OFDMA configuration is shown in Table 2.2. One frame consists of 64 symbols and is divided in an uplink transmission time interval (TTI) and a downlink TTI. More information can be found on the OpenAirInterface web-site [53].

2.9.2 Sensing Demonstration

As we can see from Figure 2.7 (b), the demonstration consists of two laptops, one for transmission and one for reception, each of them is equipped with the CardBus MIMO1 data acquisition cards and two antennas. To simulate the SNR variation, the transmission gain is adjusted within the interval [0-256]. However the reception gain can be set manually or (by default) automatically. Two sensing algorithms were selected, in addition with the DAD algorithm (the ED and CD). They are running continuously and their results are graphically displayed in real time. At reception side, we developed a graphical user interface (GUI) allowing the user to select one of the four sub-bands (with 1.25MHz of width) of the EURECOM frequency allocation around 1917MHz, the transmission gain and running/stopping the transmission. At reception side, another GUI is developed and displays, in real time, the measured SNR and the detection results of the sensing algorithms in each sub-band. The GUI transmitter and receiver are given by Figure 2.8.

Sampling rate	7.68 Msamp/s
Frame length	64 symbols (2.67 ms)
Symbol (DFT/IDFT) size	256 samples
Prefix length	64 samples
Useful carriers	160

TABLE 2.2 – The transmitted OFDM signal parameters

2.10 Conclusion

Chapter 1 has introduced the problem of spectrum sensing in CR, presented an analysis of problems with existing detectors. This chapter, however, proposed a novel algorithm based on the distribution analysis of the PU signal which provides improved performance, especially in the low SNR, and, with low complexity and blindly. This chapter provided also a number of simulations aimed at assessing the performance of the proposed detector in comparison with the reference detectors. A sensing demonstrator was presented in the last part of this chapter, based on the OpenAirInterface platform at EURECOM. In the following chapter, we will present a second blind sensing detector based on the dimension estimation of the PU received signal.

Chapter 3

Dimension Estimation Based Detection

3.1 Introduction

The work presented in the previous chapter suggested to use model selection tools like AIC criteria and Akaike weight as a promising technique in the context of CR sensing. In this chapter, however, we adopt the same framework to detect PU presence in the radio spectrum. The AIC and MDL criterions were investigated in order to sense the signal presence over the spectrum bandwidth. We focus on analyzing the number of significant eigenvalues determined by the value which minimizes the AIC and/or MDL criterion and conclude on the nature of the sensed band. Specifically, we will show that the number of significant eigenvalues is directly related to the presence/absance of data in the signal. In particular, when a PU signal is present, we observe a set of dominant eigenvalues which represents the primary system subspace. This information will be used as a detection rule for the DED detector.

The rest of the chapter is organized as follows. Section 3.2 discusses the prime condition for making the information theoretic criteria applicable to spectrum sensing. We will give in this section an explicit model for the application of the information theoretic criteria in our context ; the over sampling solution. In Section 3.3 we will formulate the two users selection tools used throughout the development of the proposed algorithm. The DED algorithm will be presented in Section 3.4 using AIC and MDL criteria. We will present two kinds of algorithms : Sub-bands detection algorithm using sliding window technique and PU signal presence detection algorithm using a binary hypothesis test. Furthermore, we derive in Section 3.5 and Section 3.6 closed-form expressions of false alarm probabilities for a given threshold using both AIC and MDL criteria, respectively. Performance evaluation and advantages will be described in Section 3.7 and a comparison of the proposed detector with reference detectors will be given. The performance will be assessed under different conditions, using the three common simulation scenarios presented in Subsection 1.4.3 and experimental measurements captured by EURECOM RF Agile Platform. We will show in this section the effect of the DED detector on both non-cooperative and cooperative CRN. In addition, we will present the limits of this method by studying the complexity required for sensing. We will show that the major complexity of this method comes from the computation of the covariance matrix and the eigenvalue decomposition. Finally, Section 3.8 presents the conclusions of this chapter.

3.2 Information Theoretic Criteria Constraint

In this section, we will provide the background of information theoretic criteria. The general problem for model selection using information theoretic criteria is : Given a set of N observations $\{\mathbf{x}_1, \mathbf{x}_2, ..., \mathbf{x}_N\}$ and a family of models which are represented by a parameterized family of probability density functions f, determine the best fit model. There are two well-known criteria that have been widely used : AIC criterion and MDL criterion. Consider the system model described in (1.1) and reformulated here as a linear convolution with a discrete vector of length p represented by a matrix-vector product :

$$\mathbf{x}_i = \mathbf{A}\mathbf{s}_i + \mathbf{n}_i \tag{3.1}$$

where

$$\mathbf{x}_i=[x(ip-p+1)\ x(ip-p+2)\ \dots\ x(ip)]^T \tag{3.2}$$

$\mathbf{A}$ is a $p \times (l+p-1)$ channel matrix defined as

$$\mathbf{A}=\begin{bmatrix} a(0) & a(1) & \cdots & a(l-1) & 0 & 0 & \cdots & 0 \\ 0 & a(0) & \cdots & a(l-2) & a(l-1) & 0 & \cdots & 0 \\ \vdots & \ddots & \ddots & \ddots & \ddots & \ddots & \ddots & \vdots \\ 0 & \cdots & 0 & a(0) & a(1) & \cdots & a(l-2) & a(l-1) \end{bmatrix} \tag{3.3}$$

$$\mathbf{s}_i=[s(ip-p+1)\ s(ip-p+2)\ \dots\ s(ip)]^T \tag{3.4}$$

and

$$\mathbf{n}_i=[n(ip-p+1)\ n(ip-p+2)\ \dots\ n(ip)]^T \tag{3.5}$$

The sampled channel have a finite discrete impulse response of length l taps. From (3.1) all the possible numbers of source signals correspond to a family of different parameterized models. Therefore, the estimation of the number of source signals can be characterized as the model selection problem and both AIC criterion and MDL criterion can be applied. Motivated by the fact that the information theoretic criteria have been used to effectively estimate the number of source signals in array processing, it can certainly be applied to detect the presence of PUs. As discussed in Chapter 1, spectrum sensing can be formulated as a binary hypothesis test. When the PU is absent, the received signal $\mathbf{x}_n$ is only the white noise samples, so the estimated number of source signals via information theoretic criteria (AIC or MDL) should be zero. When the PU is present, the number of source signal (including signal transmitted by the PU) must be larger than zero, even though the exact number estimated by information theoretic criteria may not be accurate under low SNR region. Hence, by comparing the estimated number of source signals with zero, we can detect the presence of the PU.

Now, comparing (3.1) with (1.1), we find that a major difference is that the $\mathbf{A}$ in our considered system model is an under-determined matrix, i.e., the order of column is larger than the order of row. Therefore, the information theoretic criteria are not directly applicable here [49]. To construct an over-determined channel matrix $\mathbf{A}$, one needs to enlarge the observation space. Obviously, simply increasing the observation window $\mathbf{A}$ does not work. Here we propose to expand the observation space using one of the following two methods. One is to increase the spatial dimensionality by employing multiple receive antennas at the SU and the other is to increase the time dimensionality by over-sampling the received signals. It turns out that the two methods are

equivalent to each other. Hence we shall focus on the over-sampling approach hereafter. In specific, suppose that the over-sampling factor is k, i.e., the received baseband signal is sampled k times in one symbol. Redefine (3.2) and (3.5) as

$$\mathbf{x}_i=[x(ikp-kp+1)\ x(ikp-kp+2)\ \dots\ x(ikp)]^T \tag{3.6}$$

$$\mathbf{n}_i=[n(ikp-kp+1)\ n(ikp-kp+2)\ \dots\ n(ikp)]^T \tag{3.7}$$

Then, the new channel matrix $\mathbf{A}$ becomes a $kp \times (l+p-1)$ matrix

$$\mathbf{A}=\begin{bmatrix} a^1(0) & a^1(1) & \cdots & a^1(l-1) & 0 & 0 & \cdots & 0 \\ \vdots & \vdots & & \vdots & \vdots & \vdots & & \vdots \\ a^k(0) & a^k(1) & \cdots & a^k(l-1) & 0 & 0 & \cdots & 0 \\ 0 & a^1(0) & \cdots & a^1(l-2) & a^1(l-1) & 0 & \cdots & 0 \\ \vdots & \vdots & & \vdots & \vdots & \vdots & & \vdots \\ 0 & a^k(0) & \cdots & a^k(l-2) & a^k(l-1) & 0 & \cdots & 0 \\ \vdots & \ddots & \ddots & \ddots & \ddots & \ddots & \ddots & \vdots \\ 0 & \cdots & 0 & a^1(0) & a^1(1) & \cdots & a^1(l-2) & a^1(l-1) \\ \vdots & & \vdots & \vdots & \vdots & & \vdots & \vdots \\ 0 & \cdots & 0 & a^k(0) & a^k(1) & \cdots & a^k(l-2) & a^k(l-1) \end{bmatrix} \tag{3.8}$$

Here, $a^k(i)$, for $i = 0...l-1$, denotes the k-th over-sampling point of the i-th channel tap. To ensure that $\mathbf{A}$ is now an over-determined matrix (the order of row is larger than the order of column), we need to have

$$k>\frac{l+p-1}{p} \tag{3.9}$$

or, alternatively,

$$p>\frac{l-1}{k-1} \tag{3.10}$$

Given this over-determined channel matrix in (3.8), we can now readily apply the information theoretic criteria to develop a blind sensing algorithm.

3.3 Information Theoretic Criteria

The first step of the proposed sensing algorithm is the calculation of the covariance matrix $\hat{\mathbf{R}}$ of received signals $\{\mathbf{x}_1, \mathbf{x}_2, ..., \mathbf{x}_N\}$. Then, we obtain the eigenvalues of $\hat{\mathbf{R}}$ through eigenvalue decomposition technique, and we compute finally AIC and MDL values to estimate the dimension of the PU signal. In the rest of this section, we will define the covariance matrix in our context. We will reformulate also the AIC formula, based on (2.5), that will be used throughout the development of the DED algorithm. We will define also the minimum description length (MDL) used as a second tool in the development of the DED detector. To compute AIC and MDL values, we need to estimate eigenvalues according to the covariance matrix of the received signal. From the estimation values of AIC and MDL, we make decision about the presence/absence of PU signal.

Let p be the length of one observation $\mathbf{x} \in \{\mathbf{x}_1, \mathbf{x}_2, ..., \mathbf{x}_N\}$ (i.e. one PU received signal) and q the length of the transmitted signal $\mathbf{s}$ and the additive noise $\mathbf{n}$. Our goal within this part is to

determine the value of q from N observations of $\mathbf{x}$ (i.e. the dimension of the PU received signal). Because the noise is zero mean and independent of the signals, it follows that the covariance matrix of $\mathbf{x}$ is given by :

$$\mathbf{R} = \mathbf{ASA}^H + \sigma^2\mathbf{I} \tag{3.11}$$

with $\mathbf{S}$ denoting the covariance matrix of the transmitted signal $\mathbf{s}$, i.e., $\mathbf{S} = E\{\mathbf{ss}^H\}$, and σ^2 denotes the noise power. Furthermore, if q uncorrelated signals are present, the $q - p$ smallest eigenvalues of $\mathbf{R}$ are equal to σ^2. From the covariance matrix expression given by (3.11) and using linear algebra, let's consider the following family of covariance matrix :

$$\mathbf{R}^{(k)} = \sum_{i=1}^{k}(\lambda_i - \sigma^2)\mathbf{V}_i\mathbf{V}_i^H + \sigma^2\mathbf{I} \tag{3.12}$$

where $\lambda_1, ..., \lambda_k$ and $\mathbf{V}_1, ..., \mathbf{V}_k$ are, respectively, the eigenvalues and eigenvectors of $\mathbf{R}^{(k)}$. Note that k ranges over the set of all possible numbers of degrees of freedom (DoF), i.e. $k = 0, 1, ..., p-1$. The parameter vector θ given by equation (2.2), is a function of the eigenvalues and eigenvectors and is given by :

$$\theta = (\lambda_1, ..., \lambda_k, \sigma^2, \mathbf{V}_1, ..., \mathbf{V}_k) \tag{3.13}$$

The number of signals is determined from the estimated covariance matrix $\hat{\mathbf{R}}$ defined by :

$$\hat{\mathbf{R}} = \frac{1}{N}\sum_{n=1}^{N}\mathbf{x}_n\mathbf{x}_n^H \tag{3.14}$$

where $\mathbf{x}_n|_{\{n=1,...,N\}}$ are the N independent observations. Therefore, we need to compute $\hat{\theta}$, the estimated value of θ. We reformulate then the AIC criterion based on equation (2.5) as a function of (3.13). If $\hat{\lambda}_1, \hat{\lambda}_2, ..., \hat{\lambda}_q$ are the eigenvalues of $\hat{\mathbf{R}}$ in the decreasing order then [49] [12] :

$$\text{AIC}(k) = -2\log\left(\frac{\prod_{i=k+1}^{p}\hat{\lambda}_i^{\frac{1}{p-k}}}{\frac{1}{p-k}\sum_{i=k+1}^{p}\hat{\lambda}_i}\right)^{(p-k)N} + 2k(2p-k) \tag{3.15}$$

Inspired by Akaike work, Schwartz [12] and Rissanen [54] have an approach quite different. In [12], Schwartz approached the problem by bayesian arguments. However Rissanen based his work on information theoretic arguments [54]. It turns out that in the large-sample limit, both Schwartz's and Rissanen's approaches yield the same criterion, given by [49] :

$$\text{MDL}=-\sum_{n=1}^{N}\log g_{\hat{\theta}}(\mathbf{x}_n) + 2U\log N \tag{3.16}$$

A comprehensive survey of these concepts, among others, can be found in [55]. Using the same notations given in (3.15), the resulting cost function MDL has the following form

$$\text{MDL}(k) = -\log\left(\frac{\prod_{i=k+1}^{p}\hat{\lambda}_i^{\frac{1}{p-k}}}{\frac{1}{p-k}\sum_{i=k+1}^{p}\hat{\lambda}_i}\right)^{(p-k)N} + \frac{k}{2}(2p-k)\log N \tag{3.17}$$

The number of DoF, possibly the number of significant eigenvalues, is determined as the value of $k \in \{0, 1, ..., p-1\}$ which minimizes the value of AIC and/or the value of MDL. Figures 3.1

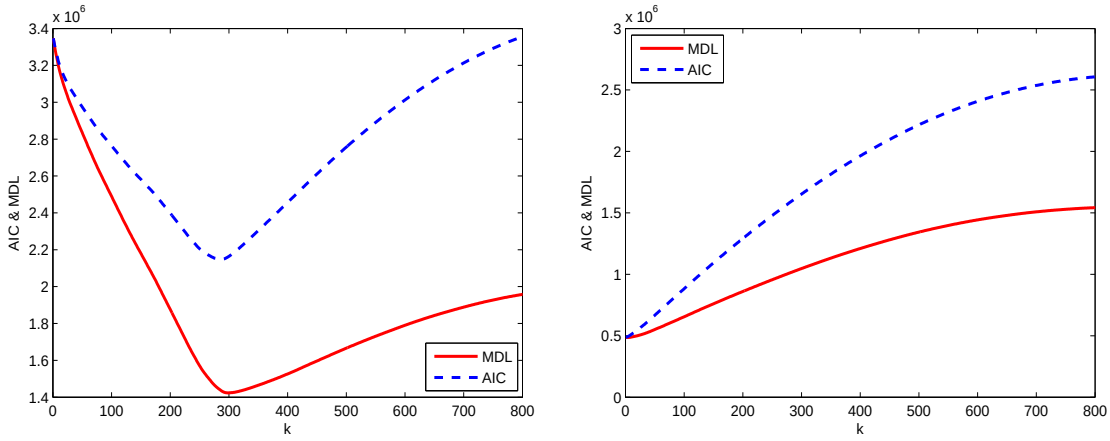

(a) Data block (b) Noise block

FIGURE 3.1 – Akaike information criterion and minimum description length of captured noise block samples and data block samples using an UMTS signal.

(a) and (b) present the computed number of DoF obtained by AIC and MDL criterion following (3.15) and (3.17), respectively. We show in these two figures the behavior of the AIC and MDL curves as function of the eigenvalues index for an occupied and vacant UMTS band, respectively. The dimension of the covariance matrix is equal to 800 (i.e. $N = 800$ observations) and the length of the received signals is 20480 samples. Based on (3.15) and (3.17), we determine the minimum of AIC and MDL and we obtain then the number of significant eigenvalues. From Figures 3.1 (a), we see clearly that the position of AIC_{min} and MDL_{min} are located at a position of $k \neq 0$ for the occupied spectrum band, and, at $k = 0$ for the vacant spectrum band as given by Figures 3.1 (b).

The number of significant eigenvalues (SE) is determined by the value which minimizes AIC and/or MDL (p and q), and is given by [56] [27] :

$$SE = \begin{cases} q & \text{noise} \\ p & \text{signal} \end{cases} \tag{3.18}$$

According to (3.18), the number of significant eigenvalues in the first case (Figures 3.1 (a)) is equal to $SE = p = 300$ and $SE = q = 1000$ for the second case (Figures 3.1 (b)).

3.4 Dimension Estimation Detector (DED)

Sub-bands Detection The previous discussion suggests that the number of significant eigenvalues concludes on the nature of the sensed sub-bands. Based on this result, we propose in the rest of this section the DED algorithm. Using the same sliding window technique as the DED given by Figure 2.2, we estimate the covariance matrix $\hat{\mathbf{R}}$ and compute AIC values for each window. The minimum of these values gives the number of significant eigenvalues. Therefore, for each sliding window, we compute the number of significant eigenvalues. If the analysis window contains a noise signal, the position of AIC_{min} and/or MDL_{min} is located at 0. Else, the position of these two values gives the dimension of the analyzed window. The idea here is to exploit the slope change of the signal space dimension curve. This slope change, from positive to negative trend, is representative of the transition from a vacant band to an occupied band (and vice versa).

PU Signal Detection Motivated by the fact that the AIC and MDL criteria have been used to effectively estimate the dimension of the PU received signals and to determine the spectrum holes in the spectrum band, it can certainly be applied to detect the presence of PUs. As discussed above, spectrum sensing can be formulated as a binary hypothesis test. When the PU is absent, the received signal $\mathbf{x}$ is only the white noise samples, so the AIC curve, for example, monotonically increases, as shown in Figure 3.1 (b). Therefore, $\text{AIC}(0) < \text{AIC}(k),\ \forall k \in \{1, ..., p-1\}$, which can be rewired as $\text{AIC}(0) < \text{AIC}(1)$. On the other hand, when the PU is present, the AIC curve monotonically decreases from $\text{AIC}(0)$ to AIC_{min}, as shown in Figure 3.1 (a). Similarly, we can write that $\text{AIC}(0) > \text{AIC}(1)$ if PU is present. Hence, the generalized blind DED using AIC criteria can be given by

$$\Upsilon_{DED-AIC}(\mathbf{x}) = \begin{cases} \text{AIC}(0) - \text{AIC}(1) < \gamma_{DED-AIC} & \text{noise} \\ \text{AIC}(0) - \text{AIC}(1) > \gamma_{DED-AIC} & \text{signal} \end{cases} \tag{3.19}$$

The same properties can be founded using MDL criteria and the DED static test is given in this case by

$$\Upsilon_{DED-MDL}(\mathbf{x}) = \begin{cases} \text{MDL}(0) - \text{MDL}(1) < \gamma_{DED-MDL} & \text{noise} \\ \text{MDL}(0) - \text{MDL}(1) > \gamma_{DED-MDL} & \text{signal} \end{cases} \tag{3.20}$$

We define here the two thresholds $\gamma_{DED-AIC}$ and $\gamma_{DED-MDL}$ in order to decide on the nature of the received signal. These thresholds depend only on P_{FA} and are calculated in Section 3.5 and Section 3.6, respectively.

3.5 DED-AIC False Alarm Probability

According to the sensing steps in Section 3.4, the false alarm of the DED using AIC criteria occurs when the estimated AIC values verify (3.19) given that the PU is absent or present. The test static $\Upsilon_{DED-AIC}(\mathbf{x})$ of the proposed detector is

$$\Upsilon_{DED-AIC}(\mathbf{x}) = \text{AIC}(0) - \text{AIC}(1) \tag{3.21}$$

Therefore, the probability of false alarm can be expressed as

$$P_{FA,DED-AIC} \approx Pr\Big(\text{AIC}(0) - \text{AIC}(1) > \gamma_{DED-AIC} | \text{H}_0\Big) \tag{3.22}$$

According to the AIC function defined in (3.15), we have

$$\begin{aligned} P_{FA,DED-AIC} &= Pr\left(-2\log\left(\frac{\prod_{i=1}^{p}\hat{\lambda}_i^{\frac{1}{p}}}{\frac{1}{p}\sum_{i=1}^{p}\hat{\lambda}_i}\right)^{pN} + 2\log\left(\frac{\prod_{i=2}^{p}\hat{\lambda}_i^{\frac{1}{p-1}}}{\frac{1}{p-1}\sum_{i=2}^{p}\hat{\lambda}_i}\right)^{(p-1)N} - 4p + 2 > \gamma_{DED-AIC}\Big|\text{H}_0\right) \\ &= Pr\left(\log\left(\frac{\left(\frac{1}{p}\sum_{i=1}^{p}\hat{\lambda}_i\right)^{p}}{\left(\frac{1}{p-1}\sum_{i=2}^{p}\hat{\lambda}_i\right)^{p-1}\hat{\lambda}_1}\right) > \frac{4p - 2 + \gamma_{DED-AIC}}{2N}\Big|\text{H}_0\right) \end{aligned} \tag{3.23}$$

At hypothesis H_0 we have

$$\frac{1}{p}\sum_{i=1}^{p}\hat{\lambda}_i \approx \frac{1}{p-1}\sum_{i=2}^{p}\hat{\lambda}_i \approx \sigma^2 \tag{3.24}$$

Substituting (3.24) into (3.23) yields :

$$P_{FA,DED-AIC}=Pr\left(\frac{\sigma^{2p}}{\sigma^{2p-2}\hat{\lambda}_1}>exp\left(\frac{4p-2+\gamma_{DED-AIC}}{2N}\right)\middle|\mathrm{H}_0\right)$$
$$=Pr\left(\frac{\hat{\lambda}_1}{\sigma^2}<exp\left(\frac{2-4p-\gamma_{DED-AIC}}{2N}\right)\middle|\mathrm{H}_0\right) \tag{3.25}$$

Let $\mu=\left(\sqrt{N}+\sqrt{p}\right)^2$ and $\nu=\left(\sqrt{N}+\sqrt{p}\right)\left(\frac{1}{\sqrt{N}}+\frac{1}{\sqrt{p}}\right)^{\frac{1}{3}}$. Then $\frac{N\frac{\hat{\lambda}_1}{\sigma^2}-\mu}{\nu}$ converges, with probability one, to the Tracy-Widom distribution of order two [57]. The false alarm probability can be rewritten as

$$P_{FA,DED-AIC}=Pr\left(\frac{N\frac{\hat{\lambda}_1}{\sigma^2}-\mu}{\nu}<\frac{Nexp\left(\frac{2-4p-\gamma_{DED-AIC}}{2N}\right)-\mu}{\nu}\middle|\mathrm{H}_0\right) \tag{3.26}$$

Let F_2 denote the cumulative density function (CDF) for the distribution of Tracy-Widom of order two given by [57] :

$$F_2(t)=\exp\left(-\int_t^{\infty}(u-t)h^2(u)du\right) \tag{3.27}$$

where $h(u)$ is the solution of the nonlinear Painlevé II differential equation [57] :

$$h(u)=uh(u)+2h^3(u) \tag{3.28}$$

Therefore, the probability of false alarm of the DED algorithm using AIC criteria can be approximated as

$$P_{FA,DED-AIC}=F_2\left(\frac{Nexp\left(\frac{2-4p-\gamma_{DED-AIC}}{2N}\right)-\mu}{\nu}\right) \tag{3.29}$$

or, equivalently

$$\frac{Nexp\left(\frac{2-4p-\gamma_{DED-AIC}}{2N}\right)-\mu}{\nu}=F_2^{-1}\left(P_{FA,DED-AIC}\right) \tag{3.30}$$

we finally obtain the threshold

$$\gamma_{DED-AIC}=2-4p-2N\ln\left(\frac{\nu F_2^{-1}\left(P_{FA,DED-AIC}\right)+\mu}{N}\right) \tag{3.31}$$

Generally, it is difficult to evaluate the function F_2. Fortunately, it can be computed using Matlab® [57].

3.6 DED-MDL False Alarm Probability

Similar with the above derivation, when the MDL criterion is applied, we only need to modify the step in (3.23) as

$$P_{FA,DED-MDL}=Pr\left(-\log\left(\frac{\prod_{i=1}^{p}\hat{\lambda}_i^{\frac{1}{p}}}{\frac{1}{p}\sum_{i=1}^{p}\hat{\lambda}_i}\right)^{pN}+\log\left(\frac{\prod_{i=2}^{p}\hat{\lambda}_i^{\frac{1}{p-1}}}{\frac{1}{p-1}\sum_{i=2}^{p}\hat{\lambda}_i}\right)^{(p-1)N}-\left(p-\frac{1}{2}\right)\log N>\gamma_{DED-MDL}\middle|\mathrm{H}_0\right)$$
$$=Pr\left(\log\left(\frac{\left(\frac{1}{p}\sum_{i=1}^{p}\hat{\lambda}_i\right)^p}{\left(\frac{1}{p-1}\sum_{i=2}^{p}\hat{\lambda}_i\right)^{p-1}\hat{\lambda}_1}\right)>\frac{\gamma_{DED-MDL}+\left(p-\frac{1}{2}\right)\log N}{N}\middle|\mathrm{H}_0\right) \tag{3.32}$$

		$p = 100$	$p = 150$	$p = 200$
Simulation results for DED detector	$P_{FA,DED-AIC}$	0.0531	0.0518	0.0504
	$P_{FA,DED-MDL}$	0.0549	0.0533	0.0520
	$\gamma_{DED-AIC}$	3.8571e04	2.5901e04	2.1521e04
	$\gamma_{DED-MDL}$	3.6133e04	2.0979e04	1.9561e04
Analytical results for DED detector	$P_{FA,DED-AIC}$	0.0500	0.0500	0.0500
	$P_{FA,DED-MDL}$	0.0500	0.0500	0.0500
	$\gamma_{DED-AIC}$	3.7623e04	2.5274e04	1.9846e04
	$\gamma_{DED-MDL}$	3.4843e04	1.8259e04	1.7540e04

TABLE 3.1 – Simulation and analytical results of thresholds values $\gamma_{DED-AIC}$ and $\gamma_{DED-MDL}$ with $P_{FA} = 0.05$ and probability of false alarm values for DED detector using AIC and MDL criteria with different p, $N = 1000$ and SNR $= -7$dB.

We consider the same supposition given by (3.24), where the received signal involves only the noise samples. Therefore, (3.32) can be written as

$$P_{FA,DED-MDL}=Pr\left(\frac{\hat{\lambda}_1}{\sigma^2} < exp\left(\frac{\gamma_{DED-MDL}+\left(p-\frac{1}{2}\right)\log N}{N}\right)\Big|\mathrm{H}_0\right) \tag{3.33}$$

Using the Tracy-Widom proposition, the false alarm probability of the DED algorithm using MDL criteria can be rewritten as

$$P_{FA,DED-MDL}=F_2\left(\frac{Nexp\left(\frac{\gamma_{DED-MDL}+\left(p-\frac{1}{2}\right)\log N}{N}\right)-\mu}{\nu}\right) \tag{3.34}$$

where μ and ν are defined in the last section, and the threshold is given by

$$\gamma_{DED-MDL}=\left(p-\frac{1}{2}\right)\log N - N\ln\left(\frac{\nu F_2^{-1}\left(P_{FA,DED-MDL}\right)+\mu}{N}\right) \tag{3.35}$$

3.7 Performance Evaluation

In this section, we will provide a number of simulations aiming to asses the performance of the proposed detector in comparison to the reference detectors presented in Chapter 1. We will present also some numerical examples to proove the effectiveness of the proposed sensing detector and to confirm the theoretical analysis.

3.7.1 Simulation and Analytical Results Comparison

When deriving the probabilities of false alarm in Section 3.5 and Section 3.6, it was assumed that $\frac{1}{p}\sum_{i=1}^{p}\hat{\lambda}_i \approx \frac{1}{p-1}\sum_{i=2}^{p}\hat{\lambda}_i \approx \sigma^2$ at hypothesis H_0. This assumption is known not to be correct, but it was argued that it should be sufficient to obtain good theoretical results for the probability of false alarm. Note that, for the DED the threshold is not related to noise power and is computed based only on N, p and P_{FA}, irrespective of signal and noise, for the two cases using AIC and MDL criteria. The comparison results for γ_{DED} and $P_{FA,DED}$ using AIC and MDL criteria are given in Table 3.1. This table shows that the simulated false alarm and thresholds performance matches the theoretical results with a high degree of accuracy.

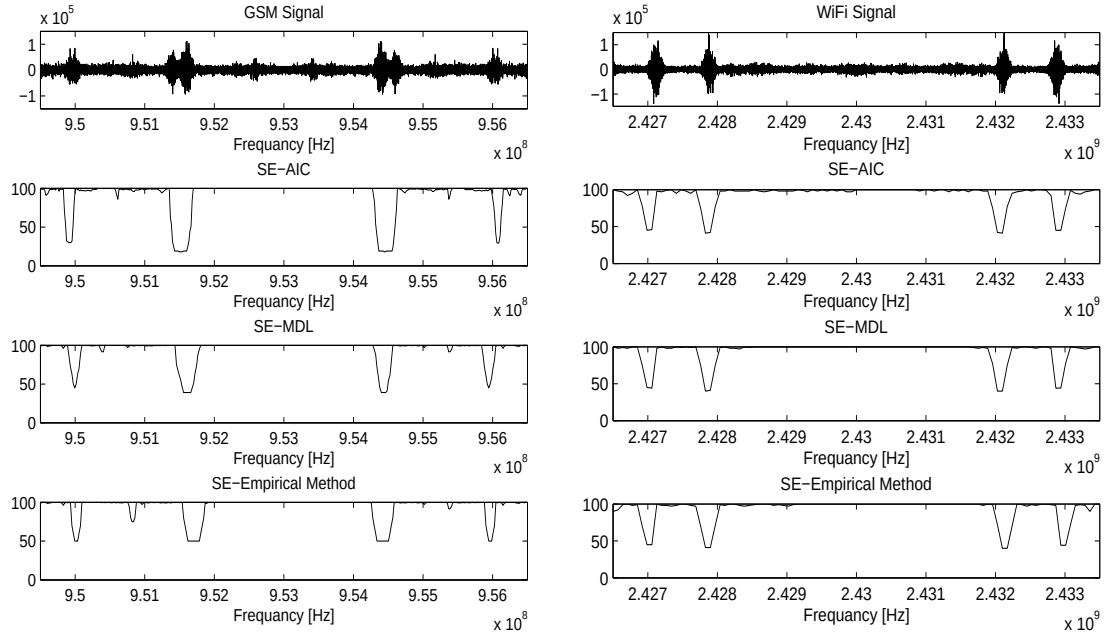

(a) GSM signal (a) WiFi signal

FIGURE 3.2 – Performance evaluation of the DED detector in terms of PU vacant sub-bands detection in the frequency domain for : (a) Baseband GSM signal at the carrier of 953MHz signal using sliding window technique with $T = 533$ samples which correspond to the GSM bandwidth (equal to 200kHz) and $L = 533$ samples, (b) Baseband WiFi signal at the carrier of 2430MHz using sliding window technique with $T = 1332$ samples which correspond to the WiFi bandwidth (equal to 500kHz) and $L = 1332$ samples.

3.7.2 Non-Cooperative Sensing Evaluation

In this subsection, we will proceed similarly as in the pervious chapter. First, we perform the proposed detector in terms of detection of vacant sub-bands in the spectrum band using sliding window in both time and frequency domains. Then, we evaluate the performances of the algorithm in terms of detection of PU presence using the binary hypothesis test.

Sub-bands Detection Figure 3.2 depicts the performance evaluation of the DED detector in terms of PU vacant sub-bands detection using GSM and WiFi signals in frequency domain. The signals parameters captured by EURECOM RF Agile Platform were given in Subsection 2.8.2. The number of observations is $N = 1000$. In a first step, we compute the covariance matrix for each analysis window. Then, we determine the position of the value that minimizes the AIC and MDL of each window, and based on these values, we can find the number of significant eigenvalues based on (3.18). The number of SE in the frequency domain is given in Figure 3.2 for both DED detectors using AIC criteria and MDL criteria. As expected, in the two cases, it is found that the numbers of SE for vacant sub-bands are clearly higher than for the other sub-bands and it is directly related to the presence/absence of data in the signal. We also compare our analytical expressions with empirical simulations. For the empirical simulations, we determine the empirical CDF of eigenvalues of each window, and based on these CDFs, we can find the number

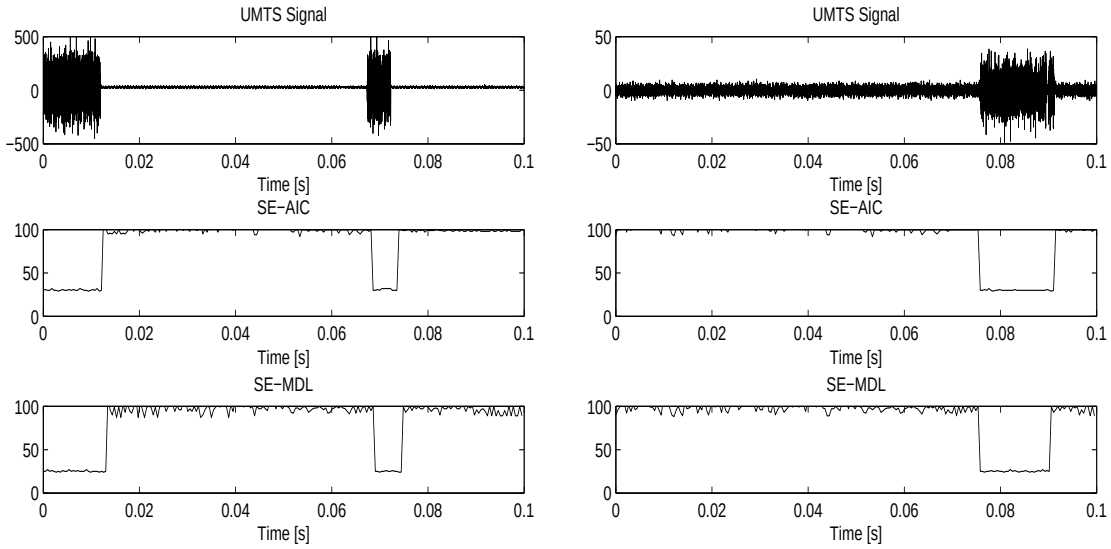

(a) SNR = 0dB (a) SNR = -10dB

FIGURE 3.3 – Performance evaluation of the DED detector in terms of PU vacant sub-bands detection in time domain for UMTS signals of duration 10ms composed by 15 slots at the carrier of 1.9GHz and a bandwidth of 5MHz.

of significant eigenvalues that capture a certain level of the signal energy (in our case 98% of the total energy for each window). The comparison shows an excellent agreement between analysis and simulation in terms of detection of vacant sub-bands in the radio band.

We consider now the sub-bands detection in time domain. A sequence of raw captured data of UMTS signals has been acquired. These signals are captured by EURECOM RF Agile Platform [51]. The raw data is represented as unsigned 16 bit integers. After this subtraction, the signals are represented with the ordinary 64 bit floating point format which is the Matlab® default. The time domain components of the captured signals are depicted in Figure 3.3 for an SNR $=$ 0dB and SNR $= -10$dB. A signal block containing 2501 samples has been extracted. A corresponding noise block is acquired by retrieving the 2501 first samples. The signal to noise ratio between these two blocks is 0dB in Figure 3.3 (a) and -10dB in Figure 3.3 (a). Note however that there is a degree of uncertainty of this estimate due to the limited number of samples. Results from the detection are summarized in Figure 3.3 using the two detection criteria AIC and MDL. From this figure, we show that, similarly to the case of frequency sub-bands detection, the proposed detector exhibits very interesting results in terms of detection holes in time domain.

PU Signal Detection Here we will assess the performance of the proposed detector in terms of PU signal detection using the binary hypothesis test expressed in (3.19) and (3.20) for the DED-AIC and the DED-MDL detectors, respectively. We will use the three different simulation scenarios presented in Subsection 1.4.3, subject to provide different attributes so that the performance can be assessed under different conditions, aiming to provide fair conditions before making conclusions. The results from these simulations can be seen in the batch Figure 3.4. The best performance is obtained from the CD detector. Subsequent is the DED using AIC criteria which has a performance in the range from approximately 0.5dB to approximately 2.5dB below the CD de-

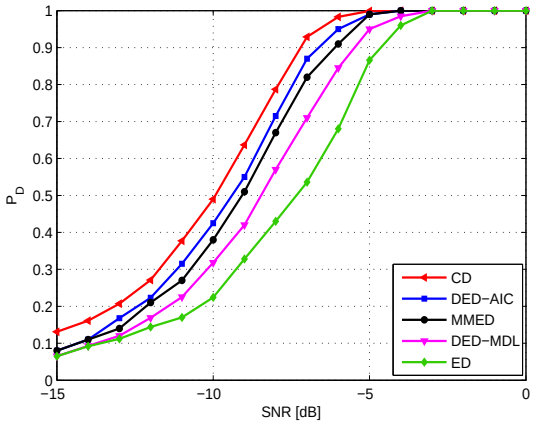

(a) P_D vs. SNR : Scenario 1

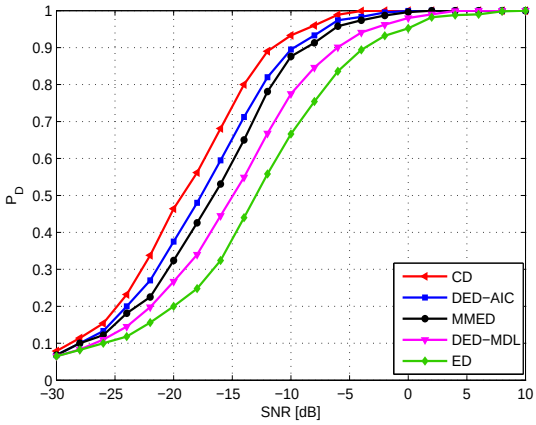

(b) P_D vs. SNR : Scenario 2

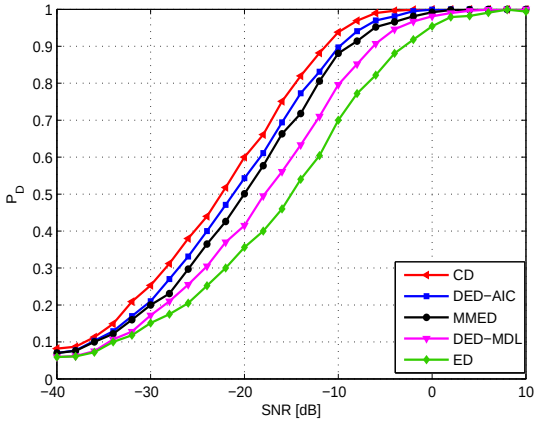

(c) P_D vs. SNR : Scenario 3

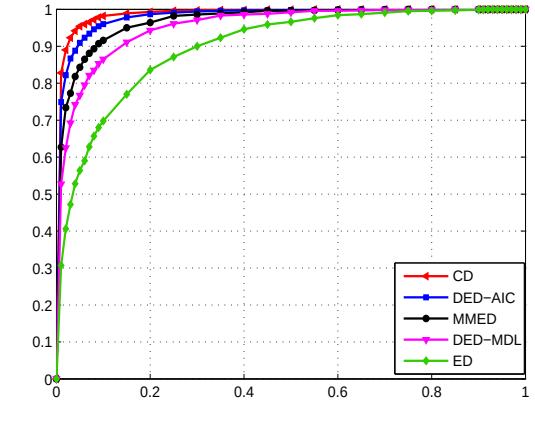

(d) ROC curves : Scenario 1

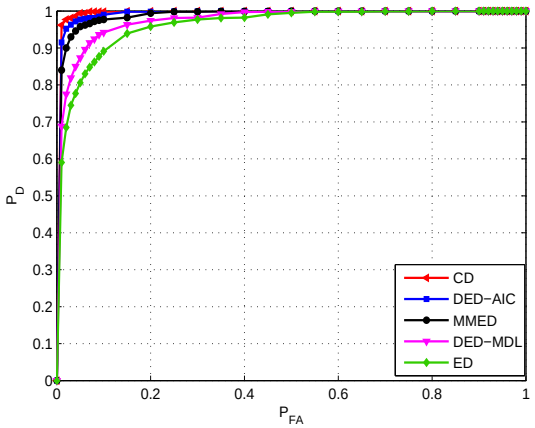

(e) ROC curves : Scenario 2

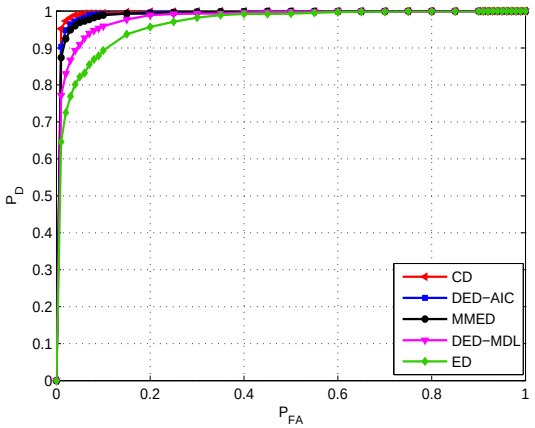

(f) ROC curves : Scenario 3

FIGURE 3.4 – Performance evaluation of the DED detector in terms of PU signal detection in non-cooperative way using an DVB-T OFDM primary user system : Probability of detection versus SNR curves with $P_{FA} = 0.05$ and ROC curves with SNR $= -7$dB, and, sensing time = $1.12ms$ and $p = 2048$.

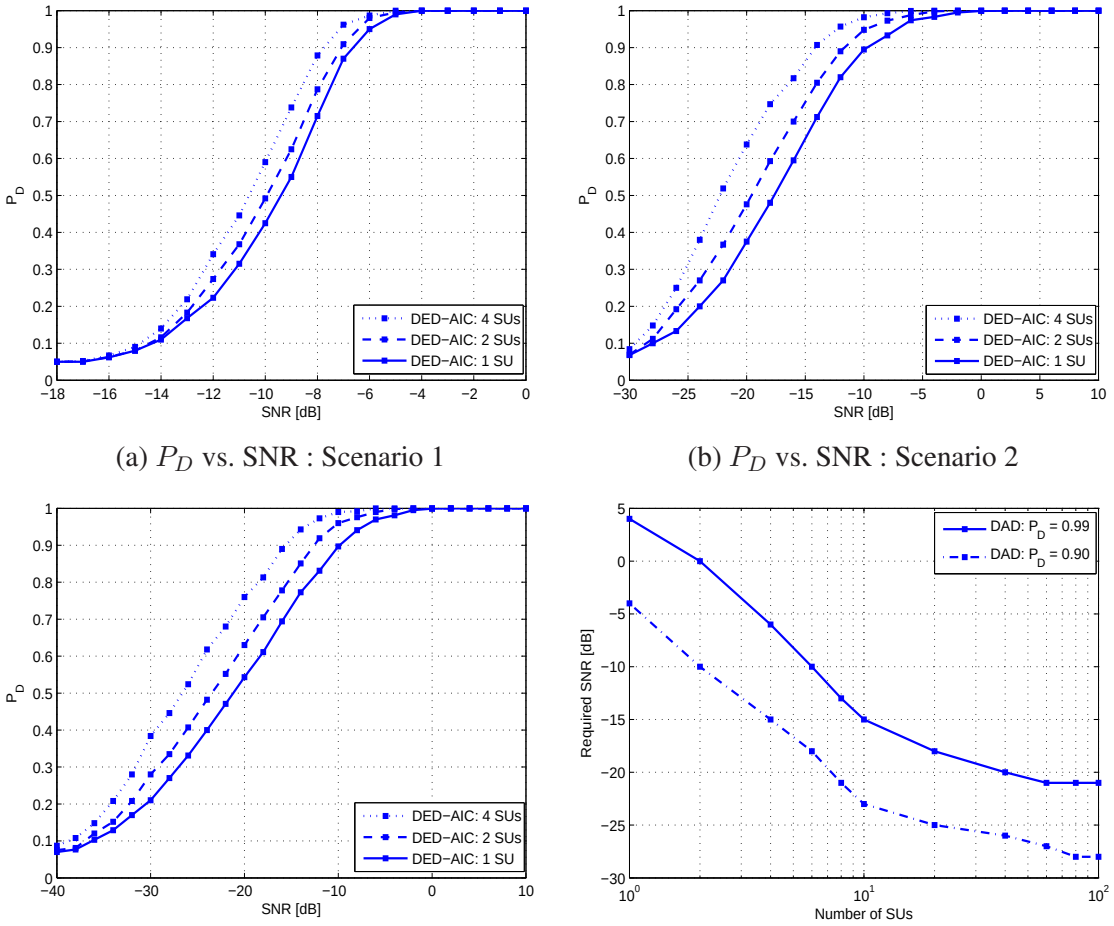

(a) P_D vs. SNR : Scenario 1

(b) P_D vs. SNR : Scenario 2

(c) P_D vs. SNR : Scenario 3

(d) ROC curves : Scenario 1

FIGURE 3.5 – Performance evaluation of the DAD detector in terms of PU signal detection in cooperative way using an DVB-T OFDM primary user system : Probability of detection versus SNR curves with $P_{FA} = 0.05$ and the required SNR versus the number of collaborating users M.

tector. Following the DED-AIC detector is the MMED detector, with a steady performance loss of approximately from 2dB to 5dB compared to CD. The worst performance is displayed by the DED-MDL detector and ED. DED-MDL performs approximately 3dB above DED-AIC, while ED differs from the DED-AIC curves with as much as approximately 8dB. In total, DED-MDL and ED can be seen to perform an average about 6dB worse than the best performance, which is obtained by the CD detector. From Figure 3.4, we remark also that relative detection results for scenario 2 and scenario 3 are to a large extent aligned with the results for scenario 1. This is expected as the underlying used signals are the same. The main difference is in absolute performance which is caused by the addition of multipath and shadow fading. It is obvious from Figures 3.4 (b) and (c) how the absolute detection performance deteriorates when the signal is subjected to channel fading. The P_D slope for all the detectors starts dropping at higher SNR values than for the AWGN case. While the P_D curves started dropping off in the range from approximately -3dB to about -5dB for the four detectors in the AWGN channel of scenario 1, all curves start dropping off before 8dB under the fading applied in scenarios 2 and 3.

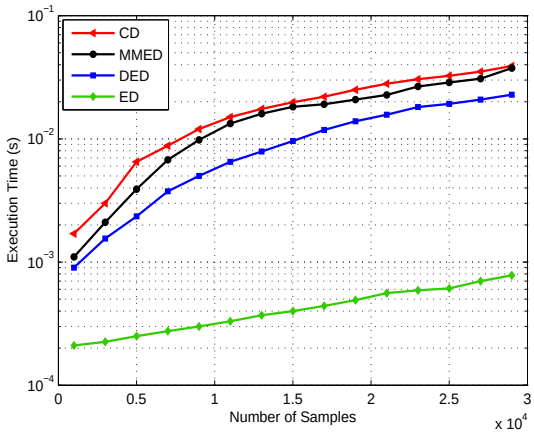

FIGURE 3.6 – Simulation results assessing the performance in terms of execution time for the DED detector compared to three detectors : Execution time versus the number of samples of the received DVB-T OFDM primary user signal.

3.7.3 Cooperative Sensing Evaluation

In this subsection, we will evaluate the performances of the DED detector in a cooperative way. Therefore, SUs share network information among each other to achieve a coordinated and efficient spectrum management and to have a better decision about the availability of the spectrum occupancy. This scenario was presented in Section 1.5. Recall, only binary decisions are shared between SUs.

Results from the simulations can be seen in the batch Figure 3.5. These figures show the impact of cooperative SUs number M in the detection performance. We plot the SNR for different numbers of cooperative users M, over the three scenarios. The false alarm probability is set to 0.05. From Figures 3.5 (a), (b) and (c) we can see that the cooperative sensing ($M > 1$) does increase the detection probability to its single user counterpart ($M = 1$), and the performance enhancement depends largely on the number of cooperative users. When M increases, the performance is getting better. These results are confirmed in Figures 3.5 (d).

3.7.4 Complexity Study

This subsection provides a brief discussion on computational complexity of the DED algorithm. In order to give an idea of the complexity of the DED algorithm, we provide in Figure 3.6 simulation results assessing the performance in terms of execution time of this algorithm in comparison with CD, MMED and ED algorithms. We use for these simulations the same conditions as in Subsection 2.8.4. From these results, we find that the CD is the most complex among all, with over 2 time complexity compared to DED. While CD and MMED have a comparable complexity. The ED is the least complex among all compared spectrum sensing algorithms.

The complexity of the DED algorithm is computed according to the different steps of the algorithm, namely computation of the covariance matrix and its corresponding eigenvalues and the derivation of AIC and MDL criterion for the DED-AIC and DED-MDL algorithms, respectively. Note that the complexity of AIC and MDL equations are equivalent because of the same number of multiplication/addition in the two equations. From the algorithm given in Section 3.4, we remark that the major complexity of this method comes from the computation of the covariance matrix

and the eigenvalue decomposition. The covariance matrix is block Toeplitz matrix and hermitian, then Np multiplications are sufficient. For the computation of eigenvalues, $O\left(p^3\right)$ multiplications are needed. MDL and AIC values are computed according to (3.15) and (3.17) with Np^2 multiplications. The total complexity of the DED algorithm is therefore

$$Np^2 + Np + O\left(p^3\right) \tag{3.36}$$

This section provided a discussion on the computational complexity of the DED algorithm. It was argued that the DED algorithm asymptotically should have a better running time than the MMED algorithm. This argument was further strengthened by simulation results. The simulations also showed that the DED algorithm have running times of approximately one to two order of magnitudes greater than the ED algorithm.

3.8 Conclusion

In the presented chapter, we have used an information theoretic based sub-space analysis for the detection of PU signal and vacant sub-bands in the primary spectrum. The proposed technique estimates the diemension of the PU received signal. Accordingly, we have explored the number of independent diversity branches, possibly the number of significant eigenvalues, determined by the value which minimizes the AIC and/or the MDL criterions.

Having looked at the spectrum sensing problem in CRN, we will address in the following chapters the problem of resource allocation.

Part II

Resource Allocation Techniques

Chapter 4

Resource Allocation for Cognitive Radio Applications

4.1 Introduction

In the second part of this thesis we address the resource allocation problem in the context of CRN with special emphasis on QoS provisioning in a number of emerging broadband wireless networks. This chapter overviews the underlying standards and/or technologies and provides a literature review of related works on resource allocation and QoS provisioning in these broadband systems. Specifically, depending on the choice of implementations, there are two approaches to allocate the spectrum resource. The first approach is based on a central controller that requires information about SUs and channel gains. This approach is referred as *centralized* solution. The second approach doesn't requires knowledge about the PU and SUs channels. This approach is so-called *distributed* solution. The centralized solution in resource allocation context demands extensive control signalling and is difficult to implement in practice if information exchange about all users and channels is limited. These two approaches will be introduced in this chapter. Particularly, we will introduce the challenges in centralized and distributed resource allocation strategies and present an overview of prior efforts. We highlight the motivation for this research, followed by a presentation of an existing resource allocation algorithm. This algorithm will serve as references when evaluating the novel approaches that resulted from the research.

The chapter is organized as follows. Section 4.2 will introduce a number of theoretical concepts of importance. It will describe the CRN that will be used throughout this second part of thesis. Section 4.3 will present the performance metrics used to evaluate the proposed resource allocation algorithms. The following two metrics are considered : PU performance metrics including the primary capacity, the outage probability and the interference outage, and, SU's performance metrics including SU's capacity, SU's sum capacity, the interference power and fairness. In Section 4.4 and Section 4.5, we will provide a rather straightforward classification of resource allocation strategies attempting to show the diversity and advantages of these techniques. Two types of resource allocation strategies, centralized strategies, and distributed strategies, are discussed in these two sections, respectively. The binary power control policy that will be used in the development of the distributed user selection strategy presented in Chapter 5, will be provided in Section 4.6. Section 4.7 describes the centralized user selection strategy that will act as reference in this part of thesis.

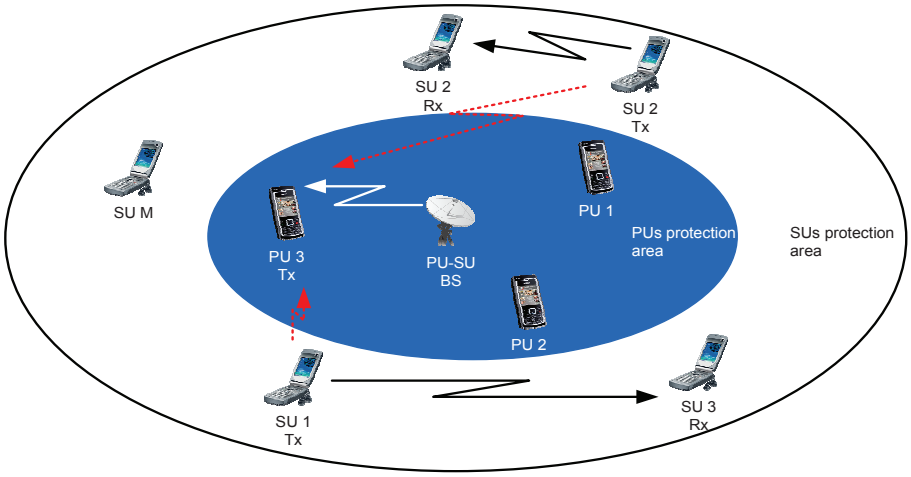

FIGURE 4.1 – The cognitive radio network with N primary users and M secondary users attempting to communicate with their respective pairs in an ad-hoc manner during a primary system transmission in downlink mode, subject to mutual interference.

4.2 Resource Allocation Goal

In order to facilitate the deployment of CR technologies for the secondary usage of spectrum, it is crucial to prove the reliable detection of PUs by SUs. In fact, primary and secondary users can coexist without a degradation of the PU transmission in order to convince regulatory authorities as well as PUs to enable such technologies. Particulary, PU will not necessarily need all that multi-rate system. In fact, the PU will experience the SU's interference, and as long as all his target rate (depending on his QoS) to be achieved, he does not care about what he leaves more. In what follows, we adopt this setting and consider a CRN in which primary and secondary users both attempt to communicate, subject to mutual interference. This is the main goal of the study in the second part of this thesis.

We consider here a wireless CRN with a collection of users randomly distributed over the geographical area considered. Users can be both transmitters and receivers. By virtue of a scheduling protocol, N PUs and M pairs of SUs are simultaneously selected from these users to communicate at a given time instant, while others remain silent. We will consider in our analysis both downlink and uplink scenarios, given in Figure 4.1 and Figure 4.2, respectively. In the downlink scenario, we assume that a BS transmits to its user which has the highest channel power gain. In the uplink scenario, its users transmit to the network's BS. We introduce also in the presented figures the interference channel gain between the n-th PU (resp. the m-th SU) and PU/BS, in the cases of the downlink/uplink scenarios, respectively. Provided that no significant scatterers are presented in the area, the channel gains between any pair of users are assumed i.i.d. in the two proposed scenarios and they depend on the position of the users in the two-dimensional plane. Each PU is allocated a unique resource slot so that it transmits in an orthogonal manner with respect to other PUs within its coverage area, i.e. no interference between different PUs like in the Orthogonal Frequency-Division Multiple Access-based (OFDMA-based). All details about the CRN parameters and the propagation model in the downlink and the uplink mode will be given in Chapter 5. In this CRN, we will consider only the case when we have one PU and M pairs of SUs.

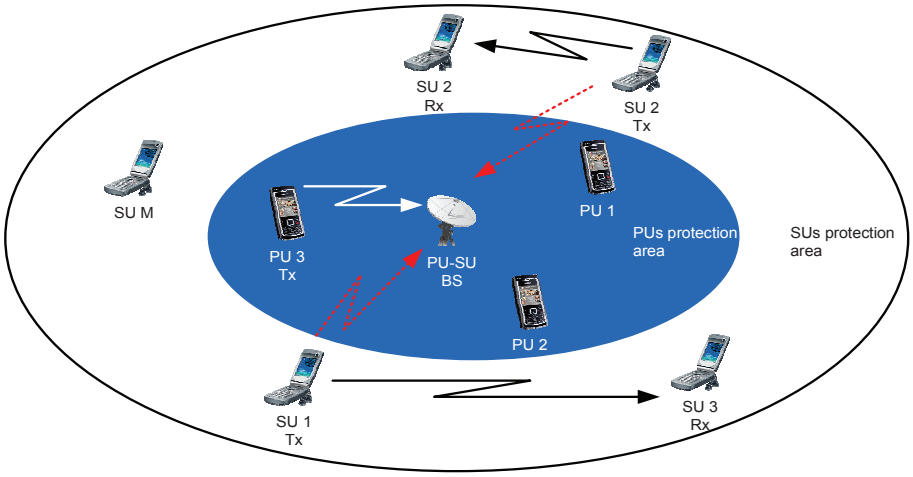

FIGURE 4.2 – The cognitive radio network with N primary users and M secondary users attempting to communicate with their respective pairs in an ad-hoc manner during a primary system transmission in uplink mode, subject to mutual interference.

In order to facilitate the problem formulation of the resource allocation problem, we state the following notations :

- the PU is indexed by pu,
- the index of SU m lies between 1 and M,
- $h_{l,m}$ denotes the channel gain from SU l to the desired user m,
- the data destined from SU m is transmitted with power p_m and a maximum power P_{max},
- $h_{pu,m}$ denotes the channel gain from the PU indexed by pu to the desired user m,
- $h_{pu,pu}$ denotes the channel gain between the BS and the PU,
- the data destined from the primary system is transmitted with power p_{pu}.

In the coverage area of the primary system, there is an *interference boundary* within which no SUs can communicate in an ad-hoc manner. Thus, as can be seen in Figures 4.1 and 4.2, for the impairment experienced by the primary system to be as small as possible, a SU must be able to detect very reliably whether it is far enough away from a primary base station, i.e., in the area of possible CR operation. Under these schemes, we allow SUs to transmit simultaneously with the PU as long as the interference from the SUs to the PU that transmits on the same band remains within an acceptable range. Specifically, we impose that SUs may transmit simultaneously with the PU as long as the PU in question does not have its QoS affected. Based on PU channel statistics, we determine a QoS bound to ensure a protection to the PU. To compute this bound, we will use the outage probability.

For system design purposes we will need to define metrics that will guide our development. These metrics need to be sufficiently broad, so that a realistic system can be designed through an optimization of all the metrics that we define. This would therefore need to include metrics to measure the performance of the CRN. These metrics will be given in the following section.

4.3 Resource Allocation Metrics

Algorithms that aid reliable resource management need to be verified and their performance has to be quantified by some metrics. In this section, we will present the performance metrics used to evaluate the proposed resource allocation algorithms.

4.3.1 Primary Users Performance Metrics

Primary Capacity In most of resource allocation strategies, algorithms must ensure that the maximum capacity of the PU resulted from the SUs transmission is no greater than some prescribed threshold. The PU instantaneous capacity is give by

$$C_{pu} = \log_2 \left(1 + \frac{p_{pu} \mid h_{pu,pu} \mid^2}{\sum_{m=1}^{M} p_m \mid h_{pu,m} \mid^2 + \sigma^2} \right) \tag{4.1}$$

where σ^2 is the ambient noise variance. Clearly, the primary capacity is directly related to the PU transmission as well as the SUs transmission.

Outage Probability The notion of *information outage probability*, defined as the probability that the instantaneous mutual information of the channel is below the transmitted code rate, was introduced in [58]. Accordingly, the outage probability can be written as :

$$P_{out}(R) = P\left\{I(\mathbf{x};\mathbf{y}) \leq R\right\} \tag{4.2}$$

where $I(\mathbf{x};\mathbf{y})$ is the mutual information of the channel between the transmitted vector $\mathbf{x}$ and the received vector $\mathbf{y}$, and R is the target data rate in (bits/s/Hz). Reliable communication can therefore be achieved when the mutual information of the channel is strong enough to support the target rate R. Thus, a $m-$th cognitive transmitter can adapt its transmit power p_m within the range of $[0; P_{max}]$ to fulfill the following two basic goals :

- *Self-goal* : Trying to transmit as much information for itself as possible,
- *Moral-goal* : Maintaining the PU's outage probability unaffected.

The outage probability can be rewritten as :

$$P_{out} = Prob\left\{\mathbf{C}_{pu} \leq R_{pu}\right\} \tag{4.3}$$

where R_{pu} is the PU transmitted data rate. The information about the outage failure can be carried out by a band manager that mediates between the primary and secondary users, or can be directly fed back from the PU to the secondary transmitters through collaboration and exchange of the CSI between the primary and secondary users.

Interference Outage The CR specific metrics relate to how well the CR is able to avoid PU and the efficiency in using available spectrum. This will require a model for PU dynamics, such as disappearance and reappearance time intervals, the amount of spectrum being used and the strength and location of the PU. In addition to the primary capacity and the outage probability, we define the interference outage meaning when the power of interference at a receiver PU exceeds a pre-defined absolute limit. Let q be this absolute limit (i.e. the maximum outage probability).

4.3.2 Secondary Users Performance Metrics

Secondary User's Capacity By making SUs access the primary system spectrum, the m-th SU experiences interference from the PU and all neighboring co-channel SU links that transmit on the same band. Accordingly, the m-th SU instantaneous capacity is given by :

$$C_m = \log_2 (1 + \text{SINR}_m) \tag{4.4}$$

where

$$\text{SINR}_m = \frac{p_m |h_{m,m}|^2}{\sum\limits_{\substack{l=1 \\ l \neq m}}^{M} p_l |h_{l,m}|^2 + p_{pu} |h_{pu,m}|^2 + \sigma^2} \tag{4.5}$$

Secondary User's Sum Capacity SUs need to recognize their communication environment and to adapt the parameters of their communication scheme in order to maximize the per-user cognitive capacity, expressed as

$$C_{su} = \sum_{m=1}^{M} C_m \tag{4.6}$$

while minimizing the interference to the PUs, in a *distributed* fashion. The sum here is made over the M SUs allowed to transmit. Moreover, we assume that the coherence time is sufficiently large so that the channel stays constant over each scheduling period length. We also assume that SUs know the channel state information (CSI) of their own links, but have no information on the channel conditions of other SUs.

Interference Power No interference cancelation capability is considered in our study. Power control is used for SUs both in an effort to preserve power and to limit interference and fading effects. The interference power (Intf) is given by :

$$\text{Intf}_m = \sum_{\substack{l=1 \\ l \neq m}}^{M} p_l |h_{l,m}|^2 + p_{pu} |h_{pu,m}|^2 + \sigma^2 \tag{4.7}$$

Combining (4.5) and (4.7), we define the SINR as a function of Intf :

$$\text{SINR}_m = \frac{p_m |h_{m,m}|^2}{\text{Intf}_m} \tag{4.8}$$

and

$$p_m = \frac{\text{SINR}_m \text{Intf}_m}{|h_{m,m}|^2} \tag{4.9}$$

Fairness In addition to the SU instantaneous capacity and the global sum capacity, other functions of SU rates are useful, as an example the fairness. Specifically, every station in the CRN transmits as much data as possible and the throughput is calculated for each of them. Both the total throughput as well as the fairness (differences in the throughput achieved by individual stations) are of interest.

4.4 Centralized Resource Allocation Strategies

In the centralized mode, the resource allocation system would require a central controller and information about all users and channels. The centralized resource allocation have been the main focus of some research efforts in CRNs. We will provide in this section some solutions to this issue that have been proposed in the literature.

The authors in [59] derived a centralized power control method for the CRN to maximize the energy efficiency of the SUs and guarantee the QoS of both the PUs and the SUs. The feasibility condition was derived in [59] and a joint power control and admission control procedure was suggested such that the priority of the PUs is ensured all the time. However, in [59] only one CRN was considered.

In [60], the authors considered spectrum sharing among a group of spread spectrum users with a constraint on the total interference temperature at a particular measurement point, and a QoS constraint for each secondary link. An optimization solution of this problem was proposed in [60] by using a game theory method. Specifically, the authors defined the secondary spectrum sharing problem as a potential game which takes different priority classes into consideration. Firstly, this game is solved through sequential play. Then a learning automata algorithm is introduced which only requires a feedback of the utility value. The same idea was proposed in [61], where the authors study a centralized auction mechanisms to allocate the received powers. They consider an objective function of maximizing utility which is a function of SINR. In [62] the authors tried to solve the centralized resource allocation problem by including a beamforming strategy. In this work, the primary systems are assumed to tolerate an amount of interference originating from secondary systems. This amount of interference is controlled by a pricing mechanism that penalizes the secondary systems in proportion to the interference they produce on the PUs.

Two centralized optimization frameworks were proposed in [63] in order to solve for the optimal resource management strategies. In the first framework, authors determine the minimum transmit power that SUs should employ in order to maintain a certain SINR and use that result to calculate the optimal rate allocation strategy across channels. In the second framework, both transmit power and rate per channel are simultaneously optimized with the help of a bi-objective problem formulation.

In [64], the authors studied the optimal power allocation strategies to achieve the ergodic capacity and the outage capacity of the SU fading channel under different types of power constraints and fading channel models. However, they ignored the QoS requirement of SU or coexistence of multiple SUs in a channel. The authors in [65] assume the same system model as in [64] and design a game to determine optimal transmit power with the objective of minimizing total transmit power. The proposed solution guarantees a level of QoS, defined by minimum rate and the target bit error rate (BER), for the primary system.

Though there have been ample research efforts on centralized resource management in CRNs, there is still a lack of a complete framework that considers QoS for SUs as well as resource management in a fair manner. One of the objective in this thesis is to take a step towards such a solution.

In a realistic network, centralized system coordination is hard to implement, especially in fast fading environments and in particular if there is no fixed infrastructure for SUs, i.e., no backhaul network over which overhead can be transmitted between users. In fact, centralized channel state information for a dense network involves immense signaling overhead and will not allow the extraction of diversity gains in fast-fading channel components. To alleviate this problem, distributed methods were proposed in the literature where SUs can get rid of PU knowledge.

4.5 Distributed Resource Allocation Strategies

In the centralized case, the need may exist, as mentioned above, for the perfect knowledge of all channel and interference state conditions for all nodes in the network. To circumvent this problem, the design of so-called distributed resource allocation techniques is crucial. Distributed optimization refers to the ability for each user to manage its local resources (e.g. rate and power control, user scheduling) based only on locally observable channel conditions such as the channel gain between the access point and a chosen user, and possibly locally measured noise and interference.

A number of distributed resource allocation strategies for CRNs have been proposed in literature. In addition to the two centralized frameworks presented in last section, the authors in [63] designed a distributed suboptimal joint coordination and power control mechanism to allocate transmit powers to SUs. A lower bound on SINR is used as a QoS constraint for SUs. In [66], the authors propose a game theoretic framework to analyze the behavior of CRs for distributed adaptive channel allocation. They define two different objective functions for the spectrum sharing games, which capture the utility of selfish users and cooperative users, respectively. The channel allocation problem is modeled in [66] to a potential game which converges to a deterministic Nash equilibrium channel allocation point. Game theory was applied in [67] to develop a distributed power allocation algorithm. In this work, each user maximizes its own utility function (which includes a pricing term) by performing a single-user price-based water-filling. However, in [67], coexistence of multiple SUs in a channel has not been considered. Also, the QoS requirement of SUs has been ignored. In [68], the authors studied the distributed multi-channel power allocation for spectrum sharing CRNs with QoS guarantee. They formulate the problem as a noncooperative game with coupled strategy space to address both the co-channel interference among SUs and the interference temperature regulation imposed by primary systems.

The authors in [69] presented a general analytical framework, in which SU's rate, frequency, and power resource can be jointly optimized under the interference temperature constraints. This framework was used to design an optimal distributed resource allocation algorithm with low polynomial time complexities in multiuser broadband CRNs. In [70], the authors focus on designing distributed resource allocation algorithms for cooperative networks. They proposed two share auction mechanisms, the SNR auction and the power auction, to distributively coordinate the relay power allocation among users. The authors in [70] demonstrate that the SNR auction achieves the fair allocation, while the power auction achieves the efficient allocation.

In [71], a framework of distributed energy efficient resource allocation was proposed for energy constrained OFDMA based CR wireless ad hoc networks. A multidimensional constrained optimization problem was formulated by minimizing the energy consumption per bit over the entire available subcarrier set for each individual user while satisfying its QoS constraints and power limit. However, in [71], the authors assume that the subcarrier detection is perfect.

In [72], the authors propose a distributed resource allocation scheme where SUs are penalized for interfering on the primary systems. The penalty is proportional to the interference rate produced from the secondary transmitter to each PU. This mechanism is referred to as pricing and is interpreted as introducing the effect of disturbance created from a user as a penalty measure in his utility function. In this means, the secondary transmitters can be controlled to choose their transmission strategies satisfying soft interference constraints on the PUs. In [73], this model of exogenous prices is used to analyze a noncooperative game between the SUs. Distributed algorithms are provided that iteratively modify the prices weights and eventually reach the Nash equilibrium that satisfies the interference temperature constraints.

4.6 Binary Power Control Policy

One basic assumption throughout this part is that a SU can vary its transmit power, under short term (minimum and peak) power constraints, in order to maximize the cognitive capacity, while maintaining a QoS guarantee to the PU. For the first proposed resource allocation algorithm, given in Chapter 5, we will use a binary power control (nodes transmitting at maximum power P_{max} or being silent). The same policy will be used in the development of the reference algorithm given in the Section 4.7.

The idea of the binary "on"/"off" power control is simple, as well as yielding quasi-optimal results in a number of cases [74]. As such, it constitutes a promising tool for making spectrum sharing a reality. Besides complexity reduction, an important additional benefit of binary power control is to allow distributed optimization. With binary power constraints, power control reduces to deciding if links should be "on" or "off". The power p_m of the m-th SU transmitter is selected from the binary set $\{0, P_{max}\}$. It is intuitively clear that if the cross-gain is sufficiently low, then all links should be "on".

The key idea within the iterative algorithm used in the development of the proposed distributed user selection algorithm is, as in [75], to subsequently limit p_m to $\{0, P_{max}\}$, i.e., to switch "off" transmission in SUs' links which do not contribute enough capacity to outweigh the interference degradation caused by them to the rest of the network. The authors in [76, 77] propose an adaptation of the distributed algorithm which allows a subset of controlled size $\tilde{M}$ of the total number of SUs M to transmit simultaneously on the same sub-band. We will give in this section a summary of the presented method in [76, 77].

Let Ψ be the set of indices of all presently active SUs. Denoting the SU which is to be potentially turned off by m, the network capacity with and without SU turned off is given by the LHS and the RHS of (4.10) respectively :

$$\sum_{l\in\Psi}\log_2\left(1+\frac{p_l \mid h_{l,l}\mid^2}{\sigma^2+p_{pu}\mid h_{pu,l}\mid^2+\sum\limits_{\substack{k\in\Psi\\k\neq l}}p_k\mid h_{k,l}\mid^2}\right)<$$
$$\sum_{\substack{l\in\Psi\\l\neq m}}\log_2\left(1+\frac{p_l \mid h_{l,l}\mid^2}{\sigma^2+p_{pu}\mid h_{pu,l}\mid^2+\sum\limits_{\substack{k\in\Psi\\k\neq l\neq m}}p_k\mid h_{k,l}\mid^2}\right) \tag{4.10}$$

We define SINR_{l_m} as :

$$\text{SINR}_{l_m}=\frac{p_l \mid h_{l,l}\mid^2}{\sigma^2+p_{pu}\mid h_{pu,l}\mid^2+\sum\limits_{\substack{k\in\Psi\\k\neq l\neq m}}p_k\mid h_{k,l}\mid^2} \tag{4.11}$$

After simple manipulations we fined :

$$(1+\text{SINR}_m)\prod_{\substack{l\in\Psi\\l\neq m}}(1+\text{SINR}_l)<\prod_{\substack{l\in\Psi\\l\neq m}}(1+\text{SINR}_{l_m}) \tag{4.12}$$

At High SINR Regime Assuming all SUs to be in "on" condition for the mentioned CRN, at high SINR regime, we have dense environment with more users within smaller geometrical area and hence a SU requires higher threshold to be active. After simple manipulation of (4.12) and assuming that $1+$ SINR $=$ SINR holds, the signal-to-interference ratio (SIR) threshold for high region comes out to be,

$$\text{SIR}_m = \frac{p_m \mid h_{m,m} \mid^2}{p_{pu} \mid h_{pu,m} \mid^2 + \sum\limits_{\substack{k \in \Psi \\ k \neq m}} p_k \mid h_{k,m} \mid^2} > e = 2.718281... \tag{4.13}$$

At Low SINR Regime By definition in the low SINR region $\ln(1+x) \simeq x$ holds with good accuracy, and binary power control is always optimal. We can go from (4.12), to come up with the active user threshold at low SINR region as,

$$\text{SIR}_m > 1 \tag{4.14}$$

Detailed derivations of the two threshold at high and low SINR are given in [76, 77]. Results given in (4.13) and (4.14) confirm, as intuition would expect, that SUs under better SINR conditions would transmit only above a higher threshold than in the low SINR regime.

4.7 Centralized User Selection Strategy

We will present in this section a centralized resource allocation strategy studied in [76, 77]. The two proposed resource allocation algorithms in Chapter 5 and Chapter 6 will be compared with this centralized one as reference algorithm. The motivation behind the centralized user selection technique is that, by opportunistically adapting their transmit power with the guide of the binary power allocation policy given in Section 4.6, SUs can maximize the achievable sum rate under the constraint of maintaining the outage probability of the PU not degraded [76, 77]. The goal within this method is thus to determine, under the assumption that the PU is oblivious to the presence of the cognitive users, what would be the cognitive system capacity (which can also be viewed as the total increase in system capacity (or spectral efficiency) due to the SUs' activity) and, at the same time, the maximum number of cognitive communication links allowed in such a system. The optimization problem was expressed as follows [76, 77] :

$$\text{Find } \; p_m|_{m=1,...,M} = \arg\max_{p_m} C_{su} \tag{4.15}$$

subject to :

$$\begin{cases} p_m \in \{0, P_{max}\}, \quad \text{for} \quad m = 1, ..., M \\ \\ P_{out} = Prob \left\{ \log_2 \left(1 + \dfrac{p_{_{pu}} \mid h_{pu,pu} \mid^2}{\sum\limits_{m=1}^{\tilde{M}_c} p_m \mid h_{pu,m} \mid^2 + \sigma^2} \right) \leq R_{pu} \right\} \leq q \end{cases} \tag{4.16}$$

where q is the maximum outage probability and $\tilde{M}_c$ is the maximum number of SUs allowed to transmit using the centralized algorithm. The centralized algorithm proposed in [76, 77] selects active SUs by checking the power and outage probability constraints iteratively.

4.8 Conclusion

This chapter presented an overview of the resource allocation problem context. We started by introducing the resource allocation goal and presenting the CRN model used in this part of thesis. We presented also the resource allocation metrics and the challenges within this research. A literature review of related works on resource allocation was discussed in this chapter. Finally, a centralized user selection strategy combined with a binary power allocation technique was presented in the last section of this chapter.

The main conclusion from the presented study is that joint resource allocation does not lend itself easily to distributed optimization because of the strong coupling between the locally allocated resources and the interference created elsewhere in the CRN. Hence the maximization of a SU capacity taken individually will not in general result in the best overall network capacity, although we suggest later cases for which the outcomes for the centralized and distributed capacity optimization will differ little. Following the above trend, we will explore in the following chapter a distributed joint resource allocation framework and then analyze what would be the loss when considering a distributed strategy. Our study will treat both downlink and uplink communications. In both cases, we will derive a distributed resource allocation algorithm and address the QoS issues for the primary system from an outage point of view.

Chapter 5

Distributed User Selection Strategy

5.1 Introduction

In this chapter, we will propose a different way to efficiently protect primary systems from SUs interference, based on outage probability. The motivation behind doing so is that, in any case, the PU will not necessarily need all that multi-rate system. In fact, the PU will experience the SU's interference, and as long as all his target rate (depending on his QoS) to be achieved, he does not care about what he leaves more. In what follows, we adopt this setting and consider a CRN in which primary and secondary users both attempt to communicate in a distributed way, subject to mutual interference. We propose a distributed CR coordination that maximizes the CRN secondary rate while keeping the interference to the PU acceptable. Our goal is to realize PU-SU spectrum sharing by optimally allocating SU transmit powers, in order to maximize the total SU throughput under interference and noise impairments, and short term (minimum and peak) power constraints, while preserving the QoS of the primary system. In particular, it is of interest to determine, in a distributed manner, the maximum number of SUs allowed to transmit threshold above which SUs can decide to transmit without affecting the PU's QoS. In such approaches, each user individually makes its decision on its transmit power so as to optimize its contribution to the system throughput. At the core of the distributed concept lies the idea that the interference is more predictable when the network is dense, and consequently the resource allocation problem of a given user becomes more dependent to the average behavior, thus facilitating distributed optimization.

Following the above trend, we will explore in this chapter a distributed joint resource allocation framework and then analyze what would be the loss when considering a distributed strategy. Our study treats both downlink and uplink communications. In both cases, we will derive a distributed power allocation algorithm and address the QoS issues for the primary system from an outage point of view.

The chapter is organized as follows. Section 5.2 describes the outage probability constraint and gives a reformulation of this probability that will be used throughout the development of the proposed user selection strategy. The same section presents also the optimization problem of the proposed strategy. In Section 5.3, the distributed user selection strategy is presented. Section 5.4 is split in two main subsections. The first subsection will introduce the propagation model that will be used to evaluate the performance of the presented strategy. The second subsection presents simulation results and a comparison with the centralized user selection strategy presented in Section 4.7. Section 5.5 concludes the chapter.

5.2 Distributed Strategy

In the current study, we adopt a QoS guarantee to the PU by means of an outage constraint. This knowledge can be obtained with a centralized mode where the resource allocation system would require information from a third party (i.e. central database maintained by regulator or another authorized entity) to schedule SUs coming. This is the case of the presented user selection strategy in Section 4.7. In fact, to compute the P_{out}, the CR system requires knowledge of the PU and SUs channels. To alleviate this problem, we propose in this chapter a distributed method where SUs can get rid of PU knowledge. In this distributed framework, the information about the outage failure can be computed without exchange of information between the primary and secondary users. In this section, we will present in a first step a reformulation of the outage probability that will be used throughout the development of the proposed user selection strategy. Then, we will present the optimization problem of this strategy.

5.2.1 Outage Probability Constraint

To proceed further with the analysis of the distributed strategy and for the sake of emphasis, we introduce the PU average channel gain estimate G_{pu} based on the following decomposition :

$$h_{pu,pu} \triangleq G_{pu} * h'_{pu,pu} \tag{5.1}$$

where $h'_{pu,pu}$ is the random component of channel gain and represents the *normalized* channel impulse response tap [74]. This gives us the following PU outage probability expression :

$$P_{out} = Prob\left\{ \log_2 \left(1 + \frac{p_{_{pu}} G_{pu}^2 \mid h'_{pu,pu} \mid^2}{\sum_{m=1}^{M} p_m \mid h_{pu,m} \mid^2 + \sigma^2} \right) \leq R_{pu} \right\} \tag{5.2}$$

Let $\tilde{M}_d$ be the maximum number of SUs allowed to transmit using the distributed method and G_{su} be the SU average channel gain estimate. If we insert these two parameters in (5.2), we obtain

$$P_{out} \simeq Prob\left\{ \frac{p_{_{pu}} G_{pu}^2 \mid h'_{pu,pu} \mid^2}{G_{su}^2 \sum_{m=1}^{\tilde{M}_d} p_m + \sigma^2} \leq 2^{R_{pu}} - 1 \right\} \leq q \tag{5.3}$$

$$\simeq Prob\left\{ \mid h'_{pu,pu} \mid^2 \leq \left(2^{R_{pu}} - 1\right) \left(\frac{\tilde{M}_d G_{su}^2 P_{max} + \sigma^2}{G_{pu}^2 p_{_{pu}}} \right) \right\} \leq q$$

From now on we assume for simplicity of analysis that the channel gains are i.i.d Rayleigh distributed. However, the results can be immediately translated into results for any other channel model by replacing the appropriate probability distribution function. Continuing from (5.3), we have :

$$P_{out} \simeq \int_0^{\left(2^{R_{pu}} - 1\right) \left(\frac{\tilde{M}_d G_{su}^2 P_{max} + \sigma^2}{G_{pu}^2 p_{_{pu}}} \right)} \exp(-t) dt \leq q \tag{5.4}$$

Finally, we get the following outage constraint :

$$P_{out} \simeq 1 - \exp\left[-\left(2^{R_{pu}} - 1\right) \left(\frac{\tilde{M}_d G_{su}^2 P_{max} + \sigma^2}{G_{pu}^2 p_{pu}} \right) \right] \leq q \tag{5.5}$$

and the maximum number $\tilde{M}_d$ of active "on" SUs that transmit with P_{max} is given by

$$0 \leq \tilde{M_d} \leq \frac{-\log(1-q)}{(2^{R_{pu}} - 1)} . \frac{G_{pu}^2 p_{pu}}{G_{su}^2 P_{max}} - \frac{\sigma^2}{G_{su}^2 P_{max}} \tag{5.6}$$

By writing SNR $= \dfrac{G_{su}^2 P_{max}}{\sigma^2}$, equation (5.6) can be expressed as :

$$0 \leq \tilde{M_d} \leq \frac{-\log(1-q)}{(2^{R_{pu}} - 1)} . \frac{G_{pu}^2 p_{pu}}{G_{su}^2 P_{max}} - \frac{1}{\text{SNR}} = \tilde{M}_{theory} \tag{5.7}$$

where $\tilde{M}_{theory}$ is the theoretic maximum number of SUs allowed to transmit. The LHS in (5.7) prevents from obtaining a negative number of users when the SNR decreases significantly. The formula in (5.7) points out that the number of SUs allowed to transmit increases as their SNR increases.

5.2.2 Optimization Problem

The SUs offer the opportunity to improve the system throughput by detecting the PU activity and adapting their transmissions accordingly while avoiding the interference to the PU by satisfying the QoS constraint on outage. We present in this subsection a distributed user selection strategy using the binary power allocation policy given in Section 4.6. The proposed strategy tries to limit the number of SUs interfering with the PU so as to guarantee the QoS for the primary system. Specifically, a SU will be deactivated if its action results in an increase in the cognitive capacity of SUs or if its transmission violates the PU outage constraint. The optimization problem can therefore be expressed as follows :

$$\text{Find } \; p_m|_{m=1,...,M} = \arg\max_{p_m} C_{su} \tag{5.8}$$

subject to :

$$\begin{cases} p_m \in \{0, P_{max}\}, \quad \text{for} \quad m = 1, ..., M \\ \\ 0 \leq \tilde{M_d} \leq \dfrac{-\log(1-q)}{(2^{R_{pu}} - 1)} . \dfrac{G_{pu}^2 p_{pu}}{G_{su}^2 P_{max}} - \dfrac{1}{\text{SNR}} \end{cases} \tag{5.9}$$

where $\tilde{M}_d$ is the maximum number of SUs allowed to transmit using the distributed algorithm and q the maximum outage probability. As we can see from (5.9), the CR system does not require knowledge about the PU and SUs channels in the sense that it decides *distributively* to either SU transmit data or stay silent over the channel coherence time depending on the specified P_{out} threshold (q). On the other hand, the optimization problem given by (4.16) requires all $h_{m,pu}$ and $h_{pu,pu}$ data to compute the outage probability and to select then the SUs able to transmit without affecting the PUs' QoS.

5.3 User Selection Algorithm

So far, we have studied the optimization problem of the distributed approach for user selection. In this section, we will present a distributed algorithm where joint power allocation and channel-aware user selection are used, in the view of maximizing the sum of users' rates. We will describe also the centralized algorithm given in Section 4.7 which observes the global network and makes decisions about the SUs that are able to transmit without affecting the PU outage probability. The goal here is to compare the centralized approach to the distributed scheme in terms of users "on" and the average rate.

The pseudo-code for the proposed approach and the centralized one are given in Algorithm 1. An iterative approach is adopted throughout this algorithm. The algorithm is first initialized with a zero power allocation vector. Each SU simultaneously measures its SIR, and depending on whether it is on high or low average SINR, respectively, he remains active or inactive during the next time slot based on (4.13) and (4.14), respectively. Similarly, at every iteration of the Monte Carlo simulation, inequality (4.13) and (4.14) are evaluated for the SU in question based on the power allocation resulting from the previous step, and the power allocation vector is updated. In Algorithm 1, $\tilde{M}_{theory}$ is the number of SUs allowed to transmit ruled by (5.7) and IT_{max} is the maximum number of iteration and is equal to 10^4 in the simulations results.

Algorithm 1 Distributed and centralized user selection strategies using binary power allocation policy

for $it = 1 : IT_{max}$ **do**
  $p_m^{(it)} = 0 \quad \forall m$
  $\tilde{M}_d^{(it)} = 0$ and $\tilde{M}_c^{(it)} = 0$
  while $\left(\tilde{M}_d^{(it)} \leq \tilde{M}_{theory}\right)$ **or** $\left(P_{out}^{(it)} \leq q\right)$ **do** ▷ Distributed and centralized constraints
    for $m = 1 : M$ **do**
▷ At high SINR regime
      if $\text{SIR}_m^{(it)} > e$ **then**
        $p_m^{(it)} \leftarrow P_{max}$
      end if
▷ At low SINR regime
      if $\text{SIR}_m^{(it)} > 1$ **then**
        $p_m^{(it)} \leftarrow P_{max}$
      end if
      if $p_m^{(it)} = P_{max}$ **then**
▷ Centralized case
        if $P_{out}^{(it)} \leq q$ **then**
          $\tilde{M}_c^{(it)} \leftarrow \tilde{M}_c^{(it)} + 1$
        end if
▷ Distributed case
        if $\tilde{M}_d^{(it)} \leq \tilde{M}_{theory}$ **then**
          $\tilde{M}_d^{(it)} \leftarrow \tilde{M}_d^{(it)} + 1$
        end if
      end if
    end for
  end while
end for

In the centralized case, where PU's QoS constraint is guaranteed based on (4.16), each PU verifies the outage probability constraint based on the resulting power allocation, within each iteration. In fact, in the first iteration SU_1 checks its power and outage probability constraints. If one of the two constraints is not verified, SU_1 will be switched "off" and will be considered inactive during the next time slot. We perform the same tests for all SUs to obtain in the last step the maximum number of active SUs $\tilde{M}_c$. In this case, the last SU entering in the system is removed from the transmission. In the distributed case, where the PU's QoS is insured by means of (5.9), we compute the number of SUs allowed to transmit using (5.7). The value of $\tilde{M}_{theory}$ is computed with a distributed manner. We choose in this case comprehensively the SUs that guarantee a QoS to PU by maintaining the PU's outage probability unaffected.

In traditional systems, a centralized entity, for instance the BS, decides which user is allowed to transmit at each time slot. If the BS cannot schedule a user which contributes enough capacity to the system to outweigh the interference produced, it will remain silent on that specific time slot. However, in current CR protocols (e.g. the IEEE 802.22 Wireless Regional Area Network (WRAN) [78]), SUs are supposed to be willing to collaboratively relay their proper SIR in order to protect the PU's instantaneous rate. Therefore, it is essential for the cognitive user to obtain the message from the other SU in real time (via a broadcast channel), and to be strictly synchronized with the rest of SU. Obviously, the SUs are supposed to be identified thanks to a specified beacon in transmission. Specifically, we will consider a system where devices are scheduled no longer by the BS but by a specified SU. Under the user selection distributed protocol, cognitive users listen to the cognitive signaling channel broadcasted by the cluster head user and, depending on the constraints considered previously, determine, either in time or frequency, the SU allowed to transmit with P_{max}.

5.4 Performance Evaluation

This section will provide a number of simulations aimed at assessing the performance of the proposed distributed user selection method in comparison with the centralized reference method. The section is split in two main subsections. The first subsection will provides the propagation model used to evaluate the performance of the proposed algorithm, and, the second subsection presents the simulations results.

5.4.1 Propagation Model

To go further with the analysis, we resort to realistic network simulations. Specifically, we consider a CRN as described in Figure 4.1 and Figure 4.2, in the downlink and the uplink mode, respectively, with one PU and M SUs attempting to communicate during a transmission, subject to mutual interference. A hexagonal cellular system functioning at 1.8GHz with a secondary cell of radius R and a primary protection area of radius R_p is considered. Secondary transmitters may communicate with their respective receivers of distances $d < R_p$ from the BS. We assume that the PU and the SUs are randomly distributed in a two-dimensional plane as shown in Figure 5.1. The BS is placed at the center $(0, 0)$. The distances, d_m, from the m-th SU to the BS, and, $d_{pu,m}$, between the PU and the m-th SU, are given by

$$d_m = \sqrt{x_m^2 + y_m^2} \tag{5.10}$$

and

$$d_{pu,m} = \sqrt{(x_{pu} - x_m)^2 + (y_{pu} - y_m)^2} \tag{5.11}$$

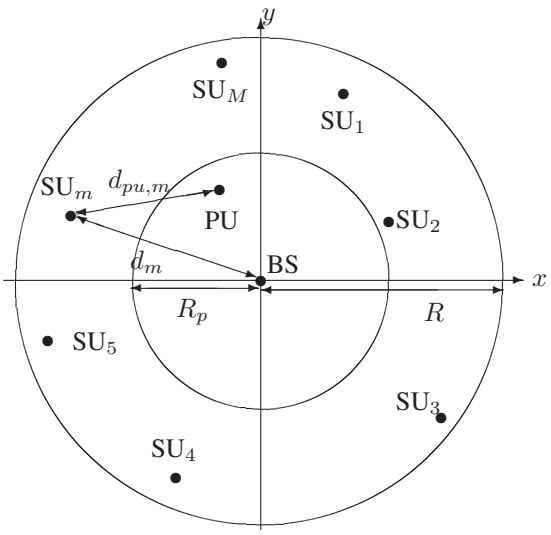

FIGURE 5.1 – Two-dimensional plane of the cognitive radio network topology with one primary user and M secondary users.

respectively, where (x_{pu}, y_{pu}) and (x_m, y_m) are the coordinates of the PU and the m-th SU, respectively. With the same manner, we can define the distance, $d_{m,l}$, between a pair of SU's, transmitter and receiver, m and l.

The channel gains are based on the COST-231 Hata model [79] including log-normal shadowing with standard deviation of 10dB, plus fast-fading assumed to be i.i.d. circularly symmetric with distribution $\mathcal{CN}(0,1)$. The basic path loss for the COST-231 Hata model (in dB) in an urban area at a distance d is defined as :

$$PL = 46.3 + 33.9\log_{10}(f_c) - 13.82\log_{10}(h_b) - A_M + (44.9 - 6.55\log_{10}(h_b))\log_{10}(d) + C_M \tag{5.12}$$

where f_c is the carrier frequency equal to 1.5GHz and h_b is the base antenna height equal to 50 meters. The distance d is computed using the formula (5.11) or (5.10). C_M is 0dB for medium sized cities and suburbs and 3dB for metropolitan areas. In the simulations, we take $C_M = 0$dB. A_M is defined for urban environment as :

$$A_M = 3.20\,(\log_{10}(11.75h_m))^2 - 4.97 \tag{5.13}$$

where h_m is the mobile antenna height equal to 10 meters. The shadowing variations of the path loss can be calculated from the log-normal distribution

$$g(x \mid \sigma) = \frac{1}{\sigma\sqrt{2\pi}} \exp\left(\frac{-x^2}{2\sigma^2}\right) \tag{5.14}$$

where σ is the variability of the signal equal to 10dB. The shadowing variation is computed using the Matlab® function $randn$. Shadowing reflects the differences in the measured received signal power with relation to the theoretical value calculated by path loss formulas. Averaging over many received signal power values for the same distance, however, yields the exact value given by path loss.

The peak power constraint is given by $P_{max} = 1$Watt while the power ratio K is taken equal to 10 for the downlink mode and equal to 1 for the uplink mode. This is justified in the light of the

fact that the power control transmitted by the BS is generally taken almost ten times the primary user transmitted power in multiple possible standards. Both centralized and distributed strategies in the downlink and the uplink scenario are implemented using the software package Matlab® R2009a.

5.4.2 Simulation Results

The performance of the proposed distributed user selection strategy is evaluated by Monte Carlo simulations ($IT_{max} = 10^4$). It is assumed that the maximum outage probability $q = 1\%$ for both distributed and centralized algorithms. We considered also that the radius of the secondary cell $R = 1000$ meters and the radius of the primary protection area $R_p = 600$ meters. The derivation of the maximum number of SUs allowed to transmit using the distributed algorithm is based on the average channel gains G_{su} and G_{pu} estimation. From the locations of the users in the two-dimensional plane and the propagation characteristics of the environment, we can estimate the two average channel gains for the downlink and the uplink mode. These values are estimated assuming a wireless ad hoc network affected by a large number of interferers. From simulation results, using $M = 500$ SUs and one PU, we find $G_{pu}^2/G_{su}^2 \simeq 15$ in the downlink mode and $G_{pu}^2/G_{su}^2 \simeq 20$ in the uplink mode.

Figure 5.2 shows the behavior of the distributed strategy in comparison with the centralized one, presented in Section 4.7, for both downlink and uplink scenarios. This figure presents the number of active SUs versus the total number of SUs ranging between 1 user and a maximum of 140 users, and using different rate values (0.1, 0.3 and 0.5bits/s/Hz). From this figure, it is clear that the distributed strategy always outperforms the centralized one. Generally, we found out that the distributed scheme presents almost 3 additional active SUs than the centralized scheme. This can be explained by the fact that, the number of active SUs in the centralized case is computed iteratively and in the distributed one, we know in advance the maximum number of active SUs (computed distributively) so, the algorithm is run until the maximum number $\tilde{M}_{theory}$ is reached. In fact, in the distributed case, we compute $\tilde{M}_{theory}$ distributively using the average channel gains G_{su} and G_{pu} and if this maximum number of active SUs is reached, all remaining SUs will be considered inactive. As explained in the first paragraph of this section, the two average gains are estimated using a large number of SUs and a number of iteration equal to 10^6 iterations. These conditions give more flexibility for the distributed algorithm and we have in this case a broader concept. In the centralized case, however, the proposed algorithm in [76, 77] selects active SUs using an iterative strategy by computing in each iteration the outage probability knowing all channel gains for the selected SUs (active) until this iteration. The majority of classic algorithms derived in the literature do not use the same concept and select active SUs with an exhaustive manner among all SUs. In fact, in the first step of this centralized algorithm, all SUs are taken inactive (”off”) and in each iteration, SU_m checks its power and outage probability constraints. If the two constraints are verified, SU_m will be switched ”on” and will be considered active during the next time slot. Here, the last SU entering in the system is removed from the transmission. We also remark from Figure 5.2 that the number of active users in the downlink always outperforms the uplink configuration. This can be explained by the fact that, as far as the downlink system is considered, the power received from BS is K times the power in the uplink. This results on better PU's QoS guarantee. In fact, at a rate $= 0.3$bits/s/Hz, 12 SUs are allowed to transmit in the downlink and 7 SUs in the uplink, when we have saturation of the number of active SUs. We also remark that, asymptotically, i.e., as the number of SUs goes large, the number of active SUs keeps constant due to the influence of interference impairments on the PU's QoS. This tends to confirm the intuition from formula (5.7) where the number of active SUs is always upper-bounded

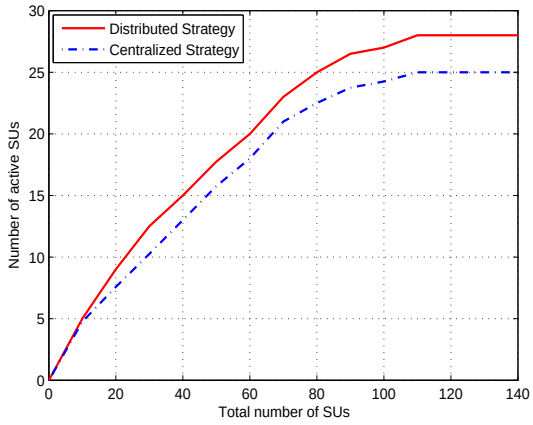

(a) Downlink : rate = 0.1bits/s/Hz

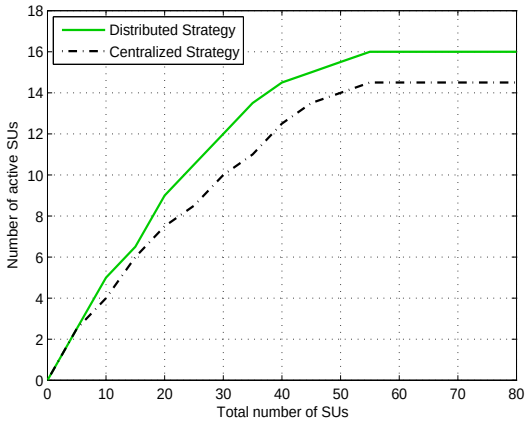

(b) Uplink : rate = 0.1bits/s/Hz

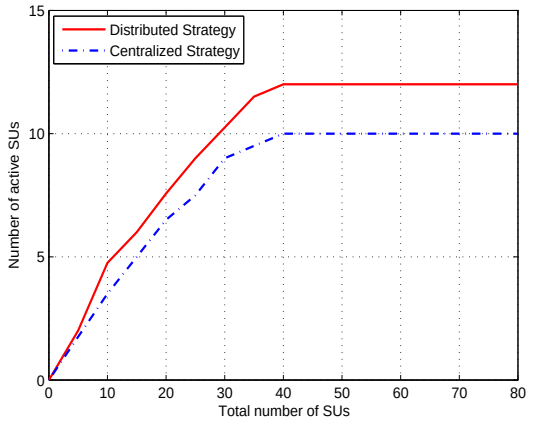

(c) Downlink : rate = 0.3bits/s/Hz

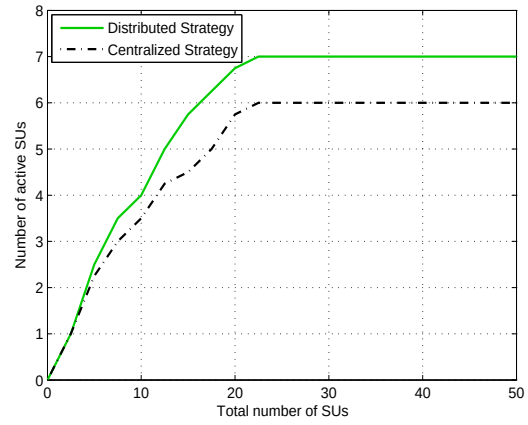

(d) Uplink : rate = 0.3bits/s/Hz

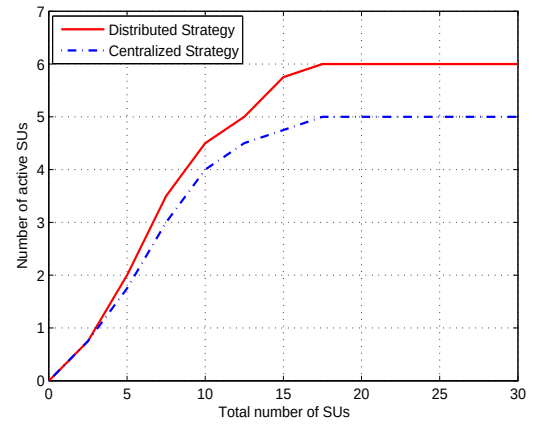

(e) Downlink : rate = 0.5bits/s/Hz

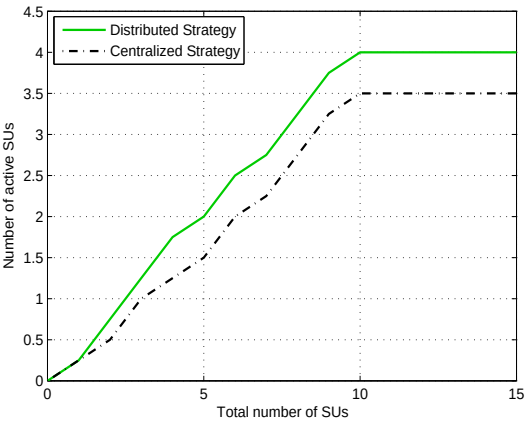

(f) Uplink : rate = 0.5bits/s/Hz

FIGURE 5.2 – Performance evaluation of the distributed user selection strategy in comparison with the centralized one : Number of active secondary users versus total number of secondary users for different rates (0.1, 0.3 and 0.5bits/s/Hz) and $q = 1\%$ in the downlink and the uplink mode.

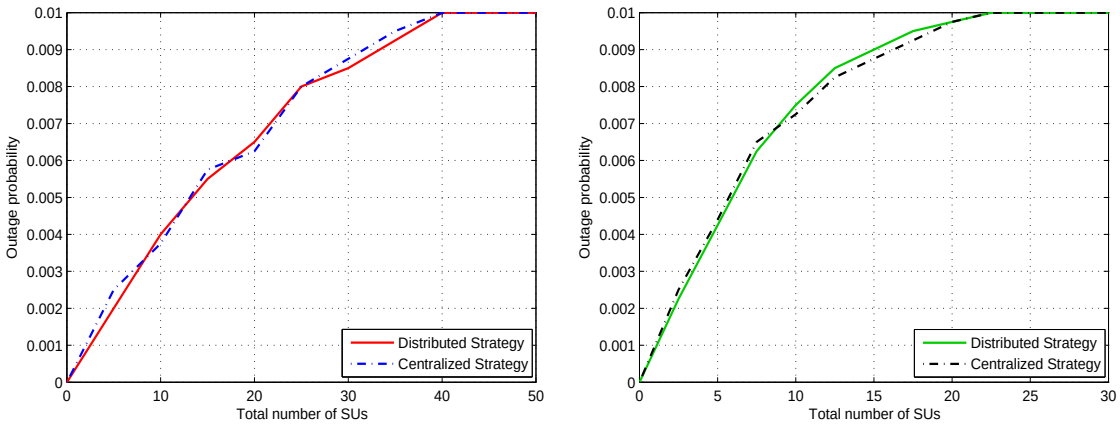

(a) Downlink (b) Uplink

FIGURE 5.3 – Performance evaluation of the distributed user selection strategy in comparison with the centralized one : Outage probability as function of the number of secondary users for a target outage probability = 1% and a rate = 0.3bits/s/Hz in the downlink and the uplink mode.

by $\tilde{M}_{theory}$ in the distributed case, and PU outage probability protection given by the maximum outage q.

In order to validate results in Figure 5.2 and the theoretical derivation given in Section 5.2, we compare the centralized outage probability expressed in (4.16) to the distributed one given in (6.15) using $\tilde{M}_{theory}$. As an example we carry out simulations for a rate = 0.3bits/s/Hz. First, it is shown from Figure 5.3 that the distributed algorithm guarantees a good protection for the PU as well as the centralized one. We also remark that, for the outage probability of interest (i.e., $q = 1\%$), the number of allowed SUs to transmit is equal to 40 for the downlink and 22 for the uplink. This is exactly what Figures 5.3 (a) and (b) show, respectively, in the saturation state at a rate = 0.3bits/s/Hz. From the presented results, we verified that we can maintain a QoS guarantee to the PU. The question now, under the assumption that the PU outage probability is unaffected, what would be the cognitive system capacity presented by the sum SU's capacity as expressed in (4.6).

Figure 5.4 (a) depicts the sum SU's capacity in the case of the distributed strategy for both downlink and uplink, and using $R = 1000$ meters and $R_p = 600$ meters. As expected, it is found that the capacity of the uplink system outperforms that of downlink system. On the other side, increasing the number of SUs yields significantly increase in capacity because the increase in degree of freedom more than compensates for the decrease in SINR due to interference. However, reaching a certain number of SUs, the sum SU's capacity stabilizes. In addition, the current curve claims that in CRN, when one attempts to maximize the number of active SUs, the cognitive capacity degrades asymptotically. Typically, there is a fundamental trade-off between cognitive capacity maximization and number of active SUs maximization. We compute also the SU's capacity in the case of the centralized user selection strategy and we find practically the same results. This confirms the very good matches between the distributed and the centralized method. Now, we change the size of the radius of the secondary cell and the primary protection area to $R = 500$ meters and $R_p = 300$ meters, respectively. From Figures 5.4 (a) and (b), we remark that, as the radius R and R_p decrease, the sum SU's capacity becomes more sensitive to the interference impairments leading to a significant decrease in the sum secondary rate.

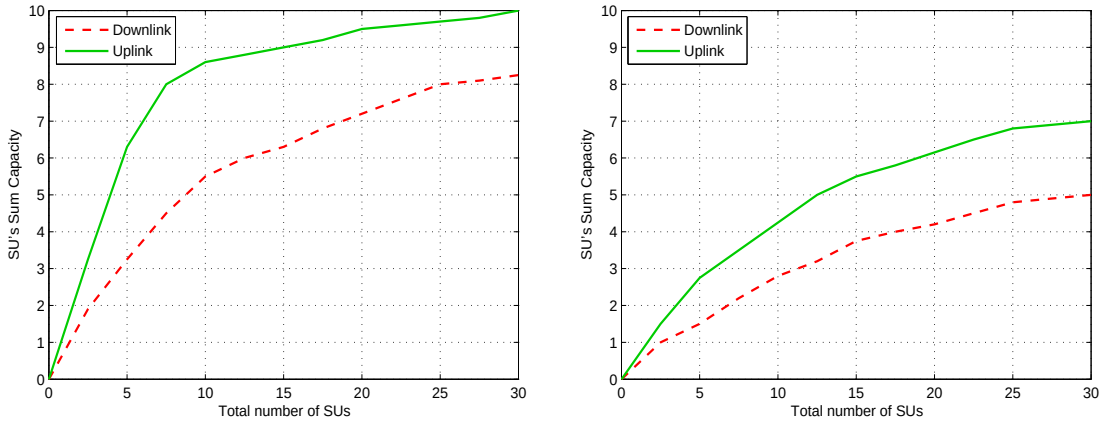

(a) $R = 1000$ and $R_p = 600$ meters (b) $R = 500$ and $R_p = 300$ meters

FIGURE 5.4 – Performance evaluation of the distributed user selection strategy in term of sum secondary user's capacity with $q = 1\%$ and a rate = 0.3bits/s/Hz in the downlink and the uplink mode using different radius of the secondary cell and primary protection area : ($R = 1000$ meters, $R_p = 600$ meters) and ($R = 500$ meters, $R_p = 300$ meters).

5.5 Conclusion

In this chapter, we explored the idea of combining multi-user diversity gains with spectral sharing techniques to maximize the SU sum rate while maintaining a QoS to a PU with a distributed manner. Our contribution within this work is the investigation of the QoS issues from an outage point of view. In particular, we explored a distributed user selection strategy. Simulation results based on a realistic network setting are shown to exhibit interesting features in terms of CRN deployment while maintaining QoS for the primary system by means of outage probability. In particular, we showed that in such CRN, one should make a trade-off between cognitive capacity maximization and number of active SUs maximization. In the following chapter, we will propose a second user selection strategy using multiuser MIMO SU system.

Chapter 6

Centralized Beamforming User Selection Strategy

6.1 Introduction

To enable the use of opportunistic spectrum sharing, many problems have to be solved. The interference caused by sharing the same radio channel becomes an obstacle that limits system performances, such as the system throughput. Thus, when sharing the spectrum with the PU, one tries to find a way to increase the throughput. It is known that the interference from SUs transmitters to a PU receiver can approach zero if it is mitigated by using an advanced signal processing technique such as beamforming on the secondary system's side. Consequently, this chapter investigates a multiuser MIMO SU system from a beamforming perspective.

Developing scheduling strategies to best exploit multiuser diversity in multiuser MIMO systems with finite number of users and evaluating the capacity limit achieved by those strategies have remained an active area of research. The authors in [80] proposed opportunistic beamforming where resources are allocated to only one user who has the best equivalent channel created by the multiple antennas and beamforming. In [81], a random beamforming technique was proposed, where the best single user is selected in communication based on the limited feedback information from the users. In [82], the authors studied multiuser diversity gain by selecting a single user or selecting multiple users simultaneously communicating in downlink.

In this chapter we focus on the beamforming problem in the context of CR using multiuser MIMO SU system in a centralized way. We consider the primary system of a single CRN, where cognitive transmitters transmit signals to a number of SUs using adaptive antennas, while the primary BS receives its desired signal from a primary transmitter and interference from all the cognitive transmitters. With the deployment of K antennas at each SU transmitter, an efficient transmit beamforming technique combined with user selection is proposed to maximize the sum throughput and satisfy the SINR constraint, thus limiting interference to the primary BS. Using this approach, transmit beamforming weights can be found.

The rest of the chapter is organized as follows. Section 6.2 describes the channel model and redefines the PU and SU's parameters given in Section 4.3. In Section 6.3, we design the transmit and receive beamvectors under the power and outage probability constraints. In Section 6.4, we present the user selection algorithm. Simulation results and a comparison with the centralized and the distributed user selection strategies are provided in Section 6.5, and Section 6.6 concludes the chapter.

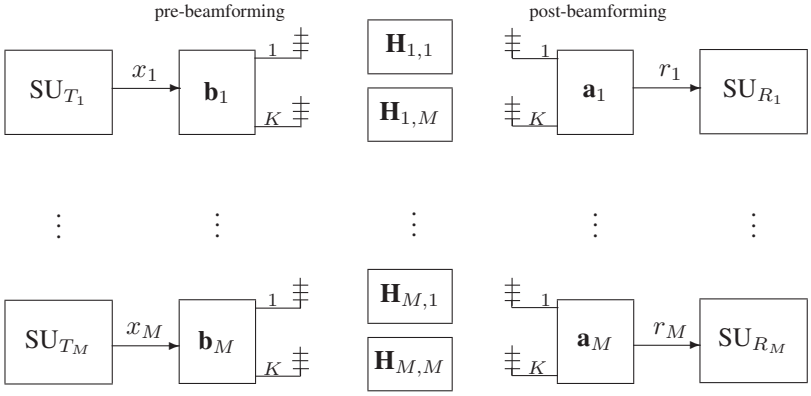

FIGURE 6.1 – Multiple transmit and receive secondary users system structure.

6.2 Secondary Users MIMO System

In this section, we will describe the SU MIMO system model and multiuser diversity scheme that we are considering in this chapter, and discuss the primary and secondary users metrics when we use a SU MIMO system. We will reformulate the resource allocations metrics given in Section 4.3 when we use a SU single-input-single-output (SISO) system.

The proposed system in this chapter consists of multiple transmit/receive SU links randomly distributed over the geographical area considered. MIMO systems have great potential to enhance the capacity in the framework of wireless cellular networks [83, 84]. Multiple antennas can for example be deployed at a cognitive BS. Many wireless network standards provision the use of transmit antenna arrays. Using baseband beamforming, it is possible to steer energy in the direction of the intended users, whose channels can often be accurately estimated [84, 85]. Beamforming has been also exploited as a strategy that can serve many users at similar throughput. Moreover, beamforming has the advantage of limiting interference. Thus, we are interested in transmit beamforming schemes for cognitive transmission. For this purpose, we utilize joint beamforming that implies an extension to the transmitter side of classical receive beamforming [86].

The SU system structure is based on beamforming at both the transmitter (K antennas) and the receiver (K antennas) for each SU link as given in Figure 6.1. The number of secondary transmitters (SU$_T$) is equal to M, and is equal to the number of secondary receivers (SU$_R$). Assuming that many scatterers are located around the transmitter and receivers, the channel coefficient matrix $\mathbf{H}_{rt}$ (the channel between the t-th transmit SU and the r-th receive SU) exhibits flat fading. The channel gain vector $\mathbf{h}_{pu,m}$ from the PU indexed by pu to a desired SU m (m between 1 and M) is given by :

$$\mathbf{h}_{pu,m} = [h_{pu,m_1} ... h_{pu,m_K}]^T \tag{6.1}$$

where the channel gains are assumed i.i.d. random variables. We consider that the channels between different users are independent. We then set the received signal of the m-th user as follows (the index of SUs m lies between 1 and M) :

$$\mathbf{y}_m = \mathbf{H}_{m,m}\mathbf{s}_m + \sum_{l=1,l\neq m}^{M} \mathbf{H}_{m,l}\mathbf{s}_l + \mathbf{h}_{pu,m}x_{pu} + \mathbf{n}_m, \quad m = 1, ..., M \tag{6.2}$$

with $\mathbf{n}_m$ of size $K \times 1$ being zero-mean i.i.d. Gaussian noise with power σ_m^2, and K being the number of antennas. $\mathbf{s}_m$ is the transmit vector of size $K \times 1$ for the m-th SU and x_{pu} being the

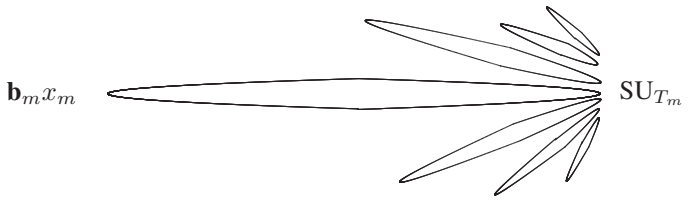

FIGURE 6.2 – Beamforming concept for the m-th secondary user transmitter.

transmit sample sent from PU. $\mathbf{y}_m$ is the receive vector of size $K \times 1$. $\mathbf{H}_{m,m}$ ($K \times K$ matrix) is the channel between the m-th SU_T and the m-th SU_R and $\mathbf{H}_{m,l}(l = 1, ..., m-1, m+1, ..., M)$ are channel matrices between the other SUs, referred to as the *interference channel matrices*.

Here, a joint beamforming approach is proposed for the SU system, that is, all the transmitters and receivers exploit a beamforming architecture [84]. The transmission scheme is characterized by the power allocation (eigenvalues of the transmit covariance matrix) and the orientation (eigenvectors of the transmit covariance matrix) [87]. This yields

$$\mathbf{s}_m = \mathbf{b}_m x_m, \quad m = 1, ..., M \tag{6.3}$$

where $\mathbf{b}_m$ is the pre-beamforming vector and x_m is the transmit sample for m between 1 and M (see Figure 6.2). The output of the m-th receiver beamformer is :

$$\begin{aligned} r_m =& \mathbf{a}_m^H \mathbf{y}_m \\ =& \mathbf{a}_m^H \mathbf{H}_{m,m} \mathbf{b}_m x_m + \mathbf{a}_m^H \sum_{l=1, l\neq m}^{M} \mathbf{H}_{m,l} \mathbf{b}_l x_l + \mathbf{a}_m^H \mathbf{h}_{pu,m} x_{pu} + \mathbf{a}_m^H \mathbf{n}_m \end{aligned} \tag{6.4}$$

where $\mathbf{a}_m$ is the post-beamforming vector at the receive SUs. $\Phi_m = E\{\mathbf{n}_m \mathbf{n}_m^H\}$ is the associated covariance matrix. The SINR defined in (4.5) at the m-th SU can be rewritten as :

$$\begin{aligned} \mathrm{SINR}_m =& \frac{E\{|\mathbf{a}_m^H \mathbf{H}_{m,m} \mathbf{b}_m x_m|^2\}}{E\left\{ \sum_{l=1, l\neq m}^{M} |\mathbf{a}_m^H \mathbf{H}_{m,l} \mathbf{b}_l x_l|^2 \right\} + E\{|\mathbf{a}_m^H \mathbf{h}_{pu,m} x_{pu}|^2\} + E\{|\mathbf{a}_m^H \mathbf{n}_m|^2\}} \\ =& \frac{|\mathbf{a}_m^H \mathbf{H}_{su_{mm}} \mathbf{b}_m|^2}{|\mathbf{a}_m^H \mathbf{h}_{pu,m}|^2 + \sum_{l=1, l\neq m}^{M} |\mathbf{a}_m^H \mathbf{H}_{m,l} \mathbf{b}_l|^2 + \mathbf{a}_m^H \mathbf{R}_m \mathbf{a}_m} \end{aligned} \tag{6.5}$$

and the capacity of PU is given in this context by :

$$\mathrm{C}_{pu} = \log_2 \left(1 + \frac{p_{pu} |h_{pu,pu}|^2}{\sum_{m=1}^{M} |\mathbf{h}_{pu,m} \mathbf{h}_{pu,m}{}^H| ||\mathbf{b}_m||^2 + \sigma^2} \right) \tag{6.6}$$

An efficient transmit beamforming technique combined with user selection will be proposed in the following section by optimizing a certain problem.

6.3 Centralized Beamforming Strategy

In this section, we will present the design of the transmit and receive beamvectors. In fact, beamvector associated with each SU is determined by optimizing a certain criterion to reach a specific purpose such as maximizing the throughput or minimizing the interference. In the literature, depending on the objective function and the constraints, the beamforming optimization problems can be divided into two classes. One is the SINR balancing problem [88], i.e., maximizing the sum SINR among all the users. The other one is the power minimization problem with SINR constraints [88], i.e., minimizing some power function with SINR constraints. In this work, we adopt the first class combined with an outage probability constraint, i. e., we will maximize the per-user sum capacity subject to minimize the mutual interference. The goal here is to choose for each user who has the best equivalent channel created by the multiple antennas and beamforming where resources are allocated. This concept is shown in Figure 6.2. In this section, we introduce the power constraints to compute beamvectors. Then, we present the outage probability constrain. Finally, we present the optimization problem of the proposed strategy.

6.3.1 Power Constraints

To compute the beamvectors, we consider just the SU MIMO system. The reason for this is that the interference among PU is nulled in SINR equation given in (6.5). In fact, we propose an algorithm that can minimize the interference between cognitive users. SUs are first pre-selected so as to maximize the per-user sum capacity, and then, the PU verifies the outage probability constraint and a number of SUs are selected from those pre-selected SUs. Specifically, beamvectors are selected such that they satisfy the interference free condition $\mathbf{a}_m^H \mathbf{h}_{pu,m} = 0$. If we consider this condition, the SINR at the m-th SU can then be written as :

$$\begin{aligned}
\text{SINR}_m =& \frac{E\{|\mathbf{a}_m^H \mathbf{H}_{m,m} \mathbf{b}_m x_m|^2\}}{E\{|\mathbf{a}_m^H \mathbf{n}_m|^2\} + E\left\{ \sum_{l=1, l\neq m}^{M} |\mathbf{a}_m^H \mathbf{H}_{m,l} \mathbf{b}_l x_l|^2 \right\}} \\
=& \frac{|\mathbf{a}_m^H \mathbf{H}_{m,m} \mathbf{b}_m|^2}{\mathbf{a}_m^H \Phi_m \mathbf{a}_m + \sum_{l=1, l\neq m}^{M} |\mathbf{a}_m^H \mathbf{H}_{m,l} \mathbf{b}_l|^2} \\
=& \frac{\left(\mathbf{a}_m^H \mathbf{H}_{m,m} \mathbf{b}_m\right)^H \left(\mathbf{a}_m^H \mathbf{H}_{m,m} \mathbf{b}_m\right)}{\mathbf{a}_m^H \left(\Phi_m + \sum_{l=1, l\neq m}^{M} \mathbf{H}_{m,l} \mathbf{b}_l \mathbf{b}_l^H \mathbf{H}_{m,l}^H \right) \mathbf{a}_m}
\end{aligned} \tag{6.7}$$

We define the total interference plus noise covariance matrix at the m-th SU as :

$$\mathbf{R}_m = \Phi_m + \sum_{l=1, l\neq m}^{M} \mathbf{H}_{m,l} \mathbf{b}_l \mathbf{b}_l^H \mathbf{H}_{m,l}^H \tag{6.8}$$

Therefore, the SINR at the m-th SU can be formulated as follows :

$$\begin{aligned}
\text{SINR}_m =& \frac{\left(\mathbf{a}_m^H \mathbf{H}_{m,m} \mathbf{b}_m\right)^H \left(\mathbf{a}_m^H \mathbf{H}_{m,m} \mathbf{b}_m\right)}{\mathbf{a}_m^H \mathbf{R}_m \mathbf{a}_m} \\
=& \left(\mathbf{a}_m^H \mathbf{H}_{m,m} \mathbf{b}_m\right)^H \left(\mathbf{a}_m^H \mathbf{R}_m \mathbf{a}_m\right)^{-1} \left(\mathbf{a}_m^H \mathbf{H}_{m,m} \mathbf{b}_m\right) \\
=& \mathbf{b}_m^H \mathbf{H}_{m,m} \mathbf{R}_m^{-1} \mathbf{H}_{m,m}^H \mathbf{b}_m
\end{aligned} \tag{6.9}$$

From (6.9), the post-beamforming vector can be expressed as follows :

$$\mathbf{a}_m = \mathbf{R}_m^{-1}\mathbf{H}_{m,m}\mathbf{b}_m \tag{6.10}$$

This gives us the following maximization of SINR at the m-th SU :

$$\mathbf{b}_m^H\mathbf{H}_{m,m}^H\mathbf{R}_m^{-1}\mathbf{H}_{m,m}\mathbf{b}_m \leq \lambda_{max}(m)p_m = \text{SINR}_m|_{max} \tag{6.11}$$

where $\lambda_{max}(m)$ is the maximum eigenvalue of $\mathbf{H}_{m,m}^H\mathbf{R}_m^{-1}\mathbf{H}_{m,m}$ and $p_m = \mathbf{b}_m^H\mathbf{b}_m$. For beamforming, the transmitted power through all the SUs for the m-th SU is proportional to $||\mathbf{b}_m||^2$. The design goal is to find the optimum transmit weight vector subject to a carrier power constraint. We consider the power allocation problem corresponding to the distribution of all the available power at the transmitter among all SUs, when the data destined from SU m is transmitted with a maximum power P_{max}. This per-user power constraint is given by :

$$||\mathbf{b}_m||^2 = p_m \leq P_{max}, \quad \forall m = 1, ..., M \tag{6.12}$$

and the global power constraint is formulated as follows :

$$\sum_{m=1}^{M} ||\mathbf{b}_m||^2 = \sum_{m=1}^{M} p_m \leq MP_{max} \tag{6.13}$$

6.3.2 Outage Probability Constraint

The outage probability is given by (4.3). In this subsection, we will reformulate this equation using the beamforming strategy. Proceeding in the same manner as in Subsection 5.2.1, the outage probability can be written as :

$$P_{out} = Prob\left\{\log_2\left(1 + \frac{p_{_{pu}}G_{pu}^2 \mid h'_{pu,pu} \mid^2}{\sum_{m=1}^{M} |\mathbf{h}_{pu,m}\mathbf{h}_{pu,m}{}^H|||\mathbf{b}_m||^2 + \sigma^2}\right) \leq R_{pu}\right\} \tag{6.14}$$

As in the development of the distributed user selection strategy in Chapter 5, we introduce here the PU and SU average channel gain estimate G_{pu} and G_{su}, respectively, defined in the Subsection 5.2.1. These assumptions give the following PU outage probability expression :

$$P_{out} \simeq 1 - \exp\left[-\left(2^{R_{pu}} - 1\right)\left(\frac{G_{su}^2\sum_{m=1}^{M} p_m + \sigma^2}{G_{pu}^2 p_{_{pu}}}\right)\right] \tag{6.15}$$

6.3.3 Optimization Problem

Concluding that the maximum eigenvalue $\lambda_{max}(m)$ must be chosen so as to maximize the capacity of SUs given a fixed transmit power. In the first step of the proposed beamforming user selection strategy, SUs are first pre-selected so as to maximize the per-user sum capacity. In the second step of the user selection strategy, the PU verifies the outage probability constraint and a

number of SUs are selected from those pre-selected SUs. If we maximize the per-user sum capacity (C_{su}) : i.e. the sum of the SINR averaged over all SUs under the constraints of maintaining the global power lower than MP_{max} and of satisfying the QoS constraint on outage, the problem can be written as :

$$\begin{cases} \text{maximize} & f(p_1,...,p_M) = \dfrac{1}{\ln 2}\displaystyle\sum_{m=1}^{M} \ln\left(1+\lambda_{max}(m)p_m\right) \\ \text{subject to} & \displaystyle\sum_{m=1}^{M} p_m \leq MP_{max} \\ & P_{out} \simeq 1-\exp\left[-\left(2^{R_{pu}}-1\right)\left(\dfrac{G_{su}^2\displaystyle\sum_{m=1}^{M} p_m+\sigma^2}{G_{pu}^2 p_{pu}}\right)\right] \leq q \end{cases} \tag{6.16}$$

To compute the transmitted power through all SUs, we define the Lagrangian expression for this maximization problem as follows :

$$\begin{aligned} J=&\frac{1}{\ln 2}\sum_{i=1}^{M} \ln\left(1+\lambda_{max}(i)p_i\right) - \mu\left(\sum_{i=1}^{M} p_i - MP_{max}\right) \\ &-\nu\left(1-\exp\left[-\left(2^{R_{pu}}-1\right)\left(\frac{G_{su}^2\displaystyle\sum_{i=1}^{M} p_i+\sigma^2}{G_{pu}^2 p_{pu}}\right)\right]-q\right) \end{aligned} \tag{6.17}$$

We introduce in (6.17) two variables, μ and ν, called Lagrange multipliers. The solution of all the system is found by calculating the derivatives of J with respect to the power allocation parameters $p_m|_{m=1..M}$ and Lagrange multipliers μ and ν. By calculating the derivatives of J with respect to the power allocation parameters p_m, we obtain :

$$\frac{\partial J}{\partial p_m}=\frac{(\ln 2)^{-1}\lambda_{max}(m)}{1+\lambda_{max}(m)p_m} - \mu - \nu\frac{\left(2^{R_{pu}}-1\right)G_{su}^2}{G_{pu}^2 p_{pu}}\exp\left[-\left(2^{R_{pu}}-1\right)\left(\frac{G_{su}^2\displaystyle\sum_{i=1}^{M} p_i+\sigma^2}{G_{pu}^2 p_{pu}}\right)\right]=0 \tag{6.18}$$

Let $g(p_i) = \frac{\left(2^{R_{pu}}-1\right)G_{su}^2}{G_{pu}^2 p_{pu}}\exp\left[-\left(2^{R_{pu}}-1\right)\left(\frac{G_{su}^2\displaystyle\sum_{i=1}^{M} p_i+\sigma^2}{G_{pu}^2 p_{pu}}\right)\right]$, we can express the solution of (6.18) as :

$$\frac{1}{(\mu+\nu g(p_i))\ln 2}\lambda_{max}(m)=1+\lambda_{max}(m)p_m \tag{6.19}$$

The solution of this problem is formulated as follows :

$$p_m = \frac{1}{(\mu + \nu g(p_i)) \ln 2} - \frac{1}{\lambda_{max}(m)} \tag{6.20}$$

The derivatives of J with respect to the power allocation parameters $p_i|_{i=1..M}$:

$$\begin{cases} p_1 = \frac{1}{(\mu+\nu g(p_i)) \ln 2} - \frac{1}{\lambda_{max}(1)} \\ p_2 = \frac{1}{(\mu+\nu g(p_i)) \ln 2} - \frac{1}{\lambda_{max}(2)} \\ \quad . \\ \quad . \\ \quad . \\ \quad . \\ p_M = \frac{1}{(\mu+\nu g(p_i)) \ln 2} - \frac{1}{\lambda_{max}(M)} \end{cases} \tag{6.21}$$

The sum of all equations in (6.21) gives :

$$\begin{aligned} \sum_{i=1}^{M} p_i &= \frac{M}{(\mu + \nu g(p_i)) \ln 2} - \sum_{i=1}^{M} \frac{1}{\lambda_{max}(i)} \\ &= M \left(p_m + \frac{1}{\lambda_{max}(m)} \right) - \sum_{i=1}^{M} \frac{1}{\lambda_{max}(i)} \\ &= M P_{max} \end{aligned} \tag{6.22}$$

Finally, we obtain the following set of equalities :

$$p_m = P_{max} - \frac{1}{\lambda_{max}(m)} + \frac{1}{M} \sum_{i=1}^{M} \frac{1}{\lambda_{max}(i)} \quad \text{for} \quad m = 1, ..., M \tag{6.23}$$

This equation gives the power allocation solution using the global power constraint given by (6.13). Firstly, the per-user power constraint given in (6.12) has been utilized to solve the problem, i.e. maximizing the per-user sum capacity under the constraint of maintaining the per-user power constraint lower than P_{max} for all users. In this case, the Lagrangian expression is given by :

$$J = \frac{1}{\ln 2} \sum_{m=1}^{M} \ln \left(1 + \lambda_{max}(i) p_i\right) - \sum_{i=1}^{M} \mu_i \left(p_i - P_{max}\right) \tag{6.24}$$

and the transmitted power through all SUs is :

$$p_m = P_{max}, \qquad m = 1, ..., M \tag{6.25}$$

but it is not the optimal solution. Besides, from (6.23), p_m can have values higher than P_{max} which contradicts condition (6.12). To optimally solve this problem, one should adopt this solution :

$$\begin{array}{rcll} p_m & = & P_{max} & \text{if } p_m > P_{max} \\ p_m & = & P_{max} - \frac{1}{\lambda_{max}(m)} + \frac{1}{M} \sum_{i=1}^{M} \frac{1}{\lambda_{max}(i)} & \text{else} \end{array} \tag{6.26}$$

Therefore, it will be shown later from simulation results that (6.26) can approximate very well the per-user sum capacity with optimal power allocation.

6.4 User Selection Algorithm

We propose here an iterative algorithm to solve the maximization problem presented in Section 2.9.2. The pseudo-code for the user selection strategy is shown in Algorithm 2. We define $\tilde{M}_b$ as the number of SUs allowed to transmit using the beamforming approach. In each iteration of the proposed algorithm, we initialize the number of transmitter SUs $\tilde{M}_b$ to 1 and the power of the first SU to P_{max}. Thus, the first SU will be selected automatically under the constraint of maintaining the outage probability of the PU not degraded ($P_{out} \leq q$). Then, each SU simultaneously measures his power based on (6.23) and we check if this value is higher than P_{max}. Similarly, at every iteration, inequality (6.15) is evaluated for the SU in question based on the resulting power allocation, and the number of SUs allowed to transmit is updated.

Algorithm 2 Resource allocation for cognitive radio networks with a centralized beamforming user selection strategy

for $it = 1 : IT_{max}$ **do**
  $p_1^{(it)} = P_{max}$
  $\tilde{M}_b^{(it)} = 1$
  while $P_{out}^{(it)} \leq q$ **do**
    for $m = 2 : M$ **do**
      $p_m^{(it)} \leftarrow P_{max} - \frac{1}{\lambda_{max}^{(it)}(m)} + \frac{1}{\tilde{M}_b^{(it)}} \sum_{i=1}^{\tilde{M}_b^{(it)}} \frac{1}{\lambda_{max}^{(it)}(i)}$
      if $p_m^{(it)} > P_{max}$ **then**
        $p_m^{(it)} \leftarrow P_{max}$
      end if
    ▷ Outage constraint
      if $P_{out}^{(it)} \leq q$ **then**
        $\tilde{M}_b^{(it)} \leftarrow \tilde{M}_b^{(it)} + 1$
      end if
    end for
  end while
end for

6.5 Performance Evaluation

This section provides a number of simulations aimed at assessing the performance of the beamforming user selection strategy in comparison with the centralized strategy presented in Section 4.7. We will use the same propagation model and CRN parameters as in Chapter 5. We ran a Monte Carlo simulations in the downlink and the uplink mode with $IT_{max} = 10^4$. The average channel gains G_{su} and G_{pu} were evaluated to $G_{pu}^2/G_{su}^2 \simeq 15$ in the downlink mode and $G_{pu}^2/G_{su}^2 \simeq 20$ in the uplink mode, through Monte Carlo simulations when the number of SUs $M = 500$. A number of simulations were performed utilizing different rate values : 0.1, 0.3 and 0.5bits/s/Hz.

In Figure 6.3, the number of active SU links under the proposed algorithm versus the total number of users, in comparison with the centralized scheme and the distributed one, using a maximum outage probability $q = 1\%$ and different rate values, is depicted. It can be seen from the figure that increasing the number of SUs produces improvements in the number of active SUs. We

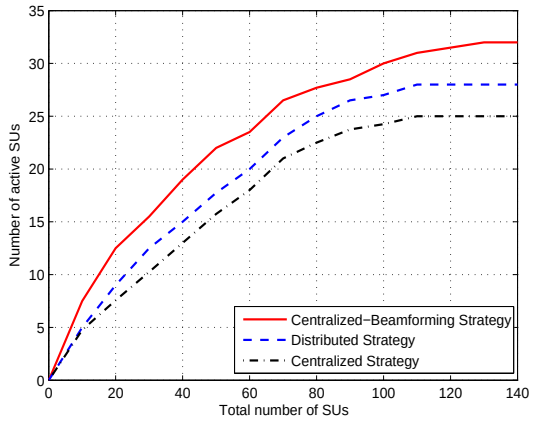

(a) Downlink : rate = 0.1bits/s/Hz

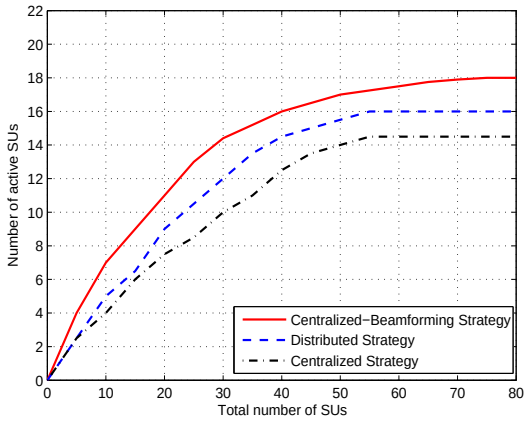

(b) Uplink : rate = 0.1bits/s/Hz

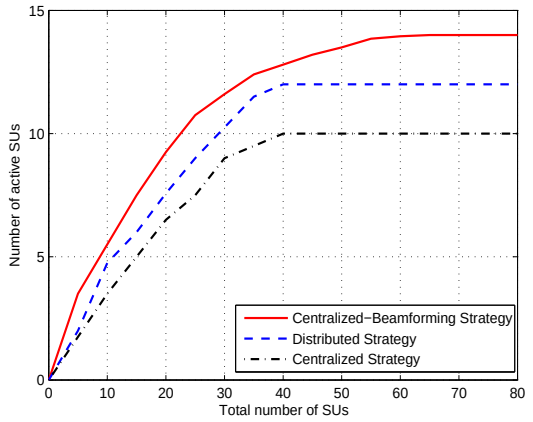

(c) Downlink : rate = 0.3bits/s/Hz

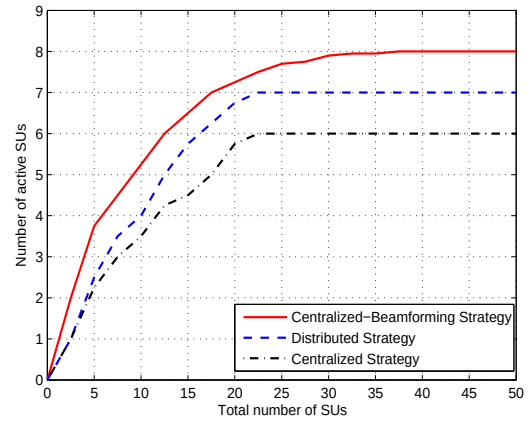

(d) Uplink : rate = 0.3bits/s/Hz

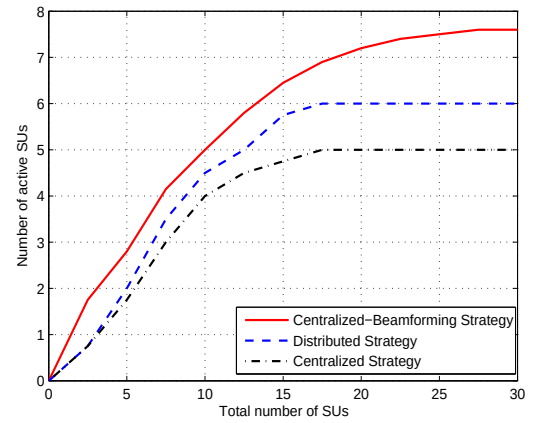

(e) Downlink : rate = 0.5bits/s/Hz

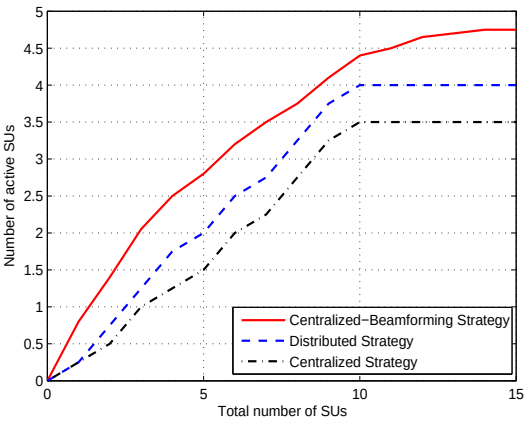

(f) Uplink : rate = 0.5bits/s/Hz

FIGURE 6.3 – Performance evaluation of the proposed user selection strategies in comparison with the centralized one : Number of active secondary users versus total number of secondary users for different rates (0.1, 0.3 and 0.5bits/s/Hz) and $q = 1\%$ in the downlink and the uplink mode.

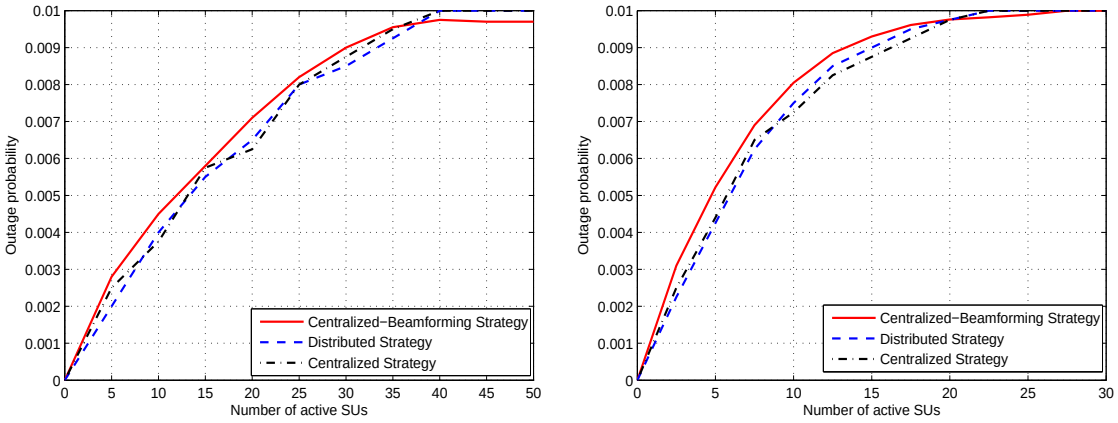

(a) Downlink (b) Uplink

FIGURE 6.4 – Performance evaluation of the centralized beamforming user selection strategy in comparison with the centralized and distributed one : Outage probability as function of the number of secondary users for a target outage probability = 1% and a rate = 0.3bits/s/Hz in the downlink and the uplink mode.

show also that the proposed user selection method outperforms the centralized and the distributed strategy. We gain almost 4 additional active SUs using the centralized beamforming strategy in comparison with the simple centralized strategy. It is obvious from Figure 6.3 that the number of active SUs slopes in the centralized strategy start dropping at a lower number of SUs than in the beamforming strategy case. While the number of active SUs curve has dropped off starting from approximately 40 SUs in the centralized algorithm, the curve of the beamforming strategy starts dropping off after 60 SUs for the beamforming strategy, in the case of downlink scenario when rate = 0.3bits/s/Hz. Observing Figure 6.3 (a), as an example, we get that the number of active SUs is lower than 20 users for any number of transmitter SUs in the system. This means that the PU outage probability is upper-bounded by the maximum outage probability q. Figure 6.4 confirms these results. As reflected in the figure, the required maximum outage probability is respected, since all outage probability values are lower then 1% for any number of SUs. From these results, the P_{out} curves in both uplink and downlink cases can be observed to have very similar slopes as in Figure 6.3. The saturation mode for the beamforming strategy is around 60 SUs in the case of downlink, and around 28 SUs for the uplink scenario.

So far, we verified the first goal of the proposed method, maintaining the outage probability of the PU not degraded. The second goal in developing this new strategy is to reduce the interference from SUs transmitters. However, we must show the impact of the proposed centralized beamforming scheme on the interference power. Figure 6.5 depicts the normalized interference power of the beamforming user selection strategy versus the number of SUs in the uplink mode, in comparison with the distributed and the centralized methods. This figure shows that the interference power increases with the increasing number of SUs. It shows as well that the beamforming strategy performs better in terms of interference power. On the other hand, the distributed and the centralized strategies have virtually identical curves. Indeed, the proposed technique reduces interfering power by about 45% in comparison with the distributed and the centralized techniques. Therefore, we conclude that the proposed beamforming strategy is highly efficient in terms of reducing the interference power as well as robust in maintaining a certain QoS to a PU.

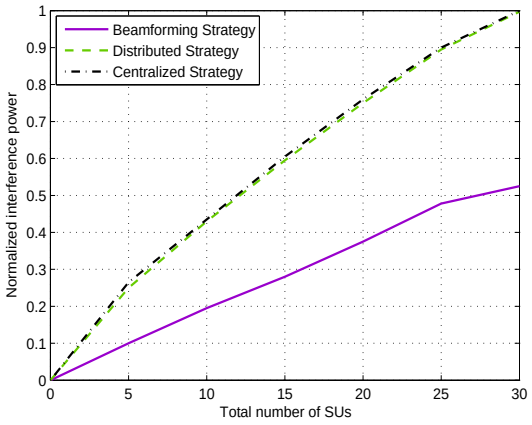

FIGURE 6.5 – Performance evaluation of the centralized beamforming user selection strategy in comparison with the distributed and the centralized one : Interference power versus number of SUs with $q = 1\%$ and a rate = 0.3bits/s/Hz in the uplink mode.

6.6 Conclusion

In this chapter, we have explored the idea of combining user selection with an efficient transmit and receive beamforming technique to maximize the SU rate while maintaining QoS to a PU. First, SUs are pre-selected so as to maximize the per-user sum capacity. Then, the PU verifies the outage probability constraint and a number of SUs are selected from those pre-selected SUs. We showed that the proposed approach exhibits a significant number of cognitive users able to transmit while constraining interference to guarantee QoS for the PU. Simulations were carried out based on a realistic network setting.

Conclusions and Perspectives

This thesis set forth exploring undiscovered ground in spectrum sensing and resource allocation for CR. Specifically, the aim of the first part of this research has been to investigate whether model selection or signal space dimension estimation and information theoretic distance measures could be used to improve spectrum detection performance in a blind way and low signal to noise region. Through a thorough research effort, two novel spectrum sensing algorithms based on distribution analysis and dimension estimation of the PU received signal were proposed and analyzed. The second part of this thesis presents and analyzes two user selection strategies based on outage probability. One explored the idea of combining multi-user diversity gains with spectral sharing techniques to maximize the SU sum rate while maintaining the outage probability of the PU not degraded with a distributed manner, the other treat the beamforming problem in the context of CR using multiuser MIMO SU system and proposes a user selection strategy based on outage probability.

Based on the first three chapters, a number of conclusions can be made for the first part of this thesis. Based on the theoretical analysis, it was shown how detectors relying on conventional sample average based estimation suffer when the signal to noise ratio decreases. In order to maintain a fixed estimation variance, a linear decrease in signal to noise ratio requires a quadratic increase in the number of samples used for the estimation. Hence, accurate estimation becomes infeasible at low signal to noise ratios. Note that the proofs are only done for signals with a circularly symmetric Gaussian distribution. Experiments with real data captured by the EURECOM RF Agile Platform revealed that the very common assumption in academia when doing spectrum sensing research, that the signal under H_0 can be modeled as circularly symmetric white Gaussian noise, can be dangerous.

It can be concluded also that the distribution analysis based detection is hard due to the similarity of signal and noise distributions in some cases. However, the dimension estimation based detection algorithm is to some extent promising. It has a performance which is lower than the CD and AD detectors, and a complexity which is higher than the ED and similar to the CD and AD detectors. This detector tray to estimate the dimension of the PU signal using AIC or MDL criteria. From these informations, it might be able to infer something about the position of the occupied sub-band in the spectrum band. The information can also be used for resource allocation. The DAD detector however outperforms the ED with comparable complexity. This detector have very good specifications, comprising especially the low estimation variance which only depends on parameters such as number of samples, which is known a priori, and its low complexity. The DAD detector compares the distribution of the received signal with a second distribution. Chapter 2 have discussed how the proposed DAD computes the Kullback-Leibler distance between the distribution of the received signal's envelope and a reference distribution, typically chosen to be a Rayleigh distribution, but we can choose other kind of reference distributions. It becomes apparent how it would be interesting to search for other areas than CR comprising detection problems with larger inherent discrepancy between the conditional distributions. One of the ideas that we propose

as perspective for work is to meet specification of standards such as GSM, WiFi and UMTS, and the distribution analysis algorithm and tray to choose the adequate distribution for each standard.

The research presented in the first part of this thesis has given rise to several scientific publications ; One journal paper and seven papers have been presented at international conferences :

- B. Zayen and A. Hayar, "Cooperative/Non-Cooperative Blind Spectrum Sensing Techniques in Cognitive Radio Networks", Submitted to IEEE Transaction on Wireless Communications.
- A. Cipriano, P. Gagneur, A. Hayar, B. Zayen and L. Le Floc'h, "Implementation and Performance of an Opportunistic Cognitive Radio System", 19th Future Network and MobileSummit'10, June 16-18, 2010, Florence, Italy.
- B. Zayen, W. Guibene and A. Hayar, "Performance Comparison for Low Complexity Blind Sensing Techniques in Cognitive Radio Systems", CIP'10, 2nd International Workshop on Cognitive Information Processing, June 14-16, 2010, Elba Island, Tuscany, Italy.
- B. Zayen and A. Hayar, "Cooperative Spectrum Sensing Technique based on Sub Space Analysis for Cognitive Radio Networks", COGIS'09, COGnitive systems with Interactive Sensors Conference, November 16-18, 2009, Paris, France.
- B. Zayen, A. Hayar, H. Debbabi and H. Besbes, "Application of Smoothed Estimators in Spectrum Sensing Technique Based on Model Selection", ICUMT'09, IEEE International Conference on Ultra Modern Telecommunications : Workshop on Cognitive Wireless Communications and Networking, October 12-14, 2009, St.-Petersburg, Russia.
- B. Zayen, A. Hayar and K. Kansanen, "Blind Spectrum Sensing for Cognitive Radio Based on Signal Space Dimension Estimation", ICC'09, IEEE International Conference on Communications, June 14-18, 2009, Dresden, Germany.
- M. Ghozzi, B. Zayen and A. Hayar, "Experimental Study of Spectrum Sensing Based on Distribution Analysis", ICT-MobileSummit'09, 18th ICT Mobile and Wireless Communications Summit, June 10-12, 2009, Santander, Spain.
- B. Zayen, A. Hayar and D. Nussbaum, "Blind Spectrum Sensing for Cognitive Radio Based on Model Selection", CrownCom'08, 3rd International Conference on Cognitive Radio Oriented Wireless Networks and Communications, Mai 15-17, 2008, Singapore.

In the last three chapters, we have focused on resource allocation and interference management. Within this setting, we have considered different system models in which SUs compete for a chance to transmit simultaneously or orthogonally with the PU. On the basis of these models, we have also defined the specific resource allocation problem and offer insights into how to design such scenario in a CRN environments and we proposed two user selection strategies. One first key idea is based on outage probability to mange the QoS of the CR system. We have derived a distributed user selection algorithm under a cognitive capacity maximization criterion and outage probability constraint. We found out that we should make a tradeoff between cognitive capacity maximization and number of active SUs maximization.

Finally, we have investigated the problem of resource allocation for multiuser multi-antenna channels using a beamforming strategy. The proposed strategy was proved to be the optimal one that achieves the maximum rate for both users under the constraint that the SU guarantees a QoS for the primary system within the outage probability constraint. We have explicitly derived the capacity of the primary as well as the SU. Both theoretical and simulation results based on a realistic network setting provide substantial throughput gains, thereby illustrating interesting features in terms of CRN deployment while maintaining QoS for the primary system by means of outage probability.

Our main contribution within this part is the QoS management of the CR system. The originality in the proposed methods is that we guarantee a QoS to PU by maintaining the PU's outage probability unaffected in addition to a certain QoS to SUs and ensuring the continuity of service even when the spectrum sub-bands change from vacant to occupied. Thus by the outage probability control, if we have a vacant spectrum holes in the PU band, we set the outage probability $P_{out} = 1$ to exploit the available spectrum band by SUs, and if we have occupied sub-bands, the outage probability is set to $P_{out} = q$ depending on the PU's QoS.

Extensions of the problem for multi-PUs are problems of timely relevance that require further research. Moreover, fairness issues between SUs, which have not been taken into account in this work, need to be incorporated in order to provide substantial throughput while satisfying certain QoS constraints between SUs.

The work in this part has been published in :

- B. Zayen, M. Haddad, A. Hayar and G. E. Oien, "Binary Power Allocation for Cognitive Radio Networks with Centralized and Distributed User Selection Strategies", Elsevier Physical Communication Journal, Vol.1, No. 3, pp. 183-193, September 2008.
- B. Zayen, A. Hayar and G. E. Oien, "Resource Allocation for Cognitive Radio Networks with a Beamforming User Selection Strategy", Asilomar'09, 43rd Asilomar Conference on Signals, Systems and Computers, pp. 544-549, November 1-4, 2009, Asilomar, California, USA.

In order to conclude, we might say that the theoretical limits of CR systems are relatively understood nowadays. However, the gap between the current practical schemes and the theoretical limits is still significant, making the design of CR networks an open and exiting issue. Notably, proposals such as ultra-wide band (UWB) and interference temperature have called into question the validity of the FCCs hierarchy and required reexamination of the source of authority for the FCCs unlicensed spectrum access rules.

Appendix A

Résumé Français

A.1 Introduction

Dans le cadre de la radio cognitive telle que définie par J. Mitola [1] [2] [3], les utilisateurs secondaires peuvent accéder de façon opportuniste aux parties du spectre détenues par les utilisateurs primaires lorsque ceux-ci ne les utilisent pas et leur en donnent l'accord. Dans ce cadre, des schémas de détection et de gestion de la ressource radio, seront supposés disposer d'informations sur l'activité des systèmes primaires (interférence, etc) et proposeront par conséquence des stratégies d'accès et d'allocation de ressource opportuniste permettant aux utilisateurs secondaires de profiter des bandes libres du primaire pour transmettre.

Dans la première partie de ce résumé nous proposons deux stratégies d'accès pour la radio cognitive basées sur la distribution et la dimension du signal primaire. Dans la deuxième partie, deux politiques d'allocation de ressources seront développées. Les deux politiques sont basées sur la probabilité outage. Des résultats de simulation seront présentés en utilisant des scenarios réels.

A.2 Stratégies d'accès pour la radio cognitive

Nous rappelons dans cette section le principe de détection dans le cadre de la radio cognitive ainsi que le contexte de notre analyse. Nous développons par la suite les deux techniques de détection qui sont proposées dans le cadre de cette thèse : une technique de détection basée sur la distribution du signal et une deuxième technique basée sur la dimension du signal primaire. Nous présentons enfin quelques résultats de simulation en comparant les méthodes proposées avec quelques méthodes de référence.

A.2.1 Principe de détection pour la radio cognitive

Nous proposons dans la Figure A.1 un exemple de scenario d'un réseau radio cognitive où nous avons un système primaire et un réseau de secondaires essayant d'exploiter les bandes libres du primaire. Désignons par $\mathbf{x}$ le signal émis sur une antenne donné par :

$$\mathbf{x} = \mathbf{As} + \mathbf{n} \tag{A.1}$$

Ce signal peut êtres un signal secondaire, un signal primaire ou deux signaux, secondaire et primaire, émis en même temps. Le problème de la détection d'une bande libre revient au test d'hypothèses suivant :

$$\mathbf{x} = \begin{cases} \mathbf{n} & \mathrm{H}_0 \\ \mathbf{As} + \mathbf{n} & \mathrm{H}_1 \end{cases} \tag{A.2}$$

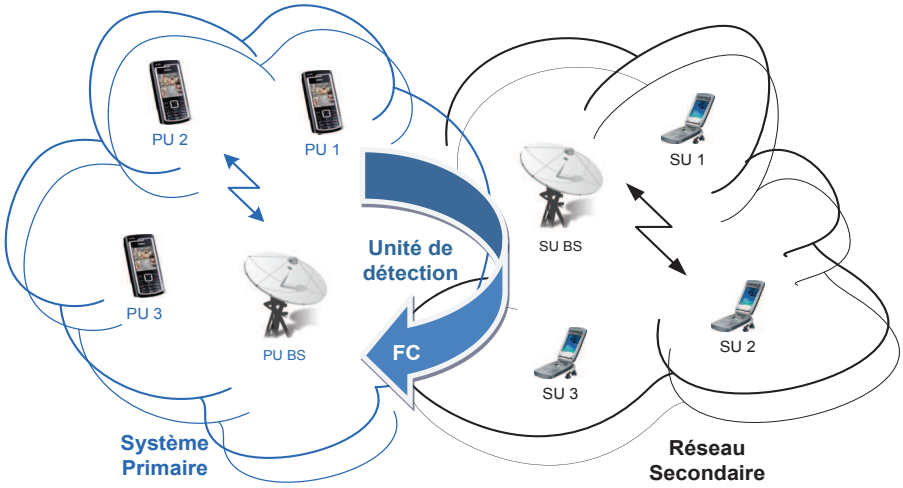

FIGURE A.1 – Exemple de scenario d'un réseau radio cognitive.

où **n** est un vecteur colonne $(q \times 1)$ représentant un bruit blanc gaussien complexe circulaire centré de matrice de covariance égale à 2 fois l'identité et **A** est une matrice $(q \times p)$ regroupant l'ensemble des coefficients d'atténuation complexes entre l'émetteur et le récepteur. **s** $(p \times 1)$ est le signal utile dont on souhaite détecter la présence.

Nous définissons aussi la probabilité de fausse alarme donnée par :

$$P_{FA} = Pr(\mathrm{H}_1 \mid \mathrm{H}_0) = Pr(\mathbf{x} \text{ est présent} \mid \mathrm{H}_0) \tag{A.3}$$

et la probabilité de détection :

$$\begin{aligned} P_D =& 1 - P_{MD} \\ =& 1 - Pr(\mathrm{H}_0 \mid \mathrm{H}_1) \\ =& 1 - Pr(\mathbf{x} \text{ est absent} \mid \mathrm{H}_1) \end{aligned} \tag{A.4}$$

où P_{MD} est la probabilité de détection manquée. La probabilité de fausse alarme peut êtres définie en fonction du seuil de détection γ donnée par :

$$P_{FA} = Pr(\Upsilon(\mathbf{x}) > \gamma | \mathrm{H}_0) \tag{A.5}$$

avec $\Upsilon(\mathbf{x})$ présentant le test statistique pour un détecteur donné.

A.2.2 Technique de détection basée sur la distribution du signal

La première technique de détection proposée dans ce travail est basée sur l'analyse de la distribution du signal reçu (DAD). L'idée principale de cette technique de détection de bande libre est basée sur la distribution du signal reçu **x**. En effet, si la distribution de **x** est une distribution Gaussienne (la distribution de la norme est Rayleigh) alors nous affirmons dans ce cas que la bande est libre (c.-à-d. il y a que du bruit **n**). Dans le cas contraire, la bande est occupée et la distribution de

la norme du signal reçu est Rice. Nous utilisons pour cela le critère d'information d'Akaike (AIC) résumé dans cette équation [11] [10] :

$$\text{AIC}=-2\sum_{n=1}^{N}\log g_{\hat{\theta}}(\mathbf{x}_n)+2U \tag{A.6}$$

où la fonction $g_{\hat{\theta}}$ représente la fonction candidate (Rayleigh ou Rice) calculée à partir des paramètres des ces deux distributions, respectivement. Le paramètre θ sera estimé également pour les deux distributions Rayleigh et Rice. Nous définissons maintenant l'Akaike weights, qui est reformulé en fonction des AIC de Rayleigh et Rice. Ce paramètre peut êtres interpréter comme la probabilité que la distribution de la norme du signal reçu est une Rayleigh dans le cas ou nous avons que de bruit (hypothèse H_0) et celle que la distribution est une Rice dans le cas contraire (hypothèse H_1). L'Akaike weights pour les deux distributions est défini comme suit [49] [12] :

$$W_{Rice}=\frac{exp\left(-\frac{1}{2}\Phi_{Rice}\right)}{exp\left(-\frac{1}{2}\Phi_{Rice}\right)+exp\left(-\frac{1}{2}\Phi_{Rayleigh}\right)} \tag{A.7}$$

$$W_{Rayleigh}=\frac{exp\left(-\frac{1}{2}\Phi_{Rayleigh}\right)}{exp\left(-\frac{1}{2}\Phi_{Rayleigh}\right)+exp\left(-\frac{1}{2}\Phi_{Rice}\right)} \tag{A.8}$$

où

$$\Phi_{Rice}=\text{AIC}_{Rice}-\min\left(\text{AIC}_{Rice},\text{AIC}_{Rayleigh}\right) \tag{A.9}$$

$$\Phi_{Rayleigh}=\text{AIC}_{Rayleigh}-\min\left(\text{AIC}_{Rayleigh},\text{AIC}_{Rice}\right) \tag{A.10}$$

et

$$\text{AIC}_{Rice}=-2L_{Rice}+2U_{Rice} \tag{A.11}$$

$$\text{AIC}_{Rayleigh}=-2L_{Rayleigh}+2U_{Rayleigh} \tag{A.12}$$

avec $U_{Rayleigh}=1$ et $U_{Rice}=2$. Par suite, un signal est présent si W_{Rice} est supérieur à $W_{Rayleigh}$ et vice versa. Par conséquent, l'algorithme de détection DAD peut être reformulé comme suit :

$$\Upsilon_{DAD}(\mathbf{x})=\begin{cases} W_{Rice}-W_{Rayleigh}<\gamma_{DAD} & \text{bruit} \\ W_{Rice}-W_{Rayleigh}>\gamma_{DAD} & \text{signal} \end{cases} \tag{A.13}$$

Le seuil de détection γ_{DAD} est calculé pour une probabilité de fausse alarme donnée $P_{FA,DAD}$. Si $\text{AIC}_{Rice}-\text{AIC}_{Rayleigh}>\gamma_{DAD}$, nous déclarons que le signal primaire est présent, sinon le signal primaire est absent. Le seuil de détection est dérivé à partir de la fonction suivante :

$$\begin{aligned} P_{FA,DAD}&=Pr\left(W_{Rice}-W_{Rayleigh}>\gamma_{DAD}|\text{H}_0\right) \\ &=Pr\left(\frac{\exp\left(-\frac{1}{2}\Phi_{Rice}\right)-\exp\left(-\frac{1}{2}\Phi_{Rayleigh}\right)}{\exp\left(-\frac{1}{2}\Phi_{Rice}\right)+\exp\left(-\frac{1}{2}\Phi_{Rayleigh}\right)}>\gamma_{DAD}\middle|\text{H}_0\right) \\ &=Pr\left(\frac{\exp\left(-\frac{1}{2}\text{AIC}_{Rice}\right)-\exp\left(-\frac{1}{2}\text{AIC}_{Rayleigh}\right)}{\exp\left(-\frac{1}{2}\text{AIC}_{Rice}\right)+\exp\left(-\frac{1}{2}\text{AIC}_{Rayleigh}\right)}>\gamma_{DAD}\middle|\text{H}_0\right) \end{aligned} \tag{A.14}$$

Après quelques dérivations, nous obtenons l'équation ci-dessous :

$$P_{FA,DAD}=Pr\left(\prod_{i=1}^{p} x_i < \left(\frac{1+\gamma_{DAD}}{1-\gamma_{DAD}}\right)^2 (4\pi K)^{-p} \exp\left(p-2\right) \middle| \mathrm{H}_0\right) \tag{A.15}$$

en introduisant le facteur de Rice K. Nous appliquons maintenant la distribution de p variables aléatoires de type Rayleigh [50], et nous obtenons :

$$F(t)=\left(2^p\sigma^{2p}\right)^{-\frac{1}{2}} tG_{1,p+1}^{p,1}\left(\left(2^p\sigma^{2p}\right)^{-1} t^2 \middle|_{\frac{1}{2},\ldots,\frac{1}{2},-\frac{1}{2}}^{\frac{1}{2}}\right) \tag{A.16}$$

avec G est la fonction Meijer [50] définie par :

$$G_{1,p+1}^{p,1}\left(u\middle|_{\frac{1}{2},\ldots,\frac{1}{2},-\frac{1}{2}}^{\frac{1}{2}}\right)=\frac{1}{j2\pi}\int_L \frac{\left(\Gamma\left(\frac{1}{2}-s\right)\right)^{p-1}\Gamma\left(\frac{1}{2}+s\right)}{\Gamma\left(\frac{3}{2}+s\right)} u^{-s} ds \tag{A.17}$$

Par suite, la probabilité de fausse alarme de l'algorithme de détection DAD est donnée par :

$$P_{FA,DAD}=F\left(\left(\frac{1+\gamma_{DAD}}{1-\gamma_{DAD}}\right)^2 (4\pi K)^{-p} \exp\left(p-2\right)\right) \tag{A.18}$$

ou, alternativement, le seuil de détection est défini par :

$$\gamma_{DAD}=\frac{\sqrt{(4\pi K)^p F^{-1}\left(P_{FA,DAD}\right)\exp\left(2-p\right)}-1}{\sqrt{(4\pi K)^p F^{-1}\left(P_{FA,DAD}\right)\exp\left(2-p\right)}+1} \tag{A.19}$$

A.2.3 Technique de détection basée sur la dimension du signal

La deuxième technique de détection proposée dans ce travail est basée sur l'estimation de la dimension du signal reçu (DED). Nous reformulons donc l'expression de la formule AIC qui sera utilisée pour le développement de l'algorithme DED. Nous définissons également la longueur de description minimale (MDL) [12] [54] utilisé comme un second outil dans le développement du détecteur DED. Pour calculer les valeurs AIC et MDL, nous estimons les valeurs propres significatives à partir de la matrice de covariance du signal reçu et nous décidons ensuite sur la présence ou l'absence de signal primaire.

Notons par p la taille d'une observation $\mathbf{x} \in \{\mathbf{x}_1, \mathbf{x}_2, ..., \mathbf{x}_N\}$ et q la taille du signal transmit en échantillons. Notre objectif est de déterminer la valeur q à partir de N observations de $\mathbf{x}$ (c.-à-d. la dimension du signal primaire reçu). La matrice de covariance du signal reçu $\mathbf{x}$ est donné par :

$$\mathbf{R} = \mathbf{ASA}^H + \sigma^2\mathbf{I} \tag{A.20}$$

avec $\mathbf{S}$ est la matrice de covariance du signal transmi $\left(\mathbf{S} = E\{\mathbf{ss}^H\}\right)$ et σ^2 est la puissance du bruit. D'après la matrice de covariance donnée par (A.20), nous pouvons avoir l'expression suivante :

$$\mathbf{R}^{(k)} = \sum_{i=1}^{k}(\lambda_i - \sigma^2)\mathbf{V}_i\mathbf{V}_i^H + \sigma^2\mathbf{I} \tag{A.21}$$

avec $\lambda_1, ..., \lambda_k$ et $\mathbf{V}_1, ..., \mathbf{V}_k$ sont, respectivement, les valeurs propres et les vecteurs propres de la matrice $\mathbf{R}^{(k)}$. Notons que, le paramètre k est lié au nombre de degré de liberté (DoF), c.-à-d.

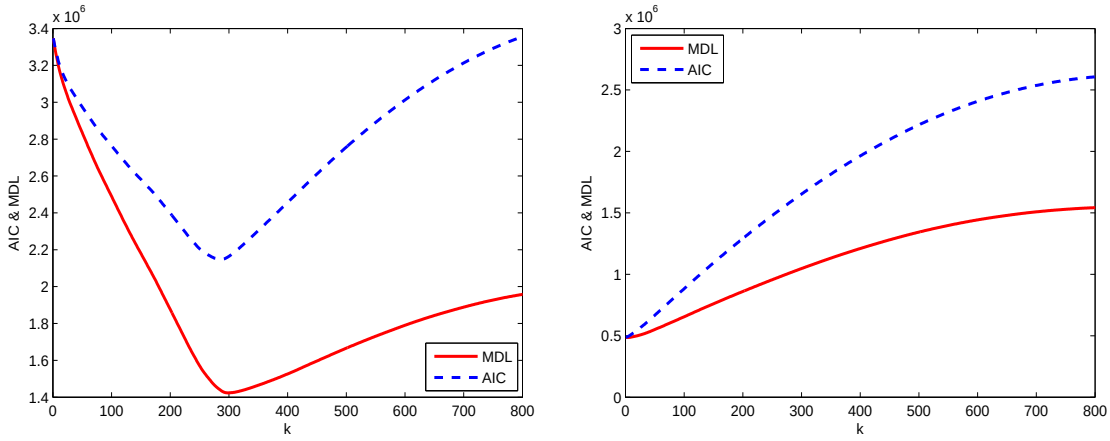

(a) Signal Utile (b) Bruit

FIGURE A.2 – Valeurs de AIC et MDL pour un block où nous avons des données utiles et un deuxième block où nous avons uniquement du bruit en utilisant un signal UMTS.

$k = 0, 1, ..., p-1$. Le vecteur de paramètres θ est une fonction des valeurs propres et des vecteurs propres et il est exprimé comme suit :

$$\theta = (\lambda_1, ..., \lambda_k, \sigma^2, \mathbf{V}_1, ..., \mathbf{V}_k) \tag{A.22}$$

et la matrice de covariance peut être estimée à partir de l'équation suivante :

$$\hat{\mathbf{R}} = \frac{1}{N} \sum_{n=1}^{N} \mathbf{x}_n \mathbf{x}_n^H \tag{A.23}$$

avec $\mathbf{x}_n|_{\{n=1,...,N\}}$ sont les N observations indépendantes du signal $\mathbf{x}$. Nous exprimons ainsi le critère AIC en fonction des valeurs propres de la matrice $\hat{\mathbf{R}}$ (c.-à-d. $\hat{\lambda}_1, \hat{\lambda}_2, ..., \hat{\lambda}_q$) :

$$\mathrm{AIC}(k) = -2 \log \left(\frac{\prod_{i=k+1}^{p} \hat{\lambda}_i^{\frac{1}{p-k}}}{\frac{1}{p-k} \sum_{i=k+1}^{p} \hat{\lambda}_i} \right)^{(p-k)N} + 2k(2p-k) \tag{A.24}$$

Nous définissons de même le critère MDL par [49] :

$$\mathrm{MDL}(k) = -\log \left(\frac{\prod_{i=k+1}^{p} \hat{\lambda}_i^{\frac{1}{p-k}}}{\frac{1}{p-k} \sum_{i=k+1}^{p} \hat{\lambda}_i} \right)^{(p-k)N} + \frac{k}{2}(2p-k) \log N \tag{A.25}$$

En se basant sur (A.24) et (A.25), nous estimons la dimension du signal reçu. En effet, nous traçons dans la Figure A.2 les valeurs de AIC et MDL pour un block où nous avons des données utiles et un deuxième block où nous avons uniquement du bruit. Nous remarquons que dans le premier cas, les valeurs minimales de AIC et MDL donnent la dimension du signal et les courbes des AIC et MDL sont strictement décroissantes jusqu'à AIC_{min} et MDL_{min}, respectivement et croissante a partir de ces valeurs. Dans le deuxième cas où il y a que du bruit, le minimum de AIC (de même pour le MDL) est égale à zéro et les deux courbes sont strictement croissantes.

D'après ces résultats, nous proposons l'algorithme de détection DED suivant en utilisant AIC comme critère :

$$\Upsilon_{DED-AIC}(\mathbf{x}) = \begin{cases} \text{AIC}(0) - \text{AIC}(1) < \gamma_{DED-AIC} & \text{bruit} \\ \text{AIC}(0) - \text{AIC}(1) > \gamma_{DED-AIC} & \text{signal} \end{cases} \tag{A.26}$$

et en utilisant le critère MDL :

$$\Upsilon_{DED-MDL}(\mathbf{x}) = \begin{cases} \text{MDL}(0) - \text{MDL}(1) < \gamma_{DED-MDL} & \text{bruit} \\ \text{MDL}(0) - \text{MDL}(1) > \gamma_{DED-MDL} & \text{signal} \end{cases} \tag{A.27}$$

Nous définissons dans les deux algorithmes proposés les seuils de détections $\gamma_{DED-AIC}$ et $\gamma_{DED-MDL}$. Ces seuils sont calculés en fixant les probabilités de fausse alarme pour chaque détecteur. Le seuil de détection en utilisant le critère AIC est dérivé à partir de la fonction suivante :

$$P_{FA,DED-AIC} \approx Pr\Big(\text{AIC}(0) - \text{AIC}(1) > \gamma_{DED-AIC} | \text{H}_0\Big) \tag{A.28}$$

En remplaçant les valeurs de AIC(0) et AIC(1) et en effectuant quelques approximations nous obtenons :

$$P_{FA,DED-AIC} = Pr\left(\frac{N\frac{\hat{\lambda}_1}{\sigma^2} - \mu}{\nu} < \frac{Nexp\left(\frac{2-4p-\gamma_{DED-AIC}}{2N}\right) - \mu}{\nu} \Big| \text{H}_0\right) \tag{A.29}$$

Notons par F_2 la CDF de la distribution de Tracy-Widom d'ordre deux donnée par [57] :

$$F_2(t) = \exp\left(-\int_t^{\infty} (u-t)h^2(u)du\right) \tag{A.30}$$

avec $h(u)$ est la solution de l'équation différentielle de Painlevé II [57] :

$$h(u) = uh(u) + 2h^3(u) \tag{A.31}$$

Par suite, la probabilité de fausse alarme de l'algorithme DED utilisant le critère AIC est donnée par :

$$P_{FA,DED-AIC} = F_2\left(\frac{Nexp\left(\frac{2-4p-\gamma_{DED-AIC}}{2N}\right) - \mu}{\nu}\right) \tag{A.32}$$

et le seuil de détection :

$$\gamma_{DED-AIC} = 2 - 4p - 2N\ln\left(\frac{\nu F_2^{-1}\left(P_{FA,DED-AIC}\right) + \mu}{N}\right) \tag{A.33}$$

avec $\mu = \left(\sqrt{N} + \sqrt{p}\right)^2$ et $\nu = \left(\sqrt{N} + \sqrt{p}\right)\left(\frac{1}{\sqrt{N}} + \frac{1}{\sqrt{p}}\right)^{\frac{1}{3}}$.

En adoptant la même démarche, nous pouvons écrire la probabilité de fausse alarme de l'algorithme DED utilisant le critère MDL comme suit :

$$P_{FA,DED-MDL} = F_2\left(\frac{Nexp\left(\frac{\gamma_{DED-MDL} + \left(p-\frac{1}{2}\right)\log N}{N}\right) - \mu}{\nu}\right) \tag{A.34}$$

		$p = 150$	$p = 200$
Résultats de simulation pour le DAD	$P_{FA,DAD}$	0.0544	0.0502
	γ_{DAD}	0.9814	0.9561
Résultats théoriques pour le DAD	$P_{FA,DAD}$	0.0563	0.0529
	γ_{DAD}	0.9907	0.9614
Résultats de simulation pour le DED	$P_{FA,DED-AIC}$	0.0518	0.0504
	$P_{FA,DED-MDL}$	0.0533	0.0520
	$\gamma_{DED-AIC}$	2.5901e04	2.1521e04
	$\gamma_{DED-MDL}$	2.0979e04	1.9561e04
Résultats théoriques pour le DED	$P_{FA,DED-AIC}$	0.0500	0.0500
	$P_{FA,DED-MDL}$	0.0500	0.0500
	$\gamma_{DED-AIC}$	2.5274e04	1.9846e04
	$\gamma_{DED-MDL}$	1.8259e04	1.7540e04

TABLE A.1 – Comparaison entre les résultats de simulation et les résultats théoriques des deux seuils de détection et les probabilités de fausse alarme pour les deux techniques DAD et DED pour différents valeurs p, $N = 1000$ et SNR $= -7$dB.

et le seuil de détection :

$$\gamma_{DED-MDL}=\left(p-\frac{1}{2}\right)\log N - N\ln\left(\frac{\nu F_2^{-1}\left(P_{FA,DED-MDL}\right)+\mu}{N}\right) \tag{A.35}$$

Le Table A.1 donne une comparaison entre les résultats de simulation et les résultats théoriques des deux seuils de détection et les probabilités de fausse alarme pour les deux techniques DAD et DED pour différents valeurs de p. Ces résultats montrent la bonne estimations théorique des seuils de détection et des probabilités de fausse alarme.

A.2.4 Résultats des simulations

Dans un premier temps, nous appliquons les deux méthodes de détection sur des signaux réels captés par la plateforme d'EURECOM où nous avons que le primaire présent : le signal primaire est envoyé seul sur l'antenne et il n'y a pas de signal secondaire. Nous présentons dans les Figures A.3 (a) et (b) un exemple de détection du signal primaire en utilisant la technique DAD et en traçant l'Akaike weights pour les deux distributions Rice et Rayleigh. Les deux signaux primaires choisis sont : un signal GSM avec une fréquence de coupure égale à 953MHz et une fenêtre d'analyse de taille $T = 533$ échantillons égale à 200kHz, et un signal WiFi avec une fréquence de coupure égale à 2430MHz et une fenêtre d'analyse de taille $T = 1332$ échantillons égale à 500kHz. La puissance à l'émission du signal primaire est de dBm. Nous remarquons, d'après ces figures, que le signal du primaire est bien localisé : Pour les sous-bandes du spectre où nous avons que du bruit, l'Akaike weights de la distribution de Rayleigh est égale à 1 et celui de la distribution de Rice est nul. Dans les sous-bandes où nous avons un signal primaire, les valeurs d'Akaike weights changent de 1 à 0 et de 0 à 1 pour Rayleigh et Rice, respectivement.

Nous nous intéressons maintenant au deuxième algorithme de détection DED. Nous traçons dans les Figures A.3 (c) et (d) la capacité de détection de l'algorithme DED des sous bandes libre dans le spectre du primaire. Nous vérifions d'après ces figures que nous assurons une bonne détection des trous dans le spectre en utilisant cette méthode.

Apres avoir étudié les performances des détecteurs proposés dans cette thèse pour la détection des sous-bandes libres dans le spectre du primaire, nous évaluons maintenant les performances

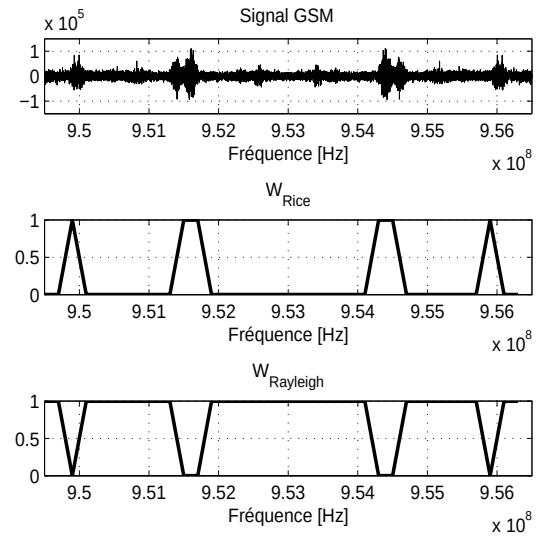

(a) Signal GSM : DAD

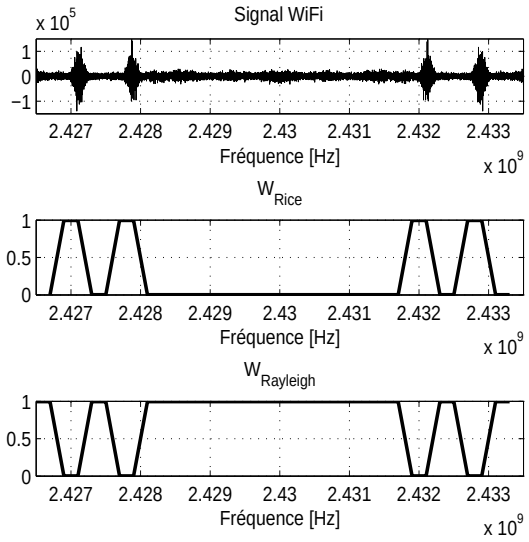

(b) Signal WiFi : DAD

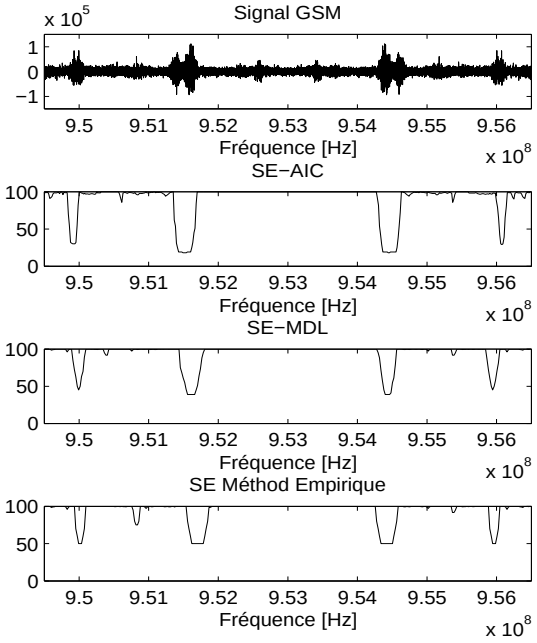

(c) Signal GSM : DED

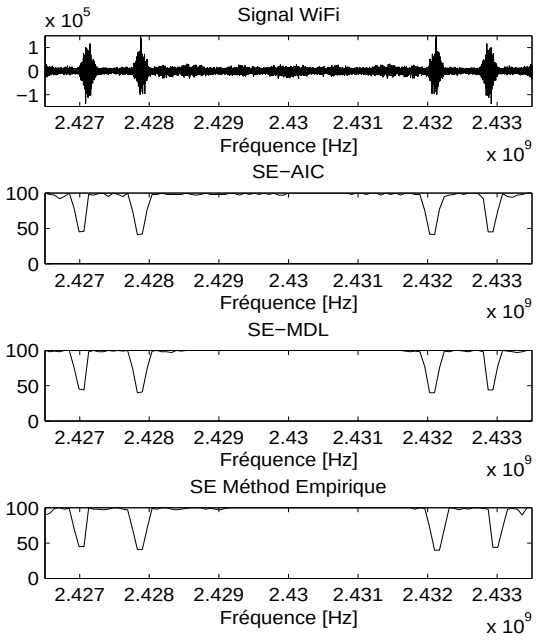

(d) Signal WiFi : DED

FIGURE A.3 – Évaluation de performances des deux techniques de détection DAD et DED pour un signal GSM avec une fréquence de coupure égale à 953MHz et une fenêtre d'analyse de taille $T = 533$ échantillons égale à 200kHz, et un signal WiFi avec une fréquence de coupure égale à 2430MHz et une fenêtre d'analyse de taille $T = 1332$ échantillons égale à 500kHz.

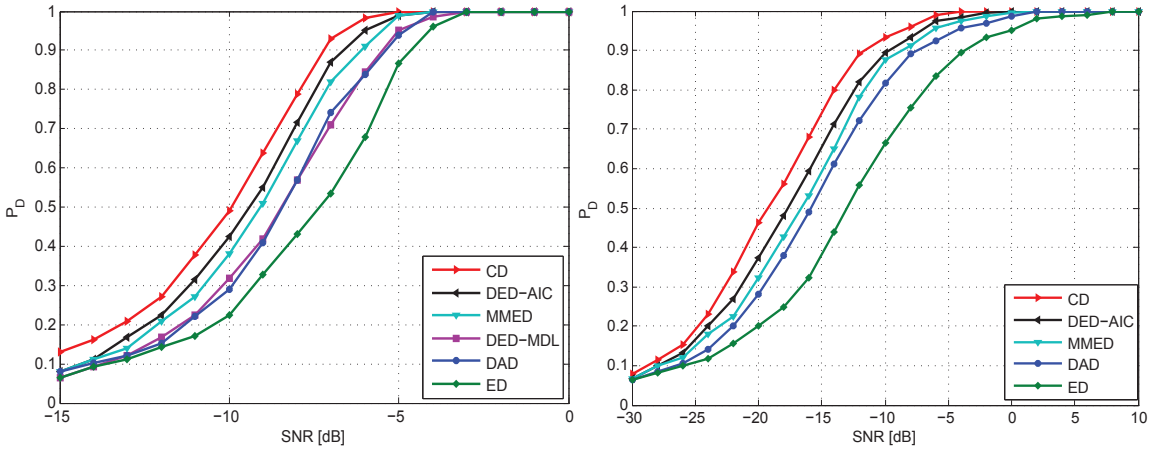

(a) P_D fct. SNR : Scenario 1

(b) P_D fct. SNR : Scenario 2

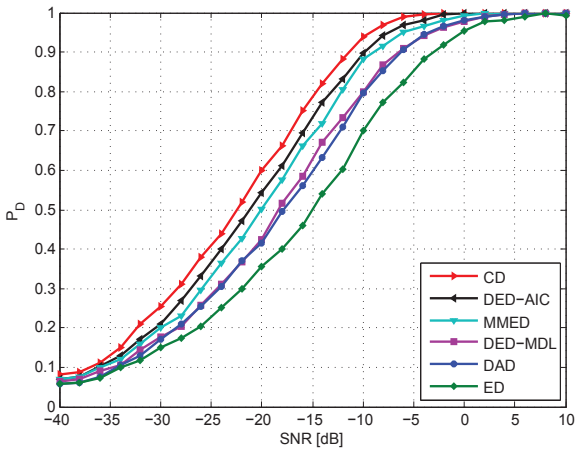

(c) P_D fct. SNR : Scenario 3

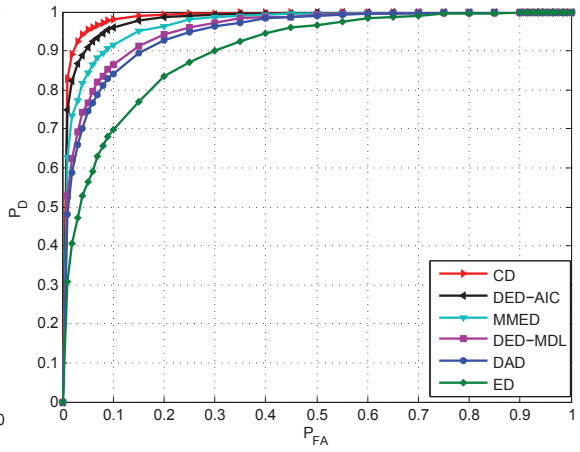

(d) Courbes ROC : Scenario 1

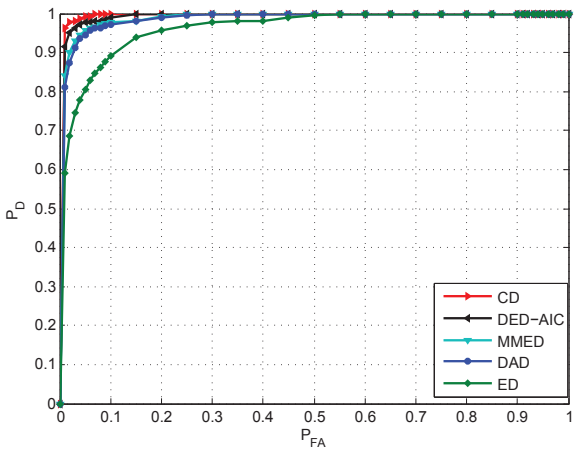

(e) Courbes ROC : Scenario 2

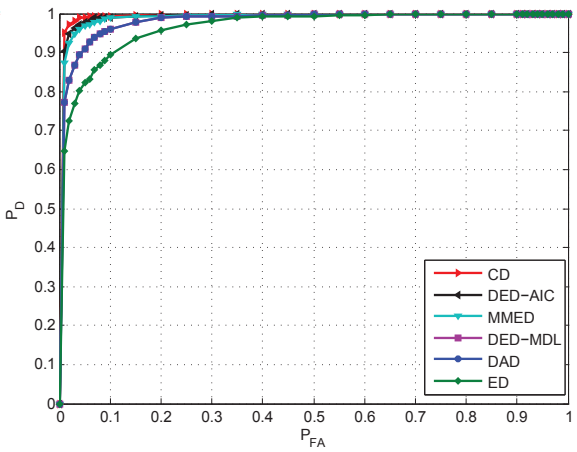

(f) Courbes ROC : Scenario 3

FIGURE A.4 – Évaluation de performances des deux techniques de détection DAD et DED en terme de détection locale du primaire en utilisant un signal DVB-T OFDM : Probabilité de détection en fonction du SNR pour une $P_{FA} = 0.05$ et courbes ROC pour un SNR $= -7$dB, et, un temps de détection = $1.12ms$ et $p = 2048$.

des détecteurs pour la détection locale du primaire. Nous considérons pour cela trois scenarios différents :

Scenario 1 Utilisant un signal OFDM avec un canal AWGN ;

Scenario 2 Utilisant un signal OFDM avec un canal multitrajets de type Rayleigh avec shadowing ;

Scenario 3 Utilisant un signal OFDM avec un canal multitrajets de type Rice avec shadowing.

La Figure A.4 montre les résultats des simulations des détecteurs DED et DAD en comparaison avec le détecteur basée sur la cyclostationarité du signal (CD) [15], le détecteur basée sur le minimum/maximum valeurs propres (MMED) [28] et le détecteur d'énergie (ED) [26], avec les trois scenarios proposés. Nous traçons dans cette figure la probabilité de détection en fonction du SNR pour les deux détecteurs proposés et les détecteurs de références ainsi que les courbes ROC (probabilité de fausse alarme en fonction de la probabilité de détection). Nous remarquons d'après ces résultats, que le détecteur CD donne les meilleurs résultats. Ce dernier en revanche a la plus grande complexité comme il nécessite quelques informations sur le signal primaire émis (n'est pas aveugle). Nous remarquons aussi que le détecteur DED donne des résultats très encourageants. Le détecteur DAD a des résultats comparables avec le détecteur ED et une complexité très faible.

Concernant la détection coopérative, chaque noeud du réseau radio cognitive renvoie une information condensée résultant de son algorithme de détection locale au centre de fusion. Ce dernier les combine pour aboutir à un état plus précis et plus fiable de la bande de fréquence testée. Ceci permettra par exemple d'éviter les problèmes de noeud caché dans lequel peut se trouver un noeud du réseau. En fonction du type de l'information renvoyée par les noeuds, le centre de fusion emploie un algorithme de combinaison différent. Si cette information est de type bit, la combinaison est dite dure. Dans le cas d'une information du type réel (mesure d'énergie, rapport de vraisemblance, etc.) la combinaison est dite douce. Ces deux techniques ont été appliquées aux algorithmes de détection proposés et nous avons obtenu les résultats donnés par la Figure A.5.

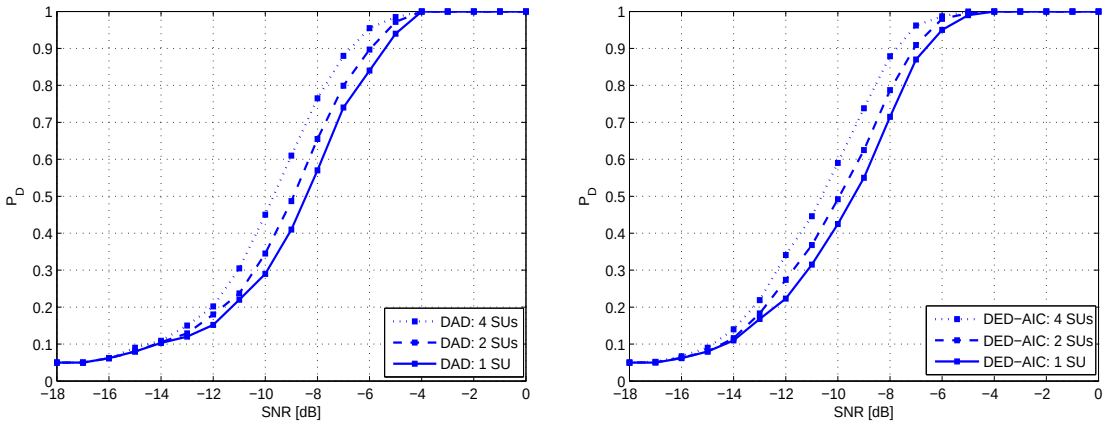

(a) P_D fct. SNR : DAD (b) P_D fct. SNR : DED

FIGURE A.5 – Évaluation de performances des deux techniques de détection DAD et DED en terme de détection coopérative en utilisant un signal DVB-T OFDM : Probabilité de détection en fonction du SNR pour une $P_{FA} = 0.05$ et un nombre de secondaires M.

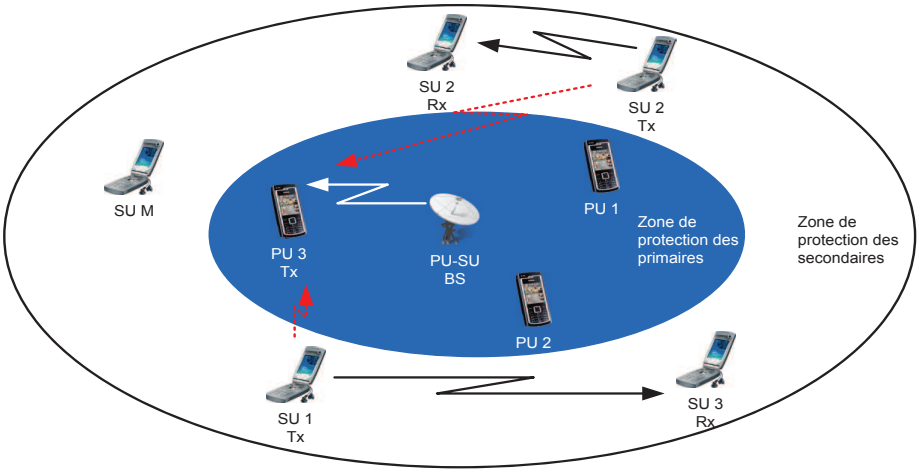

FIGURE A.6 – Réseau radio cognitif avec N utilisateurs primaires et M utilisateurs secondaires essayant de communiquer entre eux en ad-hoc, dans un système primaire en mode downlink.

A.3 Stratégies d'allocation des ressources pour la radio cognitive

Dans le cadre des politiques d'allocation de ressources dans les réseaux radio cognitive, nous avons proposé deux méthodes de sélection d'utilisateurs basées sur la probabilité outage. Nous présentons dans cette section ces deux stratégies. Nous commençons par une présentation générale du contexte d'allocation de ressource avec les définitions des différents paramètres utilisés dans notre développement. Par suite, nous présenterons les détailles des algorithmes d'allocation de ressource et quelques résultats de simulation.

A.3.1 Principe d'allocation des ressources pour la radio cognitive

L'accès opportuniste au spectre par un réseau secondaire a pour obligation de ne pas gêner le fonctionnement de l'utilisateur primaire. Nous proposons dans cette section les scenarios mises en oeuvre dans cette deuxième partie de thèse ainsi que le modèle du système cognitive adopté. Nous avons choisi les deux scenarios donnés par la Figure A.6 et la Figure A.7 dans les deux modes downlink et uplink, respectivement.

Dans le même contexte, des études théoriques sur la gestion de la ressource radio sont menées, notamment sur les points suivants :

- Modélisation et prise en compte l'environnement (interférences, technologies d'accès disponibles) ;
- Mécanismes d'allocations de ressources dans un contexte de radio opportuniste ;
- Architectures de réseau pour la gestion des ressources ;
- Interaction avec les applications en "Context Aware" et prise en compte de considérations d'usage (exploitation du profil de l'utilisateur).

Nous proposons ici deux méthodes basées sur la probabilité outage pour pouvoir satisfaire les points cités précédemment. Au cours de notre développement, nous utiliserons les paramètres suivants :

- l'utilisateur primaire est représenté par l'indice pu,

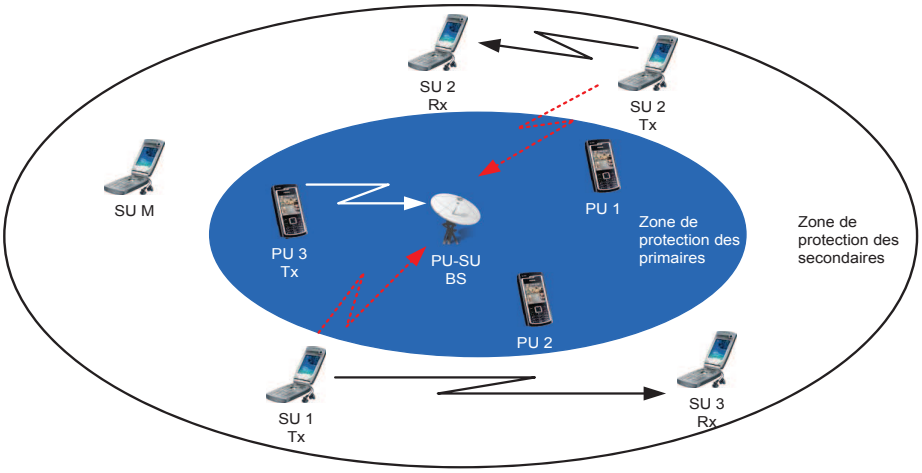

FIGURE A.7 – Réseau radio cognitif avec N utilisateurs primaires et M utilisateurs secondaires essayant de communiquer entre eux en ad-hoc, dans un système primaire en mode uplink.

- l'indice d'un utilisateur secondaire m varie de 1 à M,
- $h_{l,m}$ est le gain du canal d'un utilisateur secondaire l à un deuxième utilisateur secondaire m,
- les données destinées à un utilisateur secondaire m sont transmit avec une puissance p_m et un maximum de puissance P_{max},
- $h_{pu,m}$ est le gain du canal de l'utilisateur primaire à un utilisateur secondaire m,
- $h_{pu,pu}$ est le gain du canal entre l'utilisateur primaire et la station de base BS,
- les données destinées à l'utilisateur primaire sont transmit avec une puissance p_{pu}.

A.3.2 Technique d'allocation de ressource distribuée

Cet algorithme permet de sélectionner un nombre d'utilisateur secondaire aptes à communiquer entre eux tout en assurant une qualité de service pour le système primaire ainsi qu'une certaine qualité de service pour les secondaires. La stratégie de sélection des utilisateurs secondaires assure une protection de la probabilité outage (c.-à-d. une protection du primaire) en maximisant la somme des capacités des secondaires.

Avant d'entrer dans les détailles de l'algorithme d'allocation de ressource proposé dans cette partie, nous définissons quelques paramètres utiles pour le développement. Le premier paramètre est la capacité du système primaire donnée par :

$$C_{pu} = \log_2 \left(1 + \frac{p_{pu} \mid h_{pu,pu} \mid^2}{\sum_{m=1}^{M} p_m \mid h_{pu,m} \mid^2 + \sigma^2} \right) \tag{A.36}$$

avec σ^2 est la variance du bruit ambiant. Nous devons ainsi sélectionner le nombre d'utilisateurs secondaires pouvant transmettre dans la bande du primaire en assurant une certaine qualité de

service pour ce dernier. Cette qualité de service est vérifiée à travers la capacité du primaire, en fixant un seuil maximum R_{pu}. Nous définissons alors la probabilité outage comme suit :

$$P_{out} = Prob\left\{\mathrm{C}_{pu} \leq R_{pu}\right\} \tag{A.37}$$

Après avoir garantir une certaine qualité de service pour le système primaire, nous tenons en compte dans notre analyse une certaine qualité de service pour le système secondaire. Cette assurance est garanti par une contrainte sur la capacité de chaque secondaire définie comme :

$$C_m \ = \log_2\left(1 + \mathrm{SINR}_m\right) \tag{A.38}$$

avec

$$\mathrm{SINR}_m = \frac{p_m|h_{m,m}|^2}{\sum\limits_{\substack{l=1 \\ l\neq m}}^{M} p_l|h_{l,m}|^2 + p_{pu}|h_{pu,m}|^2 + \sigma^2} \tag{A.39}$$

et le but de l'algorithme d'allocation de ressource est de maximiser la somme des capacités des secondaires :

$$C_{su} = \sum_{m=1}^{M} C_m \tag{A.40}$$

Dans notre analyse, nous supposons que le gain du canal primaire peut être exprimé sous cette forme :

$$h_{pu,pu} \triangleq G_{pu} * h'_{pu,pu} \tag{A.41}$$

fonction du gain moyen estimé du canal primaire $h'_{pu,pu}$ et la composante aléatoire de ce gain. La probabilité outage peut s'écrire dans ce cas sous la forme suivante :

$$P_{out} = Prob\left\{\log_2\left(1 + \frac{p_{_{pu}} G_{pu}^2 \mid h'_{pu,pu} \mid^2}{\sum\limits_{m=1}^{M} p_m \mid h_{pu,m} \mid^2 + \sigma^2}\right) \leq R_{pu}\right\} \tag{A.42}$$

avec $\tilde{M}_d$ est le nombre maximum des utilisateurs secondaires pouvant transmettre sans affecter le système primaire. Si nous prenons en considération la même forme de décomposition pour le gain du canal secondaire en intégrant le gain moyen des secondaires G_{su}, nous obtenons :

$$P_{out} \ \simeq Prob\left\{\frac{p_{_{pu}} G_{pu}^2 \mid h'_{pu,pu} \mid^2}{G_{su}^2 \sum\limits_{m=1}^{\tilde{M}_d} p_m + \sigma^2} \leq 2^{R_{pu}} - 1\right\} \leq q \tag{A.43}$$

$$\simeq Prob\left\{\mid h'_{pu,pu} \mid^2 \leq \left(2^{R_{pu}} - 1\right)\left(\frac{\tilde{M}_d G_{su}^2 P_{max} + \sigma^2}{G_{pu}^2 p_{_{pu}}}\right)\right\} \leq q$$

Si nous supposons que le canal est i.i.d. distribué sous le format Rayleigh, nous avons l'équation de probabilité outage suivante :

$$P_{out} \simeq \int_0^{\left(2^{R_{pu}}-1\right)\left(\frac{\tilde{M}_d G_{su}^2 P_{max}+\sigma^2}{G_{pu}^2 p_{pu}}\right)} \exp(-t)dt \leq q \tag{A.44}$$

et finalement nous obtenons la contrainte de probabilité outage suivante :

$$P_{out} \simeq 1-\exp\left[-\left(2^{R_{pu}}-1\right)\left(\frac{\tilde{M}_d G_{su}^2 P_{max}+\sigma^2}{G_{pu}^2 p_{pu}}\right)\right] \leq q \tag{A.45}$$

Le nombre maximum d'utilisateurs secondaires actifs peut s'exprimer sous cette forme :

$$0 \leq \tilde{M}_d \leq \frac{-\log(1-q)}{(2^{R_{pu}}-1)}.\frac{G_{pu}^2 p_{pu}}{G_{su}^2 P_{max}} - \frac{1}{\mathrm{SNR}} = \tilde{M}_{theory} \tag{A.46}$$

et le problème d'optimisation de l'algorithme d'allocation de ressource distribué est

$$\text{Find } \; p_m|_{m=1,...,M} = \arg\max_{p_m} C_{su} \tag{A.47}$$

tenant compte que :

$$\begin{cases} p_m \in \{0, P_{max}\}, \quad \text{for} \quad m=1,...,M \\ \\ 0 \leq \tilde{M}_d \leq \dfrac{-\log(1-q)}{(2^{R_{pu}}-1)}.\dfrac{G_{pu}^2 p_{pu}}{G_{su}^2 P_{max}} - \dfrac{1}{\mathrm{SNR}} \end{cases} \tag{A.48}$$

A.3.3 Technique d'allocation de ressource centralisée basée sur le beamforming

Le deuxième algorithme d'allocation de ressource proposé dans ce travail est basé sur l'annulation des interférences causées par les utilisateurs secondaires. Nous avons opté pour cela une technique de beamforming au niveau du système secondaire. L'algorithme fonctionne en deux étapes indépendantes mais complémentaires : La première étape permet de sélectionner un nombre d'utilisateurs secondaires en tenant compte de la probabilité outage, après, une deuxième sélection sera effectuer parmi les utilisateurs présélectionnés en vérifiant la contrainte d'allocation de puissance assurée par le mécanisme de beamforming.

Nous proposons le système secondaire présenté par la Figure A.8. K antennes à l'émission et à la réception sont considérés. Le vecteur de gains de l'utilisateur primaire pu vers un utilisateur secondaire m est donné par :

$$\mathbf{h}_{pu,m} = [h_{pu,m_1}...h_{pu,m_K}]^T \tag{A.49}$$

et le signal reçu au niveau d'un utilisateur secondaire m est :

$$\mathbf{y}_m = \mathbf{H}_{m,m}\mathbf{s}_m + \sum_{l=1,l\neq m}^{M} \mathbf{H}_{m,l}\mathbf{s}_l + \mathbf{h}_{pu,m}x_{pu} + \mathbf{n}_m, \quad m=1,...,M \tag{A.50}$$

avec $\mathbf{n}_m$ est un bruit Gaussien de moyenne nulle et de puissance σ_m^2. $\mathbf{s}_m$ est le signal transmis pour le secondaire m et x_{pu} est l'échantillon émis par le primaire. $\mathbf{H}_{m,l}(l=1,...,m-1,m+1,...,M)$ est la matrice de canaux entre le secondaire émetteur et le secondaire récepteur m.

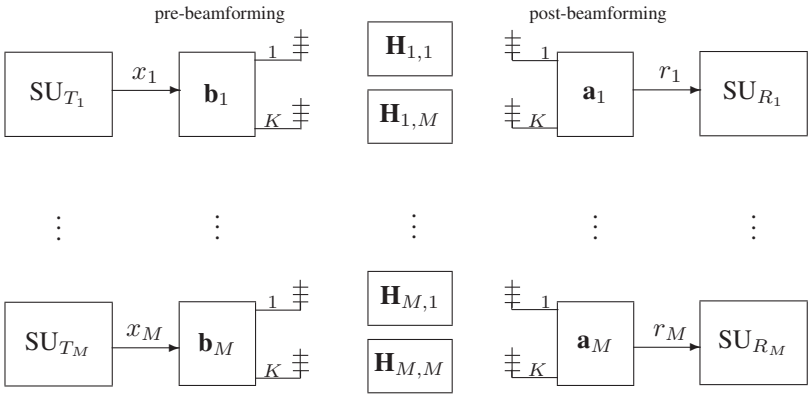

FIGURE A.8 – Strucure de réseau radio cognitive secondaire MIMO.

Le signal émis après opération de beamforming est :

$$\mathbf{s}_m = \mathbf{b}_m x_m, \quad m = 1, ..., M \tag{A.51}$$

avec $\mathbf{b}_m$ est le vecteur de pre-beamforming et x_m est l'échantillon transmis par le secondaire m. Le signal reçu est fonction du vecteur post-beamforming $\mathbf{a}_m$, donné par :

$$\begin{aligned} r_m =& \mathbf{a}_m^H \mathbf{y}_m \\ =& \mathbf{a}_m^H \mathbf{H}_{m,m} \mathbf{b}_m x_m + \mathbf{a}_m^H \sum_{l=1, l\neq m}^{M} \mathbf{H}_{m,l} \mathbf{b}_l x_l + \mathbf{a}_m^H \mathbf{h}_{pu,m} x_{pu} + \mathbf{a}_m^H \mathbf{n}_m \end{aligned} \tag{A.52}$$

Nous définissons ainsi la forme du SINR dans ce contexte :

$$\begin{aligned} \text{SINR}_m =& \frac{E\{|\mathbf{a}_m^H \mathbf{H}_{m,m} \mathbf{b}_m x_m|^2\}}{E\left\{ \sum_{l=1, l\neq m}^{M} |\mathbf{a}_m^H \mathbf{H}_{m,l} \mathbf{b}_l x_l|^2 \right\} + E\{|\mathbf{a}_m^H \mathbf{h}_{pu,m} x_{pu}|^2\} + E\{|\mathbf{a}_m^H \mathbf{n}_m|^2\}} \\ =& \frac{|\mathbf{a}_m^H \mathbf{H}_{su_{mm}} \mathbf{b}_m|^2}{|\mathbf{a}_m^H \mathbf{h}_{pu,m}|^2 + \sum_{l=1, l\neq m}^{M} |\mathbf{a}_m^H \mathbf{H}_{m,l} \mathbf{b}_l|^2 + \mathbf{a}_m^H \mathbf{R}_m \mathbf{a}_m} \end{aligned} \tag{A.53}$$

et la capacité du système primaire :

$$\text{C}_{pu} = \log_2 \left(1 + \frac{p_{pu} |h_{pu,pu}|^2}{\sum_{m=1}^{M} |\mathbf{h}_{pu,m} \mathbf{h}_{pu,m}{}^H| ||\mathbf{b}_m||^2 + \sigma^2} \right) \tag{A.54}$$

Notons par $\mathbf{R}_m$ la matrice de covariance d'interférence et bruit total pour un utilisateur secondaire m donné par :

$$\mathbf{R}_m = \Phi_m + \sum_{l=1, l\neq m}^{M} \mathbf{H}_{m,l} \mathbf{b}_l \mathbf{b}_l^H \mathbf{H}_{m,l}^H \tag{A.55}$$

avec $\Phi_m = E\{\mathbf{n}_m\mathbf{n}_m^H\}$. Par suite, le SINR du m-ème utilisateur secondaire est reformulé sous cette forme :

$$\begin{aligned}\text{SINR}_m=&\frac{\left(\mathbf{a}_m^H\mathbf{H}_{m,m}\mathbf{b}_m\right)^H\left(\mathbf{a}_m^H\mathbf{H}_{m,m}\mathbf{b}_m\right)}{\mathbf{a}_m^H\mathbf{R}_m\mathbf{a}_m}\\ =&\left(\mathbf{a}_m^H\mathbf{H}_{m,m}\mathbf{b}_m\right)^H\left(\mathbf{a}_m^H\mathbf{R}_m\mathbf{a}_m\right)^{-1}\left(\mathbf{a}_m^H\mathbf{H}_{m,m}\mathbf{b}_m\right)\\ =&\mathbf{b}_m^H\mathbf{H}_{m,m}\mathbf{R}_m^{-1}\mathbf{H}_{m,m}^H\mathbf{b}_m\end{aligned} \tag{A.56}$$

La forme (A.56) conduit à la maximisation du SINR suivante :

$$\mathbf{b}_m^H\mathbf{H}_{m,m}^H\mathbf{R}_m^{-1}\mathbf{H}_{m,m}\mathbf{b}_m\leq\lambda_{max}(m)p_m = \text{SINR}_m|_{max} \tag{A.57}$$

avec $\lambda_{max}(m)$ représente le maximum des valeurs propres de la matrice $\mathbf{H}_{m,m}^H\mathbf{R}_m^{-1}\mathbf{H}_{m,m}$ et $p_m = \mathbf{b}_m^H\mathbf{b}_m$.

Le problème d'optimisation de l'algorithme d'allocation de ressource centralisée basée sur le beamforming est donné par :

$$\begin{cases}\text{maximiser} & f(p_1,...,p_M)=\dfrac{1}{\ln 2}\displaystyle\sum_{m=1}^{M}\ln\left(1+\lambda_{max}(m)p_m\right)\\ \text{tenant compte} & \displaystyle\sum_{m=1}^{M}p_m\leq MP_{max}\\ & P_{out}\simeq 1-\exp\left[-\left(2^{R_{pu}}-1\right)\left(\dfrac{G_{su}^2\displaystyle\sum_{m=1}^{M}p_m+\sigma^2}{G_{pu}^2p_{pu}}\right)\right]\leq q\end{cases} \tag{A.58}$$

La solution de ce dernier probleme donne la forme suivante de la puissance p_m d'un utilisateur secondaire m :

$$p_m=P_{max}-\frac{1}{\lambda_{max}(m)}+\frac{1}{M}\sum_{i=1}^{M}\frac{1}{\lambda_{max}(i)}\quad\text{for}\quad m=1,...,M \tag{A.59}$$

En tenant compte d'une deuxème contrainte sur la puissance, $||\mathbf{b}_m||^2 = p_m \leq P_{max}$, nous obtenons la solution d'allocation de puissance ci-dessous :

$$\begin{array}{lcll}p_m & = & P_{max} & \text{si } p_m > P_{max}\\ p_m & = & P_{max}-\frac{1}{\lambda_{max}(m)}+\frac{1}{M}\sum_{i=1}^{M}\frac{1}{\lambda_{max}(i)} & \text{sinon}\end{array} \tag{A.60}$$

A.3.4 Résultats des simulations

Nous présentons dans cette section quelques résultats de simulation des deux algorithmes d'allocation de ressource proposés dans cette partie. Le scenario du réseau radio cognitive choisi est donné par la Figure A.9. Nous considérons un utilisateur primaire pouvant se déplacer sur un disque de rayon R_p et un ensemble de secondaires occupant une bande de rayon R comme montre la Figure A.9. Dans les simulations qui seront présentées, nous avons fixé $R = 1000$ mètres et $R_p = 600$ mètres. Le modèle de propagation utilisé est COST-231 Hata [79] et la puissance maximale d'émission des utilisateurs P_{max}, primaire et secondaires, est égale à 1 Watt.

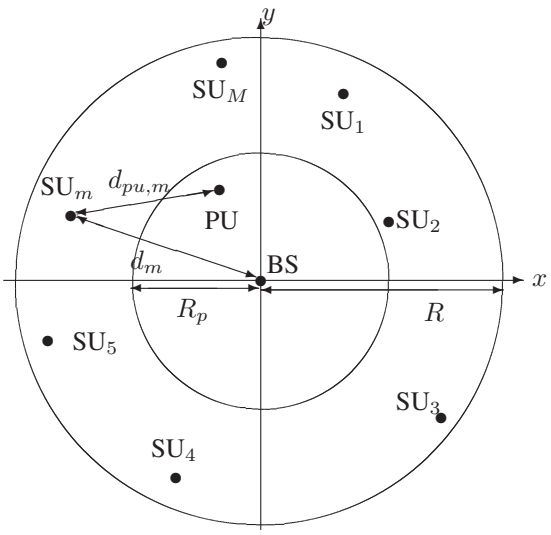

FIGURE A.9 – Réseau radio cognitive avec un utilisateur primaire et M utilisateurs secondaires.

La Figure A.10 montre le nombre maximum d'utilisateurs secondaires actifs d'un tel scénario en fonction du nombre total de tous les utilisateurs pour différents débits et dans les deux cas downlink et uplink. Nous remarquons que plus le débit est faible, plus le nombre d'utilisateurs actifs est grand. Nous remarquons aussi que l'algorithme d'allocation de ressource centralisée basée sur le beamforming donne les meilleurs résultats. Ceci est expliqué par le fait que cet algorithme prend en considération l'annulation des interférences causées par les secondaires sur le système primaire. Aussi, l'algorithme d'allocation de ressource distribuée permet de sélectionner plus d'utilisateurs actifs comparé au centralisé. En effet, l'algorithme distribué calcule le nombre d'utilisateurs sans avoir besoin d'informations sur les conditions du canal (comme les gains, etc.). Par suite, à partir de ce nombre connu au préalable, nous choisissons les utilisateurs qui causent moins d'interférences. Par contre, dans le cas de l'algorithme centralisé, le nombre d'utilisateurs actifs est estimé au fur et à mesure le nombre d'itérations augmente. En effet, nous initialisons tous les utilisateurs actifs. Nous calculons pour chaque utilisateur la probabilité outage et la capacité et nous maximisons la capacité moyenne C_{su}. Si cet utilisateur vérifie les deux contraintes mentionnées, il est maintenu actif, sinon cet utilisateur change d'état à inactif. Cette opération est répétée pour chaque utilisateur rentrant dans le système.

La Figure A.11 présente l'évaluation des performances des deux stratégies d'allocation de ressource pour garantir la qualité de service pour l'utilisateur primaire. En effet, la probabilité outage est majorée par un seuil maximum q et au delà de cette valeur le système primaire sera perturbé. Nous remarquons d'après la Figure A.11 que le système primaire reste protégé dans les trois cas de figure. Ces résultats montrent également la performance du développement réalisé surtout dans le cas de l'algorithme distribué et celui basé sur le beamforming.

Nous vérifions d'après la Figure A.12 un des objectifs fixé lors du développement de l'algorithme d'allocation de ressource centralisé basé sur le beamforming, la minimisation des interférences générées par les secondaires. En effet, le but d'applique cette stratégie était de choisir une meilleur combinaison beamforming et d'allouer le plus optimum possible les puissances d'émission des secondaires. La Figure A.12 montre que l'interférence du système secondaire a diminué en utilisant la technique du beamforming.

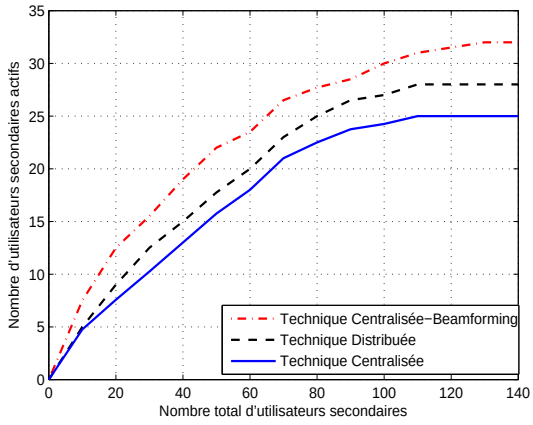

(a) Downlink : Débit = 0.1bits/s/Hz

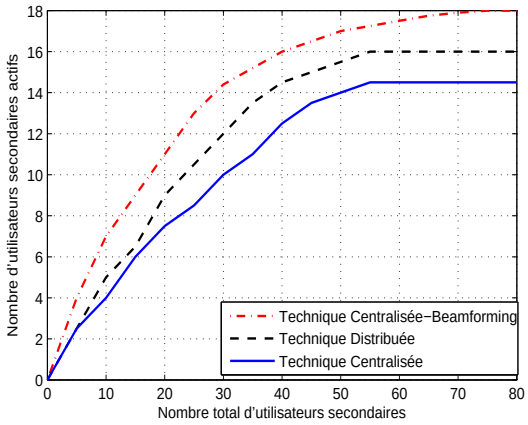

(b) Uplink : Débit = 0.1bits/s/Hz

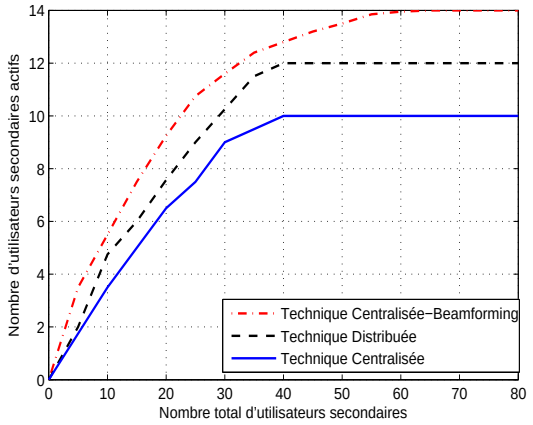

(c) Downlink : Débit = 0.3bits/s/Hz

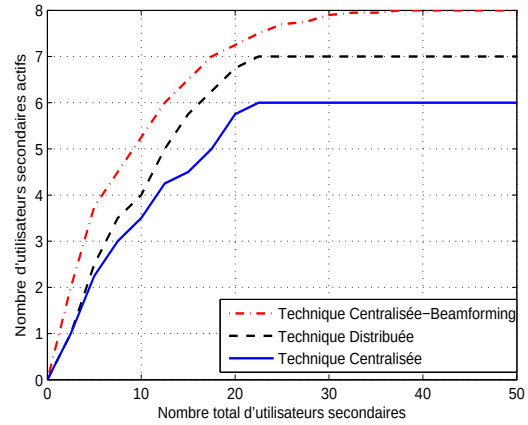

(d) Uplink : Débit = 0.3bits/s/Hz

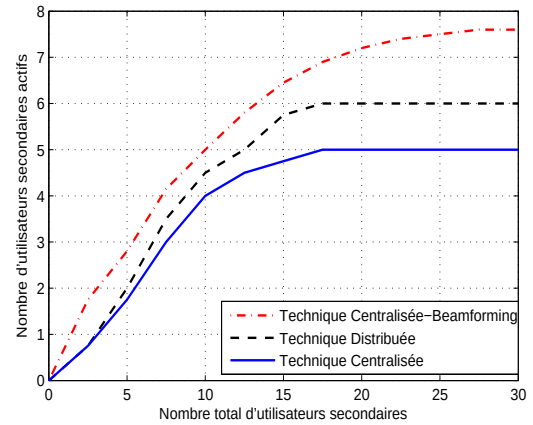

(e) Downlink : Débit = 0.5bits/s/Hz

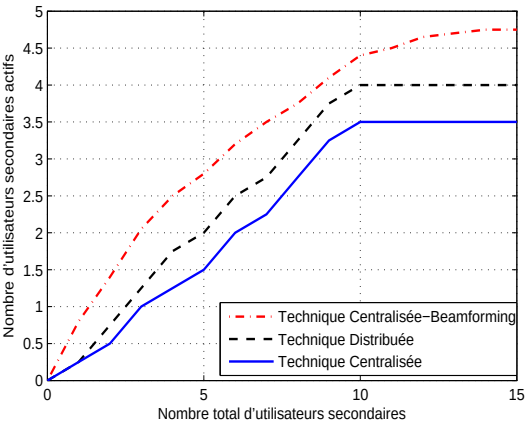

(f) Uplink : Débit = 0.5bits/s/Hz

FIGURE A.10 – Évaluation de performances des deux techniques d'allocation de ressource en comparison avec la technique centralisée : nombre maximum d'utilisateurs secondaires actifs pour différents débits (0.1, 0.3 et 0.5bits/s/Hz) dans les deux cas downlink et uplink pour $q = 1\%$.

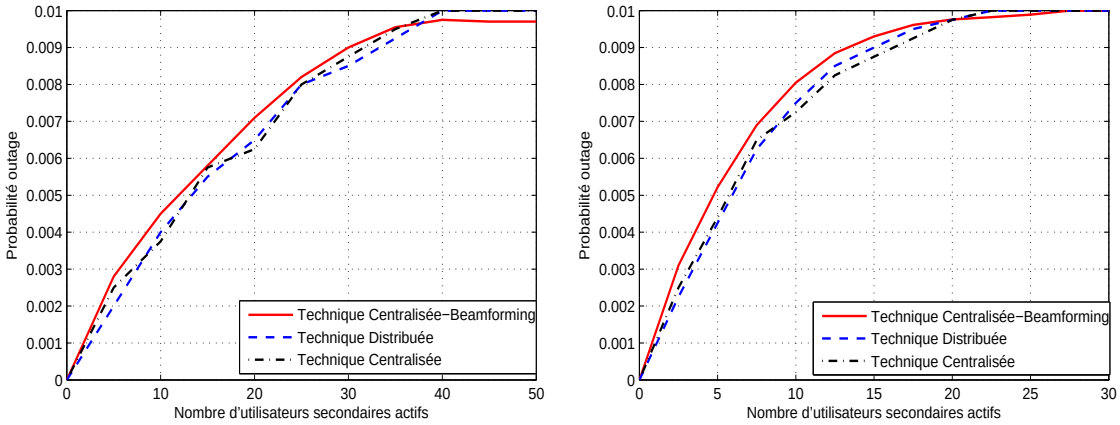

(a) Downlink (b) Uplink

FIGURE A.11 – Évaluation de performances des deux techniques d'allocation de ressource en comparison avec la technique centralisée en terme de probabilité outage pour un débit = 0.3bits/s/Hz et probabilité outage maximale = 1% dans les deux cas downlink et uplink.

A.4 Conclusion

Dans cette thèse, nous avons mis l'accent sur deux domaines qui touchent la radio cognitive : les techniques de détection spectrales et les politiques d'allocation de ressources. Dans la première partie, nous avons proposé deux méthodes de détection : le détecteur basé sur la distribution du signal primaire et le détecteur basé sur la dimension du signal. Nous avons donné dans ce résumé les détailles des deux algorithmes ainsi que le développement des seuils de détection en fonction des probabilités de fausse alarme pour les deux détecteur. Des résultats de simulation basés sur des scenarios radio cognitive réels ont été présentés. Dans la deuxième partie, nous avons proposé aussi deux stratégies d'allocation de ressource basées sur la probabilité outage. La première stratégie essaye de garantir une certaine qualité de service pour le système primaire tout en assurant une qualité de service pour les secondaires par le moyen de maximisation des capacités. La deuxième méthode proposée utilise une technique de beamforming pour minimiser les interférences générées par le système secondaire. L'originalité de ces deux stratégies est le fait de garantir une continuité du service même lorsque les trous détectés par les méthodes de détection deviennent occupés et ceux au moyen du control de la probabilité outage. En effet, si la totalité de la bande est libre (le système primaire est silencieux), nous fixons la probabilité outage à 1 (le maximum). Dans ce cas, les utilisateurs secondaires peuvent profiter de la totalité de la bande avec un maximum de flexibilité. Si la bande du primaire est partiellement occupée, nous fixons une probabilité outage maximale et nous vérifions cette condition pour chaque secondaire entrant dans le réseau pour sélectionner les secondaires pouvant émettre dans les sous-bandes libres. Nous avons ainsi une continuité de service quelque soit le résultat du système de détection.

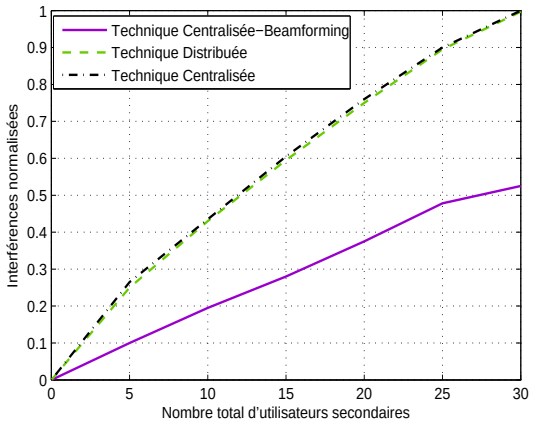

FIGURE A.12 – Évaluation de performances des deux techniques d'allocation de ressource en comparison avec la technique centralisée en terme de minimisation des interférences générées par les secondaires pour un débit = 0.3bits/s/Hz et probabilité outage maximale = 1% dans le mode uplink.

Bibliography

[1] J. Mitola and G.Q. Jr. Maguire. Cognitive radio : making software radios more personal. *IEEE Personal Communications*, 6(4) :13–18, Aug. 1999.

[2] J. Mitola. Cognitive radio for flexible mobile multimedia communications. In *Mobile Multimedia Communications (MoMUC)*, New York, Nov. 1999.

[3] J. Mitola. *Cognitive radio : An integrated agent architecture for software defined radio*. Doctor of Technology, Royal Inst. Technol. (KTH), Stockholm, Sweden, 2000.

[4] S. Seidel. Raytheon. ieee 802 tutorial. Web Page, http ://www.ieee802.org/802_tutorials/05-July/IEEE2080220CR20Tutorial207-18-0520seidel20input.pdf, 2005.

[5] SENDORA. Sensor network for dynamic and cognitive radio access. site internet, http ://www.sendora.eu/.

[6] J. M. Peha. Approaches to spectrum sharing. *IEEE Communications Magazine*, 43(2) :10–12, February 2005.

[7] FCC. Cognitive radio technologies proceeding. Web Page, http ://www.fcc.gov/oet/cognitiveradio/, 2003.

[8] FCC. Spectrum access and the promise of cognitive radio technology. Web Page, ftp ://ftp.fcc.gov/pub/Bureaus/Engineering_Technology/Documents/cognitive_radio/vanwazercognitive_radio_presentation.ppt, 2003.

[9] Cognitive Radio Technologies Federal Communications Commission. http ://hraun-foss.fcc.gov/edocs public/attachmatch/fcc−07−78a1.doc.

[10] H. Akaike. On the likelihood of a time series model. *The Statistician*, 27(3) :217–235, Dec. 1978.

[11] H. Akaike. Information theory and an extension of the maximum likelihood principle. In *2nd International Symposium on Information Theory*, Budapest, Hungary, 1973.

[12] G. Schwartz. Estimating the dimension of a model. *Annals of Statistics*, 6 :497–511, 1978.

[13] A. Ghasemi and E.S. Sousa. Spectrum sensing in cognitive radio networks : Requirments, challenges and design trade-offs. *IEEE Communications Magzine*, pages 32–39, Apr. 2008.

[14] S. M. Mishra, A. Sahai and R.W. Brodersen. Cooperative sensing among cognitive radios. *IEEE Int. Conf. Communications*, 4 :1658–1663, Jun. 2006.

[15] A.V. Dantawate and G.B. Giannakis. Statistical tests for presence of cyclostationarity. *IEEE Transactions on Signal Processing*, 42(9) :2355–2369, Sept. 1994.

[16] W. A. Gardner, A. Napolitano and L. Paura. Cyclostationarity : Half a century of research. *Signal Processing*, 86(4) :639–697, Apr. 2006.

[17] W. A. Gardner. Signal interception : A unifying theoretical framework for feature detection. *IEEE Transactions on Communications*, 36(8) :897–906, Aug. 1988.

[18] A.V. Dandawaté and G.B. Giannakis. Statistical tests for presence of cyclostationarity. *IEEE Transactions on Signal Processing*, 42(9) :2355–2369, Sep. 1994.

[19] J. Lundén, V. Koivunen, A. Huttunen and H. V. Poor. Spectrum sensing in cognitive radios based on multiple cyclic frequencies. In *2nd International Conference on Cognitive Radio Oriented Wireless Networks and Communications (CrownCom)*, pages 37–43, Orlando, FL, USA, Jul. 31-Aug. 3 2007.

[20] M. Abramowitz and I.A. Stegun. *Handbook of Mathematical Functions with Formulas, Graphs, and Mathematical Tables*. 10th ed. Washington, D. C. : U.S. National Bureau of Standards, 1972.

[21] S. Chaudhari, V. Koivunen, and H.V. Poor. Autocorrelation-based decentralized sequential detection of ofdm signals in cognitive radios. *IEEE Transactions on Signal Processing*, 57(7) :2690–2700, Jul. 2009.

[22] M. Naraghi-Pour and T. Ikuma. Autocorrelation-based spectrum sensing for cognitive radios. *IEEE Transactions on Vehicular Technology*, 59(2) :718–733, Feb. 2010.

[23] J.G. Proakis. *Digital Communications*. 4th ed. McGraw-Hill Higher Education, 2001.

[24] R. Tandra and A. Sahai. Fundamental limits on detection in low snr. In *WirelessComm05 Symposium on Signal Processing*, Jun. 2005.

[25] S. Haykin. Cognitive radio : brain-empowered wireless communications. *IEEE J. Sel. Areas Commun.*, 23 :201–220, Feb. 2005.

[26] H. Urkowitz. Energy detection of unknown deterministic signals. *Proceeding of the IEEE*, 55(5) :523–531, 1967.

[27] M. Haddad, A.M. Hayar, H. Fetoui and M. Debbah. Cognitive radio sensing information-theoretic criteria based. *CrownCom, Orlando, USA*, August 1-3 2007.

[28] Y. Zeng and Y.C. Liang. Eigenvalue-based spectrum sensing algorithms for cognitive radio. *IEEE Transactions on Communications*, 57(6) :1784–1793, Jun. 2009.

[29] T. J. Lim, R. Zhang, Y. C. Liang and Y. Zeng. Glrt-based spectrum sensing for cognitive radio. In *IEEE GLOBECOM*, Nov. 30-Dec. 4 2008.

[30] D. Ramirez, J. Via, I. Santamaria and P. Crespo. Entropy and kullback-leibler divergence estimation based on szego's theorem. In *17th European Signal Processing Conference (EUSIPCO)*, Aug. 2009.

[31] F. Perez-Cruz. *Kullback-leibler divergence estimation of continuous distributions*. Jul. 2008.

[32] A. Kortun, T. Ratnarajah, M. Sellathurai, C. Zhong and C.B. Papadias. On the performance of eigenvalue-based cooperative spectrum sensing for cognitive radio. *IEEE Journal of Selected Topics in Signal Processing*, 5(1) :49–55, Feb. 2011.

[33] N.M. Neihart, S. Roy and D.J. Allstot. A parallel, multi-resolution sensing technique for multiple antenna cognitive radios. In *International Symposium on Circuits and Systems (ISCAS)*, New Orleans, LA, USA, May 2007.

[34] Q. Zhang, A.B.J. Kokkeler and G.J.M. Smit. An efficient multi-resolution spectrum sensing method for cognitive radio. In *3rd International Conference on Communications and Networking in China*, Hangzhou, China, Aug. 2008.

[35] Z. Tian and G.B. Giannakis. A wavelet approach to wideband spectrum sensing for cognitive radios. In *Conf. on Cognitive Radio Oriented Wireless Networks and Communications (CROWNCOM)*, Jun. 2006.

[36] M.A. Lagunas-Hernandez, M.A. Rojas, and P. Stoica. New spectral estimation based on filterbank for spectrum sensing. *IEEE International Conference on Acoustics, Speech and Signal Processing*, April 2008.

[37] Official Web Page. European telecommunications standards institute. *http ://www.etsi.org*.

[38] A. Goldsmith. *Wireless Communications*. Cambridge Univ. Press, New York, 2005.

[39] T.H. Cormen, C.E. Leiserson, R.L. Rivest and C. Stein. *Introduction to Algorithms*, pages 141–145. MIT Press, 2001.

[40] T. Yucek and H. Arslan. A survey of spectrum sensing algorithms for cognitive radio applications. *IEEE Communications Surveys and Tutorials*, 11(1) :116–130, 2009.

[41] G. Ganesan and Y. Li. Cooperative spectrum sensing in cognitive radio networks. In *IEEE Int. Symposium on New Frontiers in Dynamic Spectrum Access Networks*, pages 137–143, Baltimore, Maryland, USA, Nov. 2005.

[42] J. Hillenbrand, T. Weiss and F. Jondral. Calculation of detection and false alarm probabilities in spectrum pooling systems. *IEEE Commun. Lett.*, 9(4) :349–351, Apr. 2005.

[43] E. Visotsky, S. Kuffner and R. Peterson. On collaborative detection of tv transmissions in support of dynamic spectrum sharing. In *IEEE Int. Symposium on New Frontiers in Dynamic Spectrum Access Networks*, pages 338–345, Baltimore, Maryland, USA, Nov. 2005.

[44] H. Tang. Some physical layer issues of wide-band cognitive radio systems. In *IEEE Int. Symposium on New Frontiers in Dynamic Spectrum Access Networks*, pages 151–159, Baltimore, Maryland, USA, Nov. 2005.

[45] R. Saadane, D. Aboutajdine, A. Hayar and R. Knopp. On the estimation of the degrees of freedom of indoor uwb channel. In *VTC 2005-Spring*, Jun. 2005.

[46] D. Bertsekas and J. Tsitsiklis. *Introduction to Probability*. Athena Scientific, 2002.

[47] D. Parsons. *The Mobile Radio Propagation Channel*. London, U.K. : Pentech, 1992.

[48] L. Lauwers, K. Barbe, W.V. Moer and R. Pintelon. Estimating the parameters of a rice distribution : a bayesian approach. *I2MTC 2009 - International Instrumentation and Measurement Technology Conference, Singapore, May 2009*.

[49] M. Wax and T. Kailath. Detection of signals by information theoretic criteria. *IEEE Trans. on ASSP*, 33(2) :387–392, 1985.

[50] J. Salo, H.M. El-Sallabi and P. Vainikainen. The distribution of the product of independent rayleigh random variables. *IEEE Transactions on Antennas and Propagation, Vol. 54, No. 2, Februray 2006*.

[51] F. Kaltenberger, R. Ghaffar, R. Knopp, H. Anouar and C. Bonnet. Design and implementation of a single-frequency mesh network using openairinterface. *EURASIP Journal on Wireless Communications and Networking*, 2010, Article ID 719523 2010.

[52] L. Maurer, T. Dellsperger, T. Burger, D. Nussbaum, R. Knopp and H. Callewaert. Medium term evolution for reconfigurable rf transceivers. In *Software Defined Radio Technical Conference and Product Exposition*, Orlando, USA, Nov. 2006.

[53] OpenAirInterface Web Page. *http ://www.openairinterface.org/.*

[54] J. Rissanen. Modeling by shortest data description. *Automatica*, 14 :465–471, 1978.

[55] H. Linhart and W. Zucchini. *Model Selection*. Wiley, New York, 1986.

[56] A. Hayar. Process for sensing vacant bands over the spectrum bandwidth and apparatus for performing the same based on sub space and distributions analysis. *European patent 08368002.5*, 1st February 2008.

[57] I.M. Johnstone. On the distribution of the largest eigenvalue in principal components analysis. (The Annals of Statistics) :vol. 29, no. 2, pp. 295Ű327, 2001.

[58] L. H. Ozarow, S. Shamai and A.D. Wyner. Information theoretic considerations for cellular mobile radio. *IEEE Trans. Veh. Technol.*, 43(5) :359–378, May 1994.

[59] L. Qian, X. Li, J. Attia and Z. Gajic. Power control for cognitive radio ad hoc networks. In *IEEE Workshop on Local and Metropolitan Area Networks*, pages 07–12, Jun. 2007.

[60] Y. Xing, C.N. Mathur, M.A. Haleem, R. Chandramouli and K.P. Subbalakshmi. Dynamic spectrum access with qos and interference temperature constraints. *IEEE Transactions on Mobile Computing*, 6 :423–433, Apr. 2007.

[61] J. Huang, R.A. Berry and M.L. Honig. Auction-based spectrum sharing. In *Mobile Networks and Applications*, volume 11, pages 405–418, 2006.

[62] E. Jorswieck and R. Mochaourab. Beamforming in underlay cognitive radio : Null-shaping design for efficient nash equilibrium. In *International Workshop on Cognitive Information Processing*, Jun. 2010.

[63] L. Akter and B. Natarajan. Qos constrained resource allocation to secondary users in cognitive radio networks. *Elsevier, Computer Communications*, Jun. 2009.

[64] X. Kang, R.Y. Liang and A. Nallanathan. Optimal power allocation for fading channels in cognitive radio networks under transmit and interference power constraints. In *IEEE International Conference on Communications*, May 2008.

[65] A. Attar, M.R. Nakhai and A.H. Aghvami. Cognitive radio game : a framework for efficiency, fairness and qos guarantee. In *IEEE International Conference on Communications*, May 2008.

[66] N. Nie and C. Comaniciu. Adaptive channel allocation spectrum etiquette for cognitive radio networks. In *New Frontiers in Dynamic Spectrum Access Networks*, 2005.

[67] F. Wang, M. Krunz and S. Cui. Spectrum sharing in cognitive radio networks. In *IEEE Conference on Computer Communications*, pages 1885–1893, Jan. 2008.

[68] Y. Wu and D.H.K. Tsang. Distributed power allocation algorithm for spectrum sharing cognitive radio networks with qos guarantee. In *IEEE INFOCOM*, 2009.

[69] P. Cheng, Z. Zhang, H. Huang and P. Qiu. A distributed algorithm for optimal resource allocation in cognitive ofdma systems. In *IEEE International Conference on Communications*, May 2008.

[70] J. Huang, Z. Han, M. Chiang and V. Poor. Auction-based distributed resource allocation for cooperation transmission in wireless networks. In *IEEE Global Communications Conference (GLOBECOM)*, Nov. 2007.

[71] S. Gao, L. Qian and D. Vaman. Distributed energy efficient spectrum access in cognitive radio wireless ad hoc networks. *IEEE Transactions on Wireless Communications*, 8(10), 2009.

[72] D. Schmidt, C. Shi, R. Berry, M. Honig and W. Utschick. Distributed resource allocation schemes. *IEEE Signal Process. Mag.*, 26(5) :53–63, Sep. 2009.

[73] J. S. Pang, G. Scutari, D. Palomar and F. Facchinei. Design of cognitive radio systems under temperature-interference constraints : A variational inequality approach. *IEEE Trans. Signal Process.*, 58(6) :3251–3271, Jun. 2010.

[74] A. Gjendemsjø, D. Gesbert, G. E. Øien and S.G. Kiani. Binary power control for multi-cell capacity maximization. *IEEE Trans. Wireless Comm.*, Aug. 2007.

[75] Saad G. Kiani and David Gesbert. Optimal and distributed scheduling for multicell capacity maximization. Submitted to IEEE International Conference on Communications 2006.

[76] M. Haddad, A. Hayar and G.E. Øien. Uplink distributed binary power allocation for cognitive radio networks. In *CrownCom*, Singapore, Mai 2008.

[77] M. Haddad, A. Hayar and G.E. Øien. Downlink distributed binary power allocation for cognitive radio networks. In *PIMRC*, Cannes, France, Sep. 2008.

[78] The charter of ieee 802.22, the working group on wireless regional area networks (wrans).

[79] Urban transmission loss models for mobile radio in the 900 and 1800 MHz bands, 1991.

[80] X. Shao and J. Yuan. Multiuser scheduling for mimo broadcast and multiple access channels with linear precoders and receivers. *IEE Proc.-Commun.*, 153(4) :541–547, Aug. 2006.

[81] J. Chung, C.S. Hwang, K. Kim and Y.K. Kim. A random beamforming technique in mimo systems exploiting multiuser diversity. *IEEE Journal on Selected Areas in Communications*, 21 :848–855, Jun. 2003.

[82] R. W. Heath, Jr., M. Airy and A.J. Paulraj. Multiuser diversity for mimo wireless systems with linear receivers. In *Asilomar Conference on Signals, Systems and Computers*, Pacific Grove, CA, Oct. 2001.

[83] C.N. Chuah, D.N.C. Tse, J.M. Kahn and R.A. Valenzuela. Capacity scaling in mimo wireless systems under correlated fading. *IEEE Transactions on Information Theory*, 48(3) :637Ű–650, 2002.

[84] E.A. Jorswieck and H. Boche. Channel capacity and capacity-range of beamforming in mimo wireless systems under correlated fading with covariance feedback. *IEEE Transactions on Wireless Communications*, 3(5), Sep. 2004.

[85] A. Tarighat, M. Sadek and A.H. Sayed. A multi user beamforming scheme for downlink mimo channels based on maximizing signal-to-leakage ratios. *IEEE International Conference on Acoustics, Speech, and Signal Processing, ICASSP*, Mar. Philadelphia, PA, USA.

[86] P. Viswanath, D. Tse and R. Laroia. Random beamforming for mimo systems with multiuser diversity. *IEEE Personal, Indoor and Mobile Radio Commun. Conf.*, 1 :290–294, Sep. 2004.

[87] D. Tse. *Fundamentals of Wireless Communication*. University of California, Berkeley Pramod Viswanath, University of Illinois, Urbana-Champaign, Sep. 2004.

[88] M. Schubert and H. Boche. Solution of the multiuser downlink beamforming problem with individual sinr constraints. *IEEE Trans. Veh. Technol.*, 53(1) :18–28, Jan. 2004.